Important Notice

UNIVERSITY OF CALGARY

Direct Measurement of Frequency Dependent Phase Velocity and Seismic Attenuation from the Snowflake Dataset

by

Chioma Agatha Chineke

A THESIS

SUBMITTED TO THE FACULTY OF GRADUATE STUDIES

IN PARTIAL FULFILMENT OF THE REQUIREMENTS FOR THE

DEGREE OF MASTER OF SCIENCE

GRADUATE PROGRAM IN GEOSCIENCE

CALGARY, ALBERTA

OCTOBER, 2024

Abstract

Carbon Capture and Storage (CCS) stands out as an effective technique for mitigating the CO2 footprint in the atmosphere. Ensuring the containment of sequestrated CO2 within geological storage is crucial, necessitating continuous monitoring. The research presented here leverages data from the Newell County facility, a shallow CO2 injection project actively promoting advancements in measurement, monitoring, and verification technologies related to CCS. The seismic method proves valuable for estimating frequency-dependent phase velocities of seismic waves. The concept of dispersion reveals that seismic waves of varying frequencies travel with distinct velocities, primarily due to non-uniform elastic properties in the subsurface, leading to frequency-dependent attenuation. As a preliminary step in estimating frequency-dependent seismic attenuation, this study aims to estimate the frequency-dependent phase velocities of the seismic waves as they propagate through the earth. The chosen method involves the analysis of uncorrelated vibroseis data, with a specific emphasis on the frequency dependence of seismic velocities. The estimated phase velocities were further utilized in predicting Q using the Kolsky dispersion model. The lateral and VSP azimuth changes in the phase velocity and seismic attenuation reflect the spatial heterogeneity in the near surface.

Acknowledgement

My sincere appreciation goes to my supervisor, Professor Kris Innanen, for his immense support, insights, guidance, and encouragement during the analysis of this work and throughout my MSc. Program.

I would like to thank Joe Wong for his guidance, and support and for permitting me to use his modified energy ratio (MER) code for picking the arrival and departure times of seismic frequencies.

Thank you, Kevin, for always being ready to provide answers to my many questions as it relates to the acquisition of Snowflake II.

Thank you, Dave Henley, for proofreading and making suggestions on my thesis write-up, it brought out the best version of my thesis.

Thank you, Zhang, and Seun, for always being ready to break down concepts, it made me better in my analysis.

It was great to belong to the CREWES family, thank you all for your support.

To my acquaintances who made it easy for me to adapt to an unfamiliar environment during my early days in Canada, I say a big thank you.

My sincere appreciation goes to my husband Casmir, and my four wonderful children, Chidera, Chikamso, Chimamanda and Ugochinyere for their support.

Finally, I would like to thank God Almighty who made it possible for me to complete my MSc. Program.

Dedication

This work is dedicated to God Almighty, He has been my overall help and confidant and to my family for their support in this journey.

Table of contents

List of Figures and Illustrations

List of Tables

List of Symbols, Abbreviations and Nomenclature

Symbol or Abbreviation	Definition
CO2	Carbon dioxide
NOAA	National Oceanic and Atmospheric Administration
GML	Global monitoring laboratory
CCS	Carbon Capture and Storage
Mt	Mega tonnes
Km	Kilometres
CMC	Carbon Management Canada
VSP	Vertical Seismic Profiling
CREWES	Consortium for Research in Elastic Waves Exploration Seismology
%	Percentage
*	Multiplication
CaMI	Containment and Monitoring Institute
MMV	Monitoring, Measurement and Verification
P-wave	Compressional wave
MER	Modified Energy Ratio
SNR	Signal-to-Noise Ratio

Tcal	Calibration time

Chapter 1-Introduction

1.1 Project Motivation

Seismic attenuation, the gradual loss of amplitude or energy experienced by seismic waves as they propagate through the subsurface, presents opportunities for monitoring sequestered Carbon Dioxide (CO_2). While traditionally considered a negative effect, seismic attenuation can be a valuable tool for understanding subsurface dynamics, especially when we consider the frequency-dependent attenuation to which seismic waves are exposed as they propagate at different velocities in an anelastic medium.

1.1.1 Carbon dioxide Capture and storage

Global warming and climate change result from the effects of the presence of Carbon dioxide in the atmosphere. In the 2023 annual report from the National Oceanic and Atmospheric Administration (NOAA) Climate, as shown in Figure 1.1, a Global Monitoring Laboratory (GML) observed that despite the fact that the recorded quantity of the three trapping gases in air samples obtained in 2023 was lower than in previous years, they follow the same pattern as the rises documented ten years ago. As a result, the report emphasized the importance of continuing to work to lower greenhouse gas levels in the atmosphere (National Oceanic and Atmospheric Administration, 2023).

The presence of Carbon dioxide in the atmosphere can be reduced or eliminated by Carbon Capture and Storage (CCS) technology. In CCS (International Energy Agency, 2023), carbon dioxide is extracted from large point sources, such as factories or power plants that run on biomass or fossil fuels. It is also possible, but more difficult, to extract CO_2 directly from the atmosphere. When not needed immediately, the compressed CO_2 is injected into the target

reservoirs (such as saline or depleted oil and gas reserves) to trap it for long-term storage, or it is transported by pipeline, ship, rail, or truck for use in a variety of applications.

Today, more than 40 Mega tonnes (Mt) of CO_2 can be captured annually by CCS facilities worldwide (International Energy Agency, 2023). Several of these facilities (International Energy Agency, 2023) have been in operation since the Val Verde, Texas, natural gas processing plants started providing CO_2 to nearby oil producers for improved oil recovery activities in the 1970s and 1980s.

The adoption of CCS has grown to include other regions and applications since these first initiatives. At the Sleipner offshore gas facility in Norway (International Energy Agency, 2023), the first extensive CO_2 capture and injection project with specialized CO_2 storage and monitoring was put into service in 1996. More than 20 MtCO2 has now been stored by the project in a deep saline rock around 1 km below the North Sea.

To make sure the implementation of CCS projects is safe and effective (Daley et. al, 2019), it is critical to identify suitable storage facilities for sequestered CO_2, and many deep saline geological formations have the necessary porosity, permeability, and seal rock. The end goal of CCS is to eliminate or reduce the amount of CO_2 in the atmosphere, and this can only happen when the stored CO_2 remains in the subsurface where it was placed. To ensure the permanent containment of sequestered CO_2 within the geological formation without leakage (Daley et. al, 2019), monitoring the sequestered CO_2 at the injection stage and throughout all stages of the CCS projects is required. The seismic method (Gassmann 1951) is a useful tool for monitoring fluid movement within the subsurface since the injection of CO_2 into the geological formation

causes changes in the elastic and acoustic properties of the propagating seismic waves within the geological storage.

While the thesis did not focus on CO2 tracking, the dataset is currently being utilized to investigate CO2 plume propagation. However, these efforts are being impeded by a lack of understanding of near-surface attenuation and dispersion.

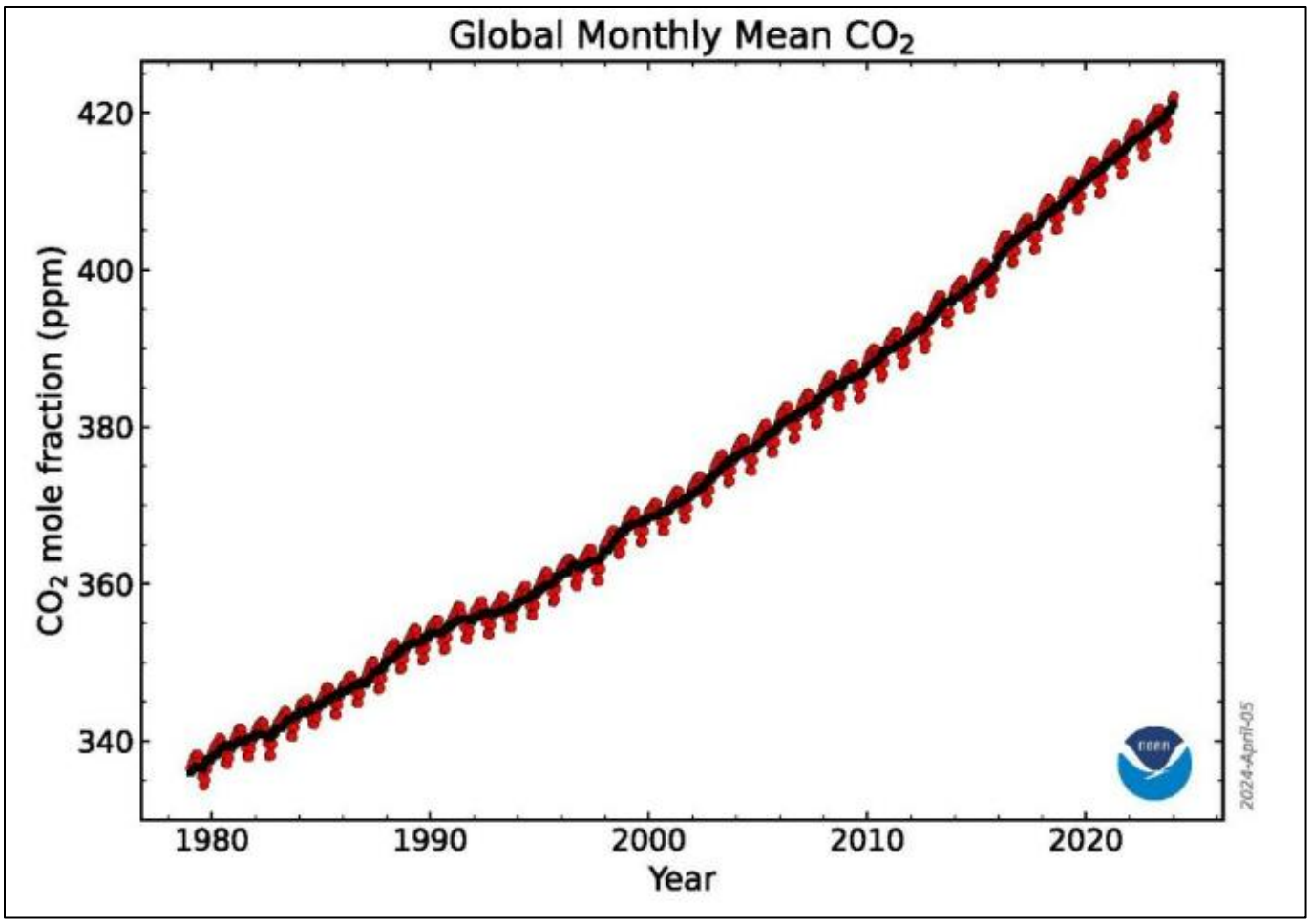

Fig 1.1: This graph shows the monthly average levels of carbon dioxide observed worldwide since 1980 at air sampling stations within the Global Monitoring Laboratory's network. The data is preliminary and may undergo quality control checks and reference gas recalibrations (source: NOAA GML).

1.1.2 Previous work on estimation of frequency-dependent phase velocities and seismic attenuation using uncorrelated VSP datasets.

This research is a continuation of Innanen (2014), where he analysed dispersion using multicomponent VSP datasets. Innanen (2014) affirms the Aki & Richards dispersion model that stipulates that higher frequencies travel faster in a dispersive medium but noted that low frequencies are typically sent into the earth before higher frequencies, but the higher frequencies travel faster and tend to catch up with lower frequencies. This travel time interplay between the higher frequencies and lower frequencies is important in estimating phase velocities which creates a pathway to estimating the Quality factor. Innanen (2014) noted that the ability of geological volumes, particularly those near the surface, to enable seismic body waves to travel dispersively is a significant barrier to Full Waveform Inversion (FWI). Anelastic parameters, such as Quality factor values of P- and S-waves QP and QS, might appear as unknowns in tractable seismic inverse algorithms if the corresponding dispersion laws are known.

Long before Innanen (2014), Dragoset et al. (1980) proposed this method of estimating phase velocities, although in a maritime context. Dragoset et al. (1980) the dispersion of a particular reflection event is determined by its frequency, sweep function type, and Doppler factor.

Sun and Milkereit (2007) expanded the concept by estimating dispersion in body waves. It was affirmed that velocity dispersion was a worry in a high-attenuation medium, and to detect velocity dispersion in the exploration seismic frequency band, a novel signal processing method was created for uncorrelated vibroseis data, cross correlation with a moving window. This approach was utilized on uncorrelated vibroseis data from places with varying geological conditions. It was observed that velocity dispersion, along with the Kramers-Krönig relation,

gives an innovative approach for calculating the quality factor Q, which can be compared to results produced using the spectral ratio method. Q is a dimensionless quantity used as a measure of seismic attenuation.

Haase et al. (2010) published tests, estimated velocity dispersion, and calculated the Q-factor from uncorrelated Vibroseis records. In this approach, pilot sweeps are divided into time segments using successive windowing, each segment featuring a different central frequency. Each segment cross-correlated with the entire received sweep at all VSP stations, enabling the automatic selection of frequency and depth-dependent travel times and the calculation of velocity dispersion. The method was tested using two synthetic zero-offset VSPs. It was observed that Q-factors can be accurately recovered, particularly away from the near-field, in the specific case of a homogeneous earth and noted that velocity dispersion and the derived Q-factor are quite sensitive to stratigraphic effects.

1.2 Newell County Facility

One CCS project in Alberta is the Newell County facility in Brooks, Southern Alberta, western Canada (Figure 1.2a), a shallow CO_2 sequestration experiment around 300m in depth, which aims to be the world's leading site for testing, and supporting the development of new Measurement, Monitoring, and Verification (MMV) technologies related to geological CO_2 sequestration. The Containment and Monitoring Institute (CaMI) operates this field research station in collaboration with the University of Calgary. The injection zone utilized in the facility corresponds to the Basal Belly River Sandstone (BBRS), a reservoir saturated with brine and possessing a porosity of 10%, situated at the bottom of the Foremost Formation (Dongas, 2016; Macquet and Lawton, 2017) as shown in Figure 1.2b. The research conducted

here utilizes the Vertical Seismic Profiles (VSP) dataset, acquired by the Consortium for Research in Elastic Waves Exploration Seismology (CREWES) in 2022. Analysing this sparse VSP dataset from the Newell County facility, despite it being a shallow CO_2 injection project, holds significant potential for increasing the understanding of seismic data behaviour in the near surface. Such insights are crucial for efficient seismic interpretation, particularly for deeper targets.

Fig1.2a: Location of Carbon Management Canada, Newell County Facility.

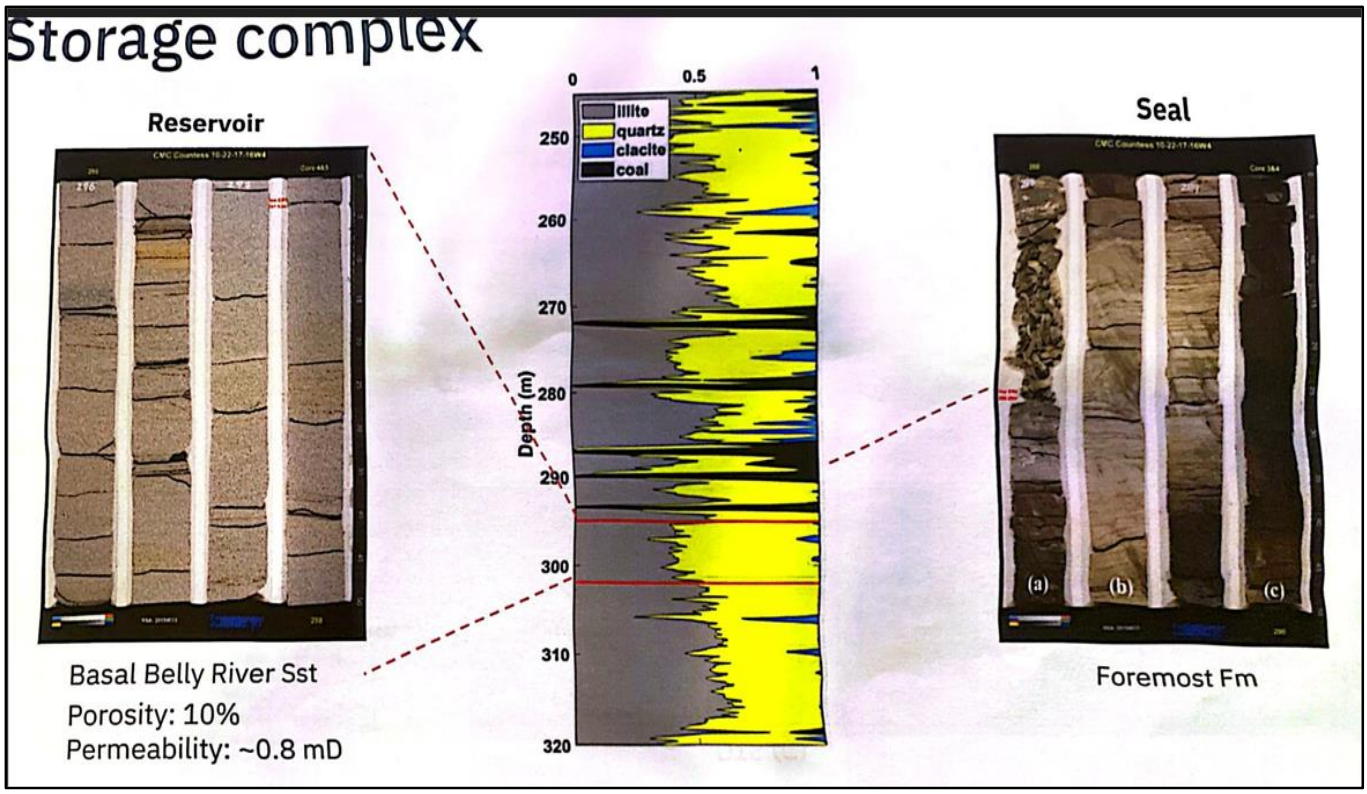

FIG1.2b: The saline storage reservoir- Basal Belly River Sandstone around depth 298-303m (from CMC research station pamphlet).

1.3 Thesis Objectives

To study the CO2 plume propagation within the Basal Belly River sandstone at the Newell County facility, I will be analysing the uncorrelated vibroseis Vertical Seismic Profiles (VSP) dataset from Snowflake II in this research, through the following objectives:

- Estimate the frequency-dependent phase velocities from the uncorrelated vibroseis Vertical Seismic Profiling (VSP) dataset.
- Determine the seismic attenuation from the phase velocities.

1.4 Data used

The uncorrelated vibroseis VSP dataset from Snowflake II acquired from the Newell County facility was analysed in this research work. Snowflake II is a walkaway VSP experiment carried out in 2022 by the CREWES research group.

1.4.1 Location of the Injection well and the observation well 2 (geophysics well)

The CO_2 is injected into the storage reservoir through the injection well and the accelerometers that measure the wave propagation are aligned along the observation well 2. The observation well 2 in the green circle is 20m away from the injection well in the red circle, as shown in Figure 1.3.

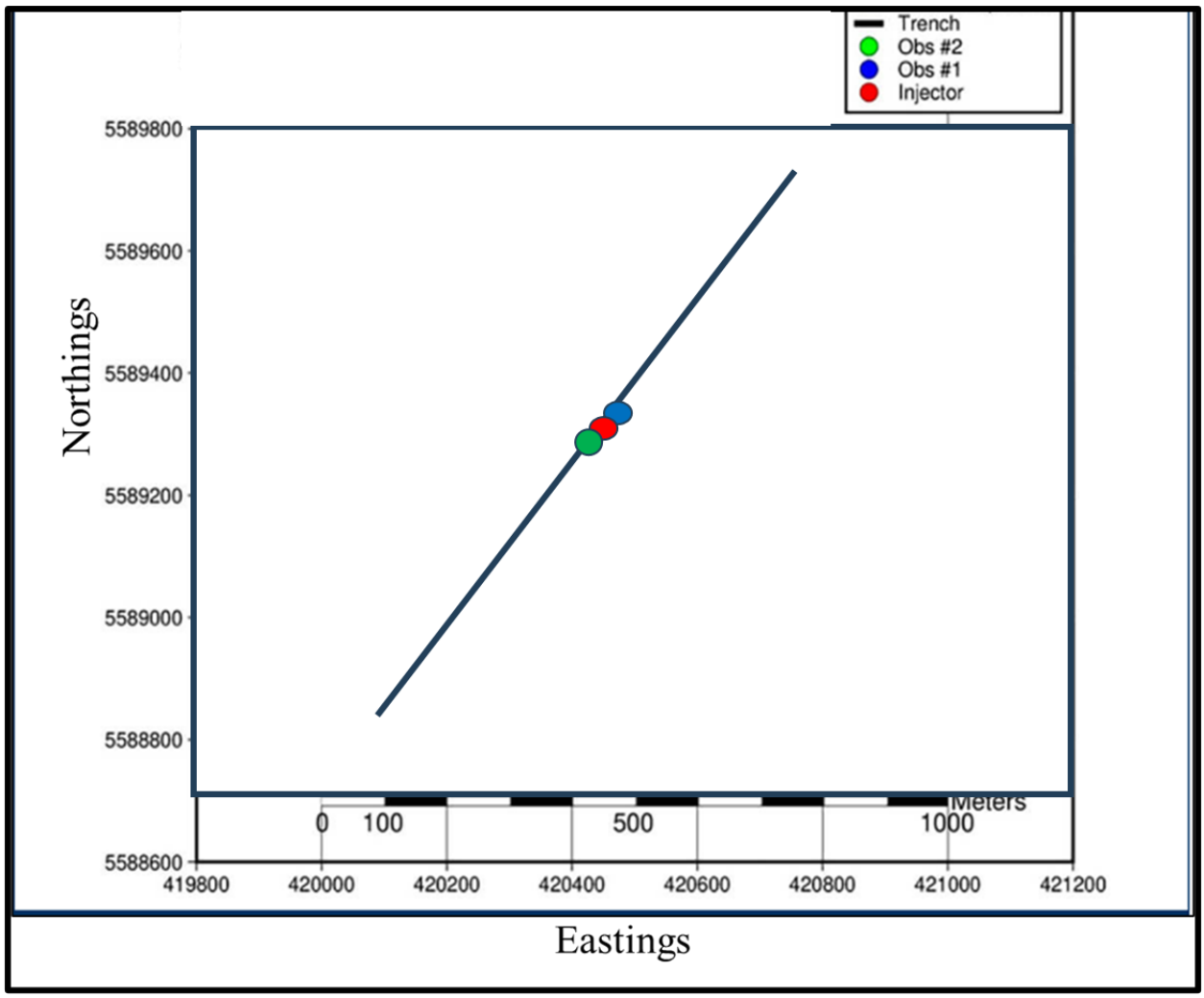

FIG 1.3: The injection well in the red circle and observation well 2 in the green circle displayed on the map of CMC Newell County facility. Source (modified from CSEG Recorder.com)

1.4.2 Walkaway VSP

The walkaway Vertical Seismic Profiling (VSP) survey was utilized in the acquisition of the two VSP datasets used in this analysis. Vertical seismic profiling (VSP) is a seismic-reflection technique that uses one or more receivers positioned at various depths within a borehole to capture seismic arrivals from surface-activated sources. VSP serves as both a well log and a seismic imaging tool, making it valuable for geophysical evaluation of the area surrounding a

well (Robert Stewart, CSEG Recorder,2001). For the acquisition of the VSP dataset, the receiver array was in a fixed position aligned along observation well 2 (geophysics well) while moving the source along multiple offset distances away from observation well 2. The multiple shot lines were important to measure the variation in elastic properties with different directions of wave propagation. A detailed description of the acquisition of the VSP dataset can be found in Hall *et al.* (2022). The acquisition geometry and the schematic diagram of the VSP technique are shown in Figure 1.4a and Figure 1.4b.

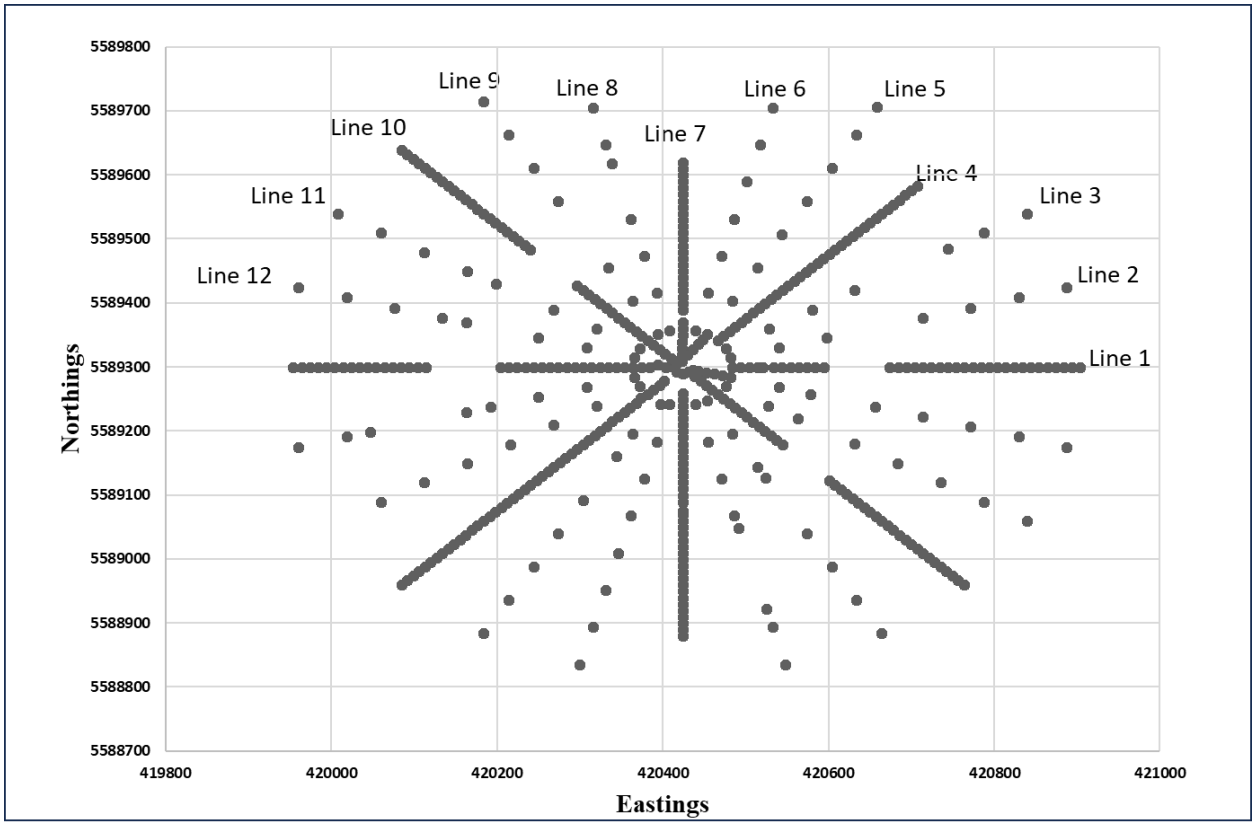

FIG 1.4a: Twelve shot lines displayed on the acquisition geometry.

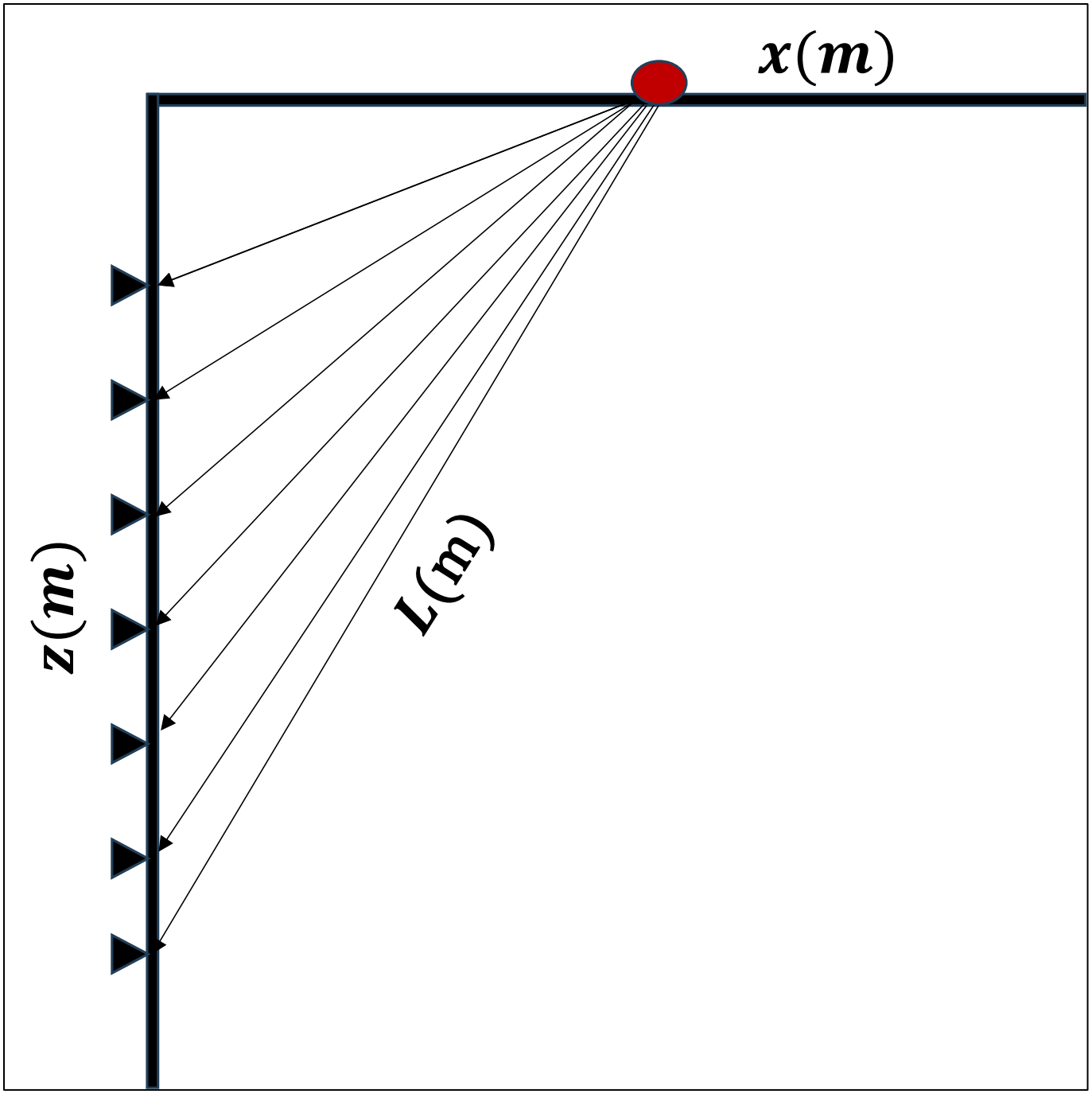

FIG 1.4b: A schematic diagram showing the location of the source (x) relative to that of the accelerometers (z) and ray path of the P-wave (L).

1.4.3 Seismic Source

The source used in the acquisition of the VSP dataset for Snowflake II was the CREWES EnviroVibe. Acoustically, it is a 2 to 300 Hz efficient vibrator with a maximum force output of 15,000 pounds. Table 1.1 contains more information about the EnviroVibe's characteristics. Twelve shot lines were utilized in the acquisition of the dataset, as displayed in Figure 1.5.

Table 1.1 Characteristics of the EnviroVibe

Specifications	Metric units	English units
Peak Force:	66,000 N	15,000 pounds
Mass Piston Area:	25.7 cm2	3.99 inches2
Reaction Mass Weight:	794 Kg	1,750 pounds
Reaction Mass Stroke:	6.99 cm	2.75 inches
Servovalve:	227 LPM	60 GPM
Servovalve Pilot Filter:	3 Micron	3 Micron
Baseplate Area:	11,675 cm2	1,810 inches2
Baseplate Assembly Weight (with pad):	895 kg	2273.3 pounds

1.4.4 Receivers

The recording sensors used in these surveys were the 3-component accelerometers. The sensors were aligned 1m apart from 0m to 140m and 2m apart from 140m to 324m in the z-direction along the Geophysics well.

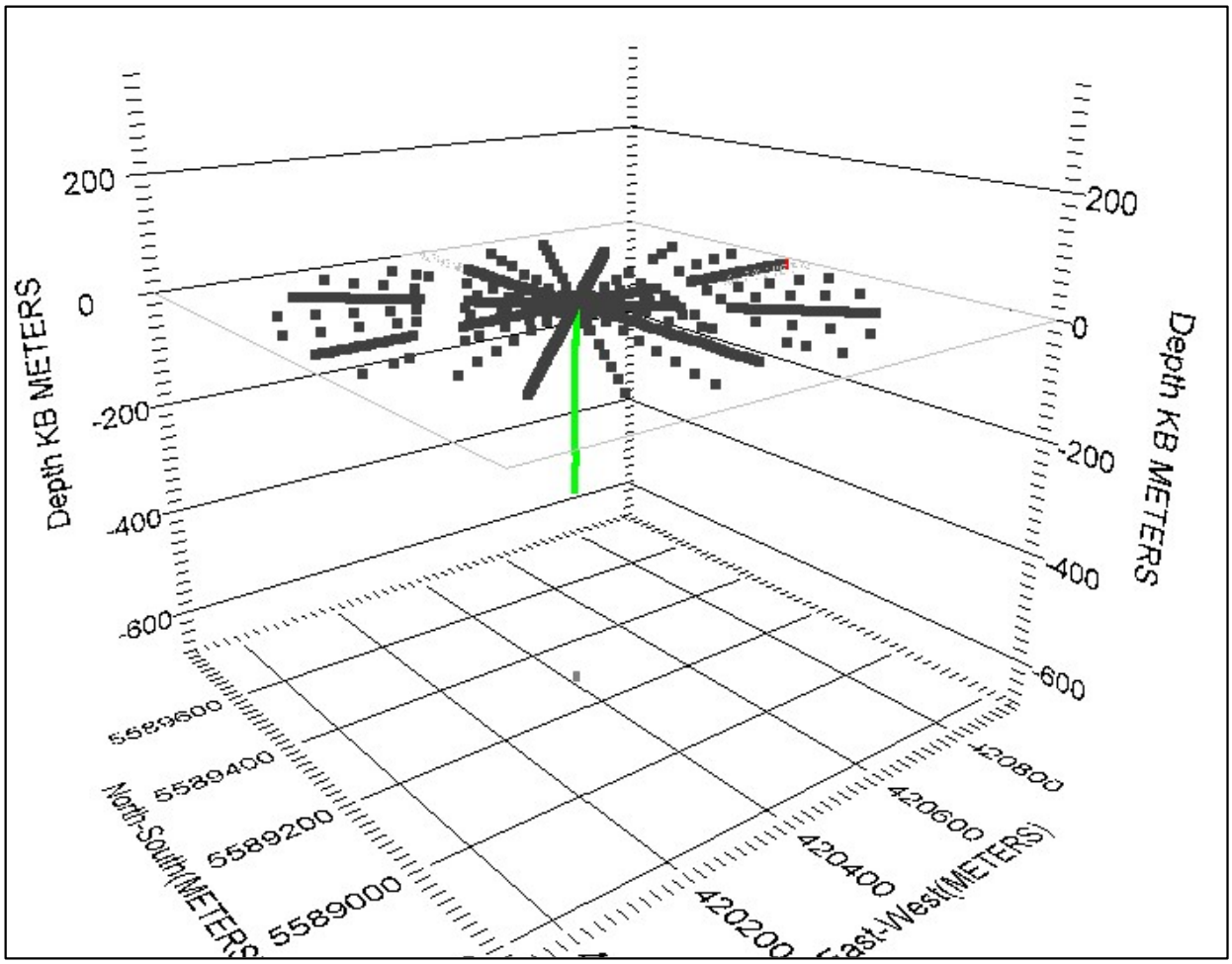

FIG 1.5: Acquisition geometry showing the arrangement of the shot lines relative to the observation well 2.

Table 1.2: Summary of data used.

Year Acquired	Seismic source	Receiver	Survey	Seismic experiment
2022	CREWES ENVROVIBE	3-Component Accelerometers	Walk-away VSP	Snowflake II

1.5 Software used

MATLAB version R2022a was used to analyse the datasets, from extracting traces and transforming them from time to frequency to estimation of phase velocities and seismic attenuation. Vista (Schlumberger) 2021 software was used to view the traces, analyse the acquisition geometry, and extract the source offsets and accelerometer location values. SeiSee software version 2.22.5 was used to visualize the traces.

Chapter 2-Theory and Methods

2.1 Introduction

The transmission of the seismic signal from the vibroseis into the earth sets the particles of the medium as well as the seismic waves into motion. The particle velocity is the speed of the particle in a medium as the seismic waves travels through it. Group velocity is the velocity at which the entire wave envelope of the seismic wave travel. It is the ratio of the change in angular frequency,w of the propagating waves to the change in their wavenumber,k .

$$v_g = \frac{\partial w}{\partial k} \quad (1)$$

Phase velocity is the velocity at which the different component of the seismic wave travels. It is defined as the ratio of the angular frequency,w of the propagating seismic wave to the wavenumber,k of the same wave.

$$v_p = \frac{w}{k} \quad (2)$$

Dispersion refers to the frequency dependence of phase velocity, while attenuation describes the decrease in seismic energy as a wave propagates through the subsurface. Aki and Richards (2002) demonstrated the interdependence of dispersion and attenuation by analysing the shape of a seismic signal traveling through an attenuating medium while neglecting dispersion. The analysis revealed that the resulting shape of the seismic signal violated the causality condition and exhibited asymmetry.

In vibroseis seismic surveys, the lower frequencies are usually sent into the earth before the higher frequencies. In a dispersive medium, the high-frequency waves propagate with a higher phase velocity than the low-frequency waves and tend to approach the lower-frequency waves as they travel (Innanen et al., 2014). Aki and Richards (2002) dispersion models of body waves predict that higher seismic frequencies propagate more quickly than lower seismic frequencies.

Thus, seismic waves of varying frequencies travel with different velocities (dispersion), which leads to frequency-dependent attenuation. This means that the seismic waves are exposed to different degrees of energy loss which depend upon their frequency content.

2.2 Methods

2.2.1 The time deviation (departure time) of a seismic wave with frequency from the sweep

The time t=0 marks the beginning of the vibroseis sweep program. A typical mathematical representation of the sweep program is expressed as:

$$S(t) = Im[a(t)e^{i\emptyset(t)}] \quad (3)$$

The amplitude function, $a(t)$ decreases as time moves away from the center of the function (exhibits a tapering effect during the early and late times) while the phase is defined as:

$$\emptyset(t) = 2\pi f(t)t \quad (4)$$

The equation shows that frequency is time-dependent, and that phase is a function of time-dependent frequency. The linear sweep can be mathematically represented as:

$$f(t) = fmin + \frac{(fmax - fmin)t}{2 \cdot T} \quad (5)$$

where $fmin$ and $fmax$ are the low and high-frequency limits, respectively, while T is the sweep length. The time, $T_s(f)$ at which the frequency f departs the vibroseis sweep is the inverse of $f(t)$.

$$T_s(f) = \frac{f-fmin}{fmax-fmin}T \quad (6)$$

2.2.2 The propagation time (arrival time) of a seismic wave of frequency f within the medium.

The time, $\Delta T(f)$ it takes the seismic signal at frequency f to travel from the source to the geophone depends on the path taken within the subsurface medium and the propagation velocity of the wave. Because of the acquisition geometry, we assume that the seismic waves travel in a straight line between the source and the receiver (straight ray path) in this study:

$$\Delta T(f)^2 = \frac{x_s^2+z_g^2}{C(f)^2} \quad (7)$$

$$T_M(f) = T_s(f) + \frac{L}{C(f)} \quad (8)$$

The dispersive phase velocity, $C(f)$ of the seismic wave can thus be calculated by the relationship:

$$C(f) = \frac{L}{T_M(f)-T_S(f)} \quad (9)$$

where L is estimated from the assumption of a straight ray path between the source location, x_s^2 and geophone depth, z_g^2.

2.2.3 Time-frequency decomposition of the vibroseis response

The uncorrelated seismic traces are in the time domain, the Gabor transform was used to transform the uncorrelated seismic traces to the time-frequency domain to estimate the travel time of the frequencies.

The Gabor transform is a mathematical transformation that yields a combined time-frequency representation of a given signal and a method to extract the signal from this time-frequency representation. The Gabor transform $G\,f(t,w)$ of a given signal $f(t)$ identifies the spectral magnitude present in the signal close to time t at frequency w as a function of two variables.

$$G\,f(t,w) = \int_{-\infty}^{\infty} f(s)g(s-t)e^{-2\pi isw}\,ds \tag{10}$$

2.2.4 Calibration of phase velocity

The wave arrival and departure times were picked with precision but were subject to a known and consistent error. To accommodate this error, calibration time, Tcal is introduced from the group velocity of the direct P wave from the near offset shot record using the correlated trace.

$$C(f) = \frac{L}{T_M(f) - T_s(f) - T(cal)} \tag{11}$$

Chapter 3-Estimation of frequency-dependent phase velocity from the VSP dataset

3.1 Summary

In this chapter, we carried out the different steps of analysis to estimate the phase velocity of seismic waves as a function of frequency. This analysis starts with identifying the seismic traces from the vertical component accelerometer and extracting the traces. These traces and the sweep were transformed using the Gabor transform and their respective arrival and departure times of the frequencies were picked.

3.1.1 The sweep

The linear sweep which is a controlled source signal emitted by the vibroseis truck has a frequency range of 2-150Hz with a sweep length of 20 seconds and a listening time of 3 seconds. The low frequencies were sent into the earth before the higher frequencies. The sweep is displayed in the time domain in Figure 3.1a. and for clarity, the first 5s of the sweep is displayed in Figure 3.1b.

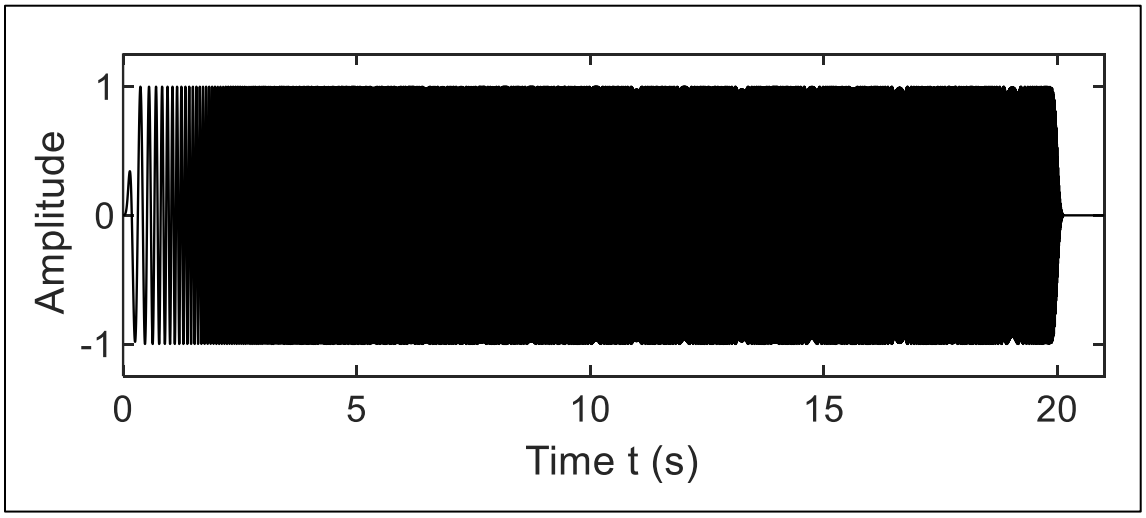

FIG 3.1a: The sweep is displayed as amplitude variation with time.

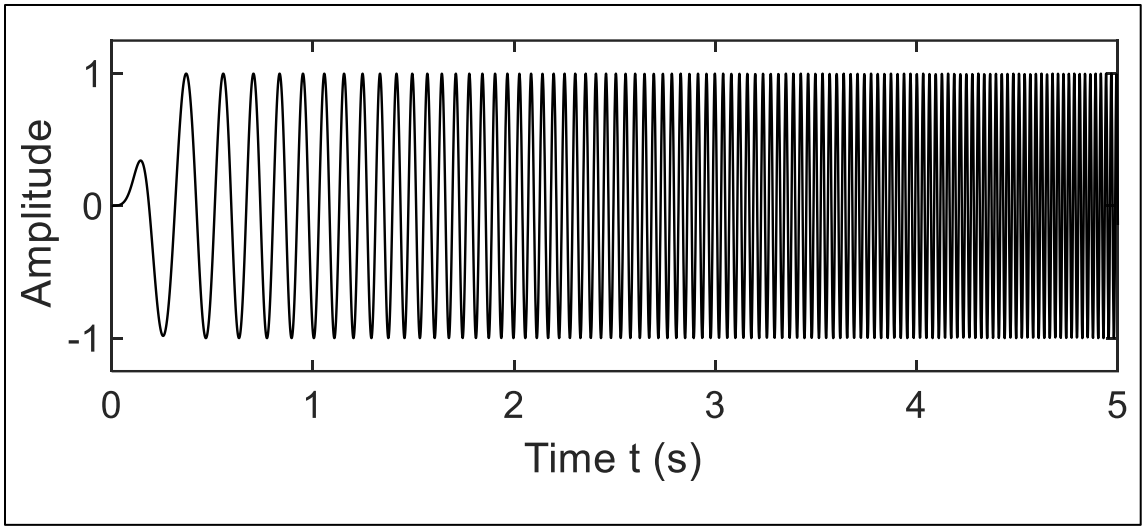

FIG 3.1b: The first 5s of the sweep.

3.1.2 Identifying vertical component in the seismic traces

The total number of traces recorded by the three component accelerometers in a shot is 705. Ignoring the first six auxiliary traces, we are left with 699 traces. The three traces 7, 8 and 9 from the first 3-component accelerometer, are seen in Figure 3.2a as an example to identify the vertical component seismic trace. We plotted the correlated seismic traces, as shown in Figure 3.2b. In Figure 3.2b, the image quality of traces from the two horizontal components is distinct from that of the vertical component. The direct P wave arrival is well imaged in the vertical component, showing little or no response of the shear wave. The shear wave is easily distinguished in both traces from the horizontal component, whereas the response of the P wave was only weakly represented.

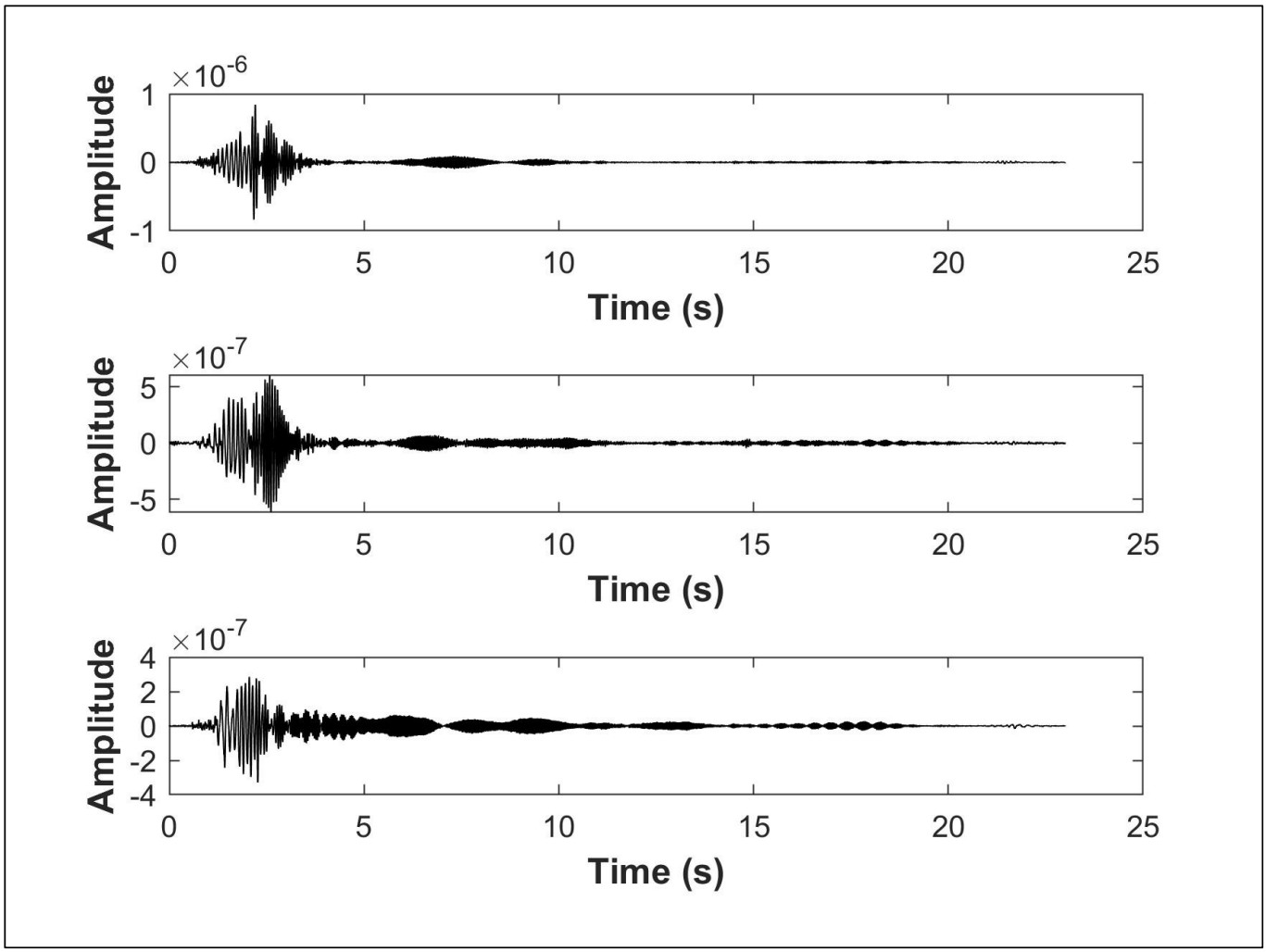

FIG 3.2a: Uncorrelated seismic traces from one 3-component accelerometer.

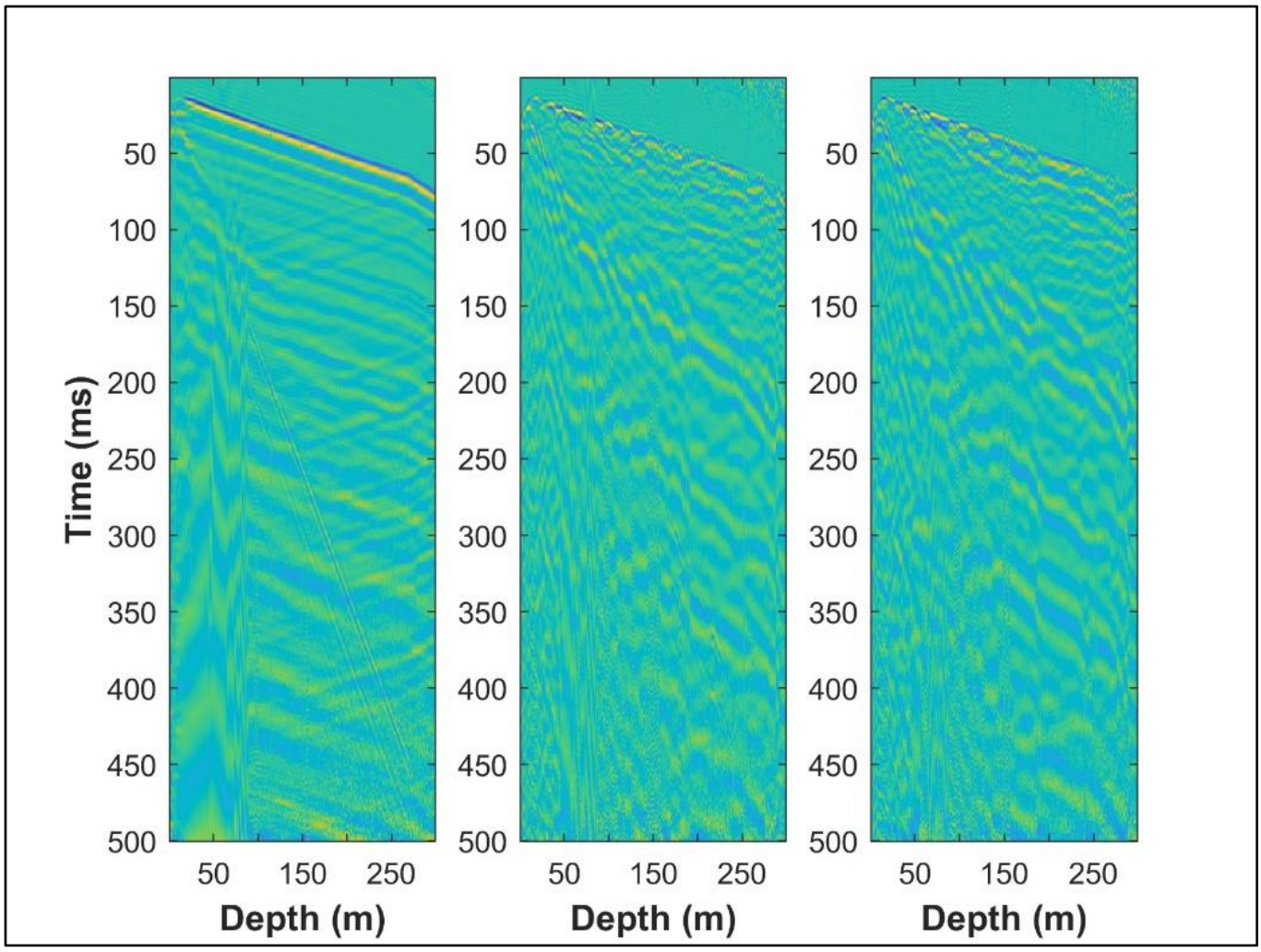

FIG 3.2b: Plots of the correlated seismic traces for identifying the vertical component.

3.1.3 Extracted vertical component traces

A total of 24 seismic traces were analysed for a shot. These traces were 30 traces apart, which is equivalent to 10m apart for depths between 0 and 140m and 20m apart for depths between 140 m and 324 m.

3.1.4 Transform of the sweep and seismic traces

The method used in estimating the phase velocities in this research requires the arrival and departure time of the signal corresponding to particular frequencies. To achieve this, we need to transform the seismic traces and the sweep from the time to the time-frequency domain

using the Gabor transform. The Gabor spectrum of a seismic trace is displayed in Figure 3.3 with different events labelled, but the event we are interested in is the event labelled vibroseis sweep.

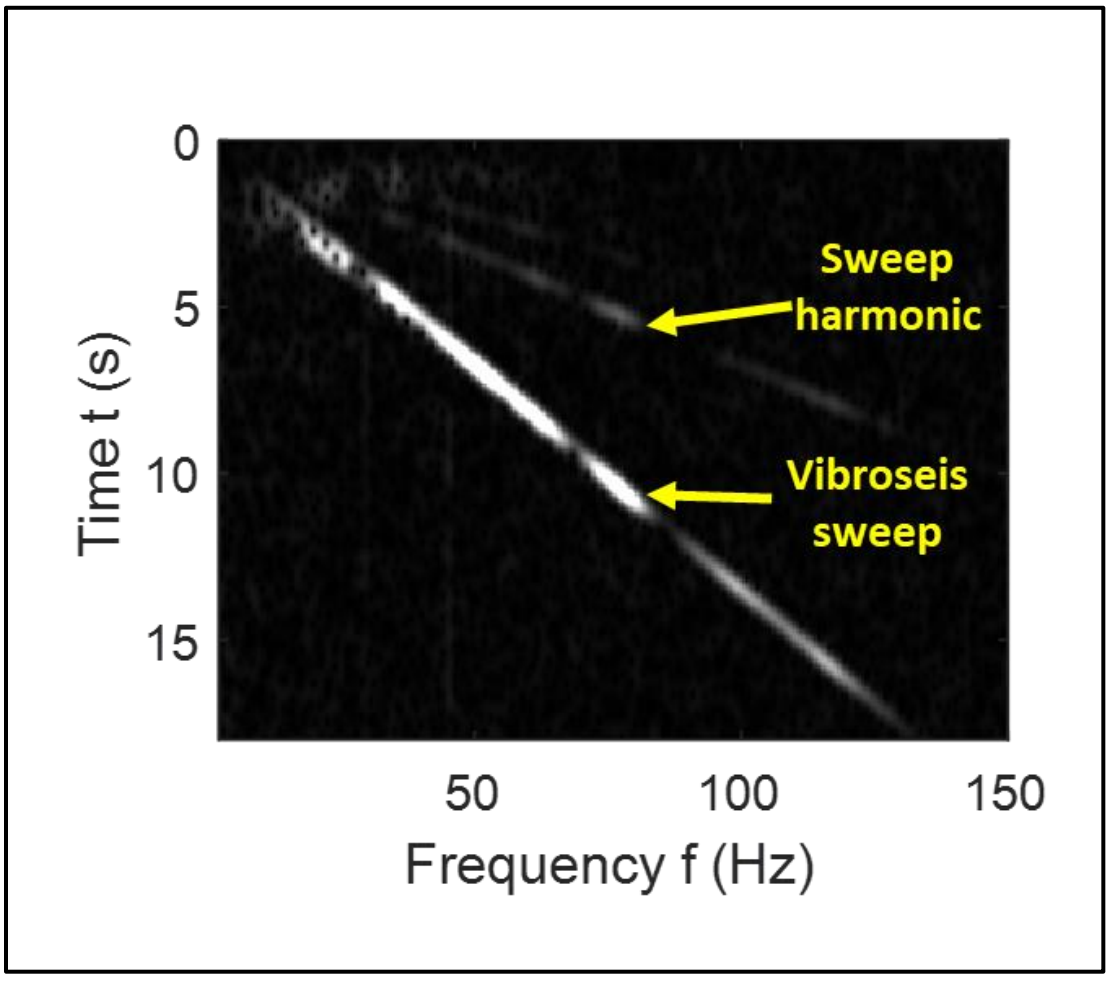

FIG 3.3: Gabor spectrum of an uncorrelated seismic trace showing different events

3.2 Picking the Times

Picking the departure time, which is the time it takes a certain frequency to depart from the source, and the arrival time, which is the time it takes for the same frequency to arrive at the accelerometer is important for this analysis.

3.2.1 Departure and Arrival Times

The arrival and departure times used in estimating the phase velocities were automatically picked using the Modified Energy Ratio (MER) code written by Wong (CREWES report, 2023). The times could be manually picked using the ginput function on MATLAB, but considering the volume of data to be analysed, to efficiently maximize time and energy, the MER code was used.

The automatic picking technique generates signal-to-noise ratio (SNR) estimates at the specified times. The modified energy ratios (MER) approach works well when SNRs are high, but for low SNRs, the selected times frequently exhibit random changes and significant outliers. These outliers deviate from a smooth curve on the frequency axis. Outliers were removed by eliminating selected times with SNRs below a predetermined decibel threshold. A nonlinear continuous non-negative function specified by a minimal number of parameters can then be used to smoothly fit the remaining selected times and fill in the gaps left by the deleted outliers. Using MATLAB's nlinfit utility function with this fitting function optimizes the fitting parameters in a least-squares manner.

The Modified Energy Ratio (MER) for a digitized seismic trace sampled at intervals of Δt is defined as a cube of the absolute product of the energy ratio at a test point (i) and the seismic trace at a test point(i).

$$MER = abs[er(i) * grm(i)]^3 \quad (12)$$

The energy ratio at a test point (i) is the ratio of the sum of the squares of the seismic trace over two different equally spaced windows centred at i, as shown in Figure 3.4

$$er(i) = \sum_{i}^{i+L} grm(j)^2 \,/\, \sum_{i-L}^{i} grm(j)^2 \qquad (13)$$

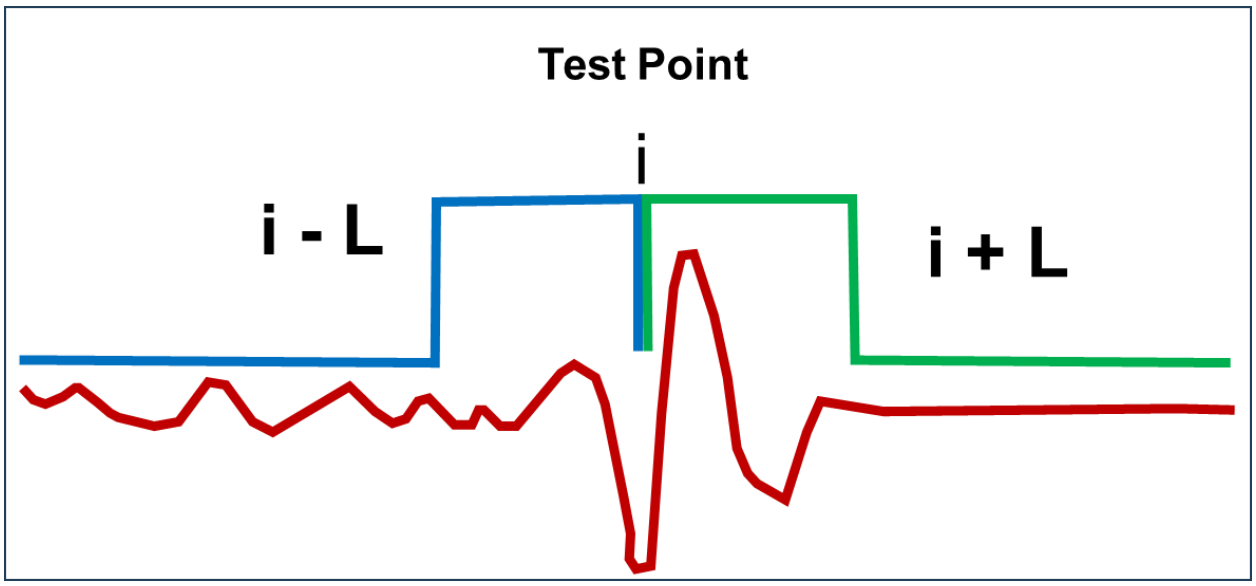

FIG 3.4: Modified Energy Ratio (MER) for a digitized seismic trace sampled with variation with time, Δt (Wong,2023).

The departure times were determined using the Gabor transform of the linear sweep as displayed in Figure 3.5a. The frequencies vary linearly with time, as intended because the frequencies were transmitted into the earth with increasing time and increasing frequencies.

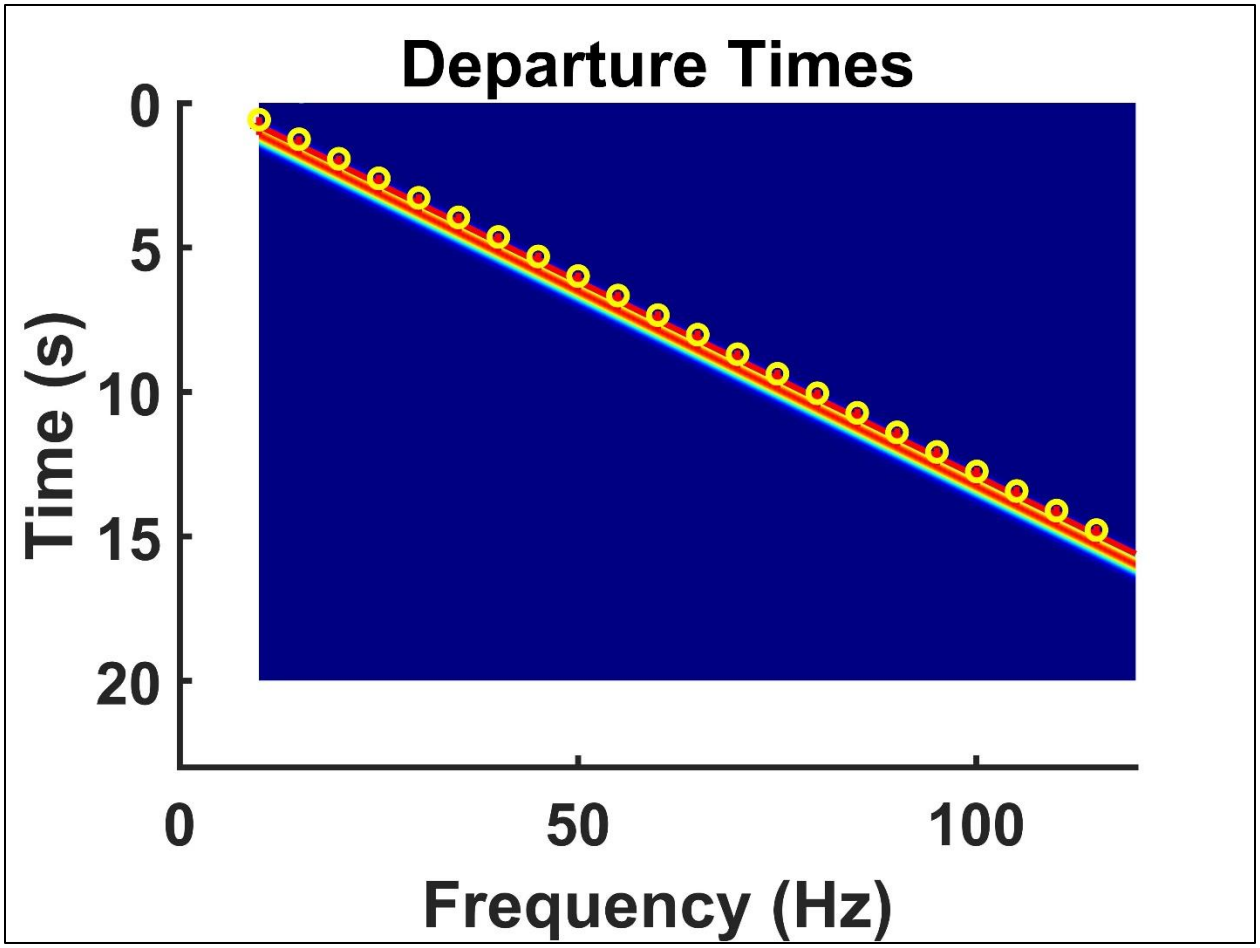

FIG 3.5a: Gabor transform of the sweep for picking departure times of the frequencies.

The arrival times were picked using the Gabor transform of the uncorrelated seismic traces as displayed in Figure 3.5b. At frequencies between 20-120Hz, the frequencies vary linearly with time, but at lower frequencies between 2-20 Hz, the relationship between time and frequency is non-linear. This can be attributed to dispersion.

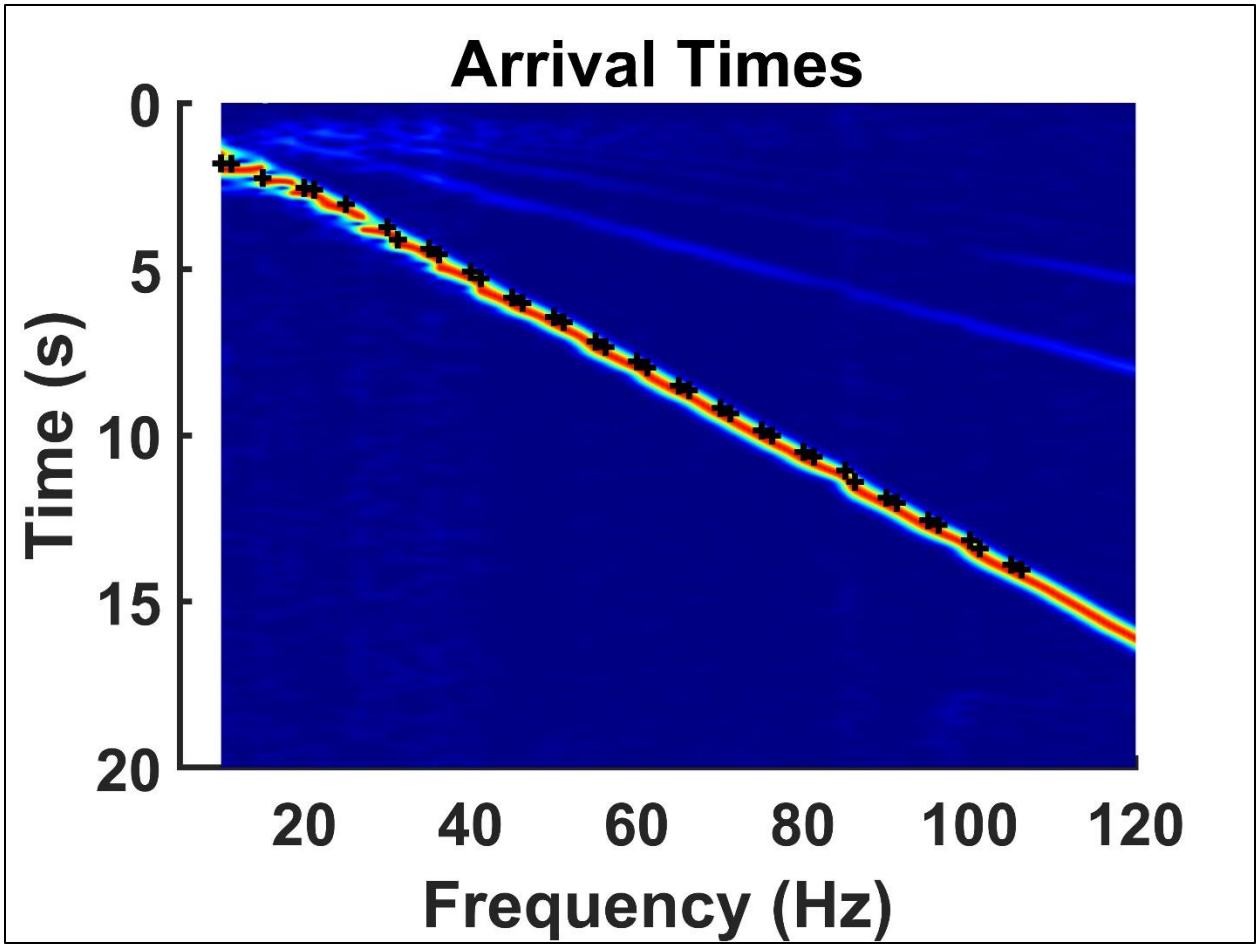

FIG 3.5b: Gabor transform of the uncorrelated seismic trace for picking arrival times of the frequencies.

3.2.2 Travel time

The method utilized in this research leverages the travel time interplay between the higher frequencies that were the last to be transmitted into the earth and the lower frequencies that were transmitted earlier.

The travel time or the propagation time of each frequency is the difference between the time it takes a frequency to arrive at the accelerometer to be measured and the time it takes the same frequency to depart from the source. In Figure 3.6a, the arrival and departure times plot for an

uncorrelated seismic trace at a depth of 100m for a source offset 250m on line 2 is displayed and in Figure 3.6b, its travel time plot is displayed.

On the arrival and departure time plot, we observed that the departure and arrival times are parallel from frequencies between 22- 100Hz, and at frequencies 2-22Hz, there is a clear deviation from the parallel, this is again attributed to dispersion.

On the travel time plot, we could see that lower frequencies have higher travel times while the higher frequencies affirm that they travel faster, hence the lower travel times. This supports the dispersion model of Aki & Richards 2002 which stipulates those higher frequencies travel faster than lower frequencies in dispersive environments.

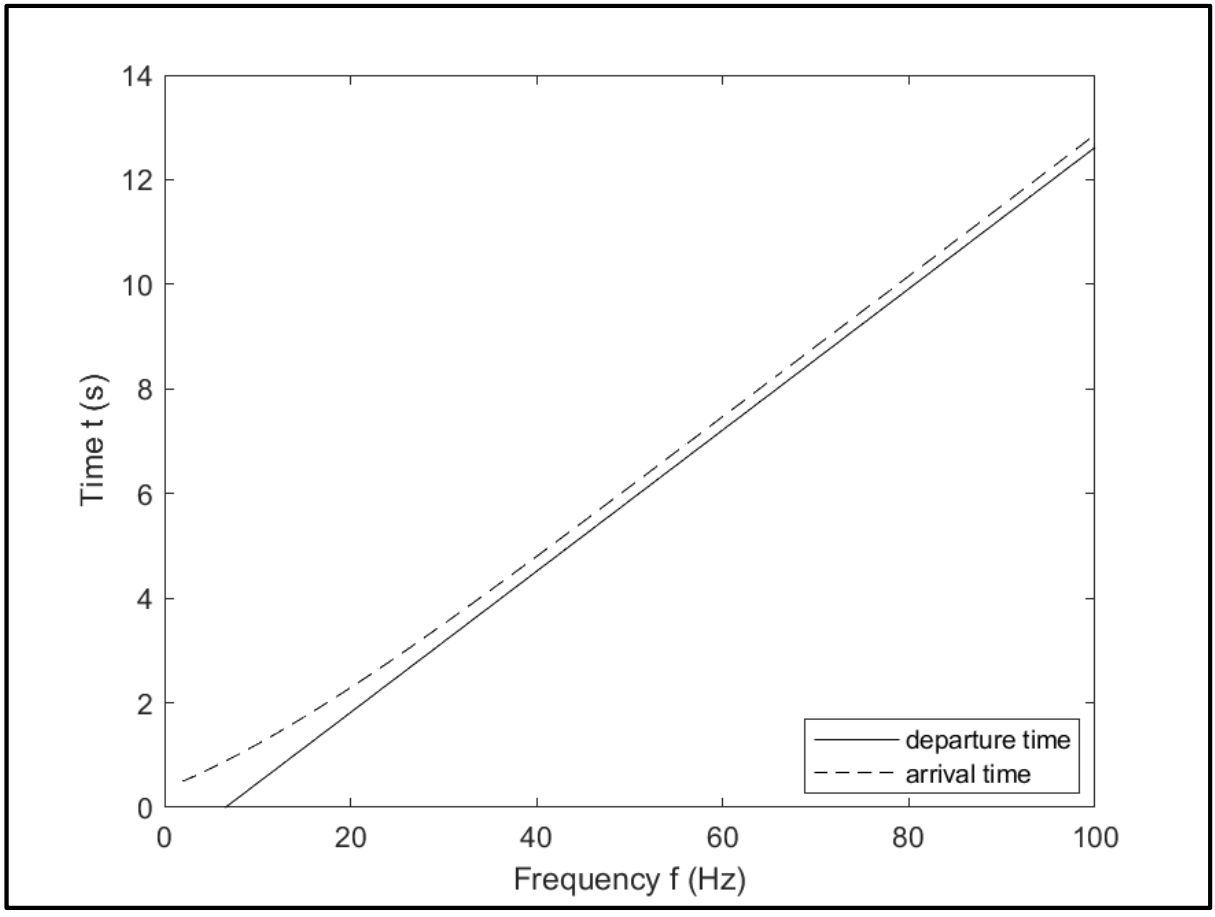

FIG 3.6a: The departure and arrival times plot of the frequencies.

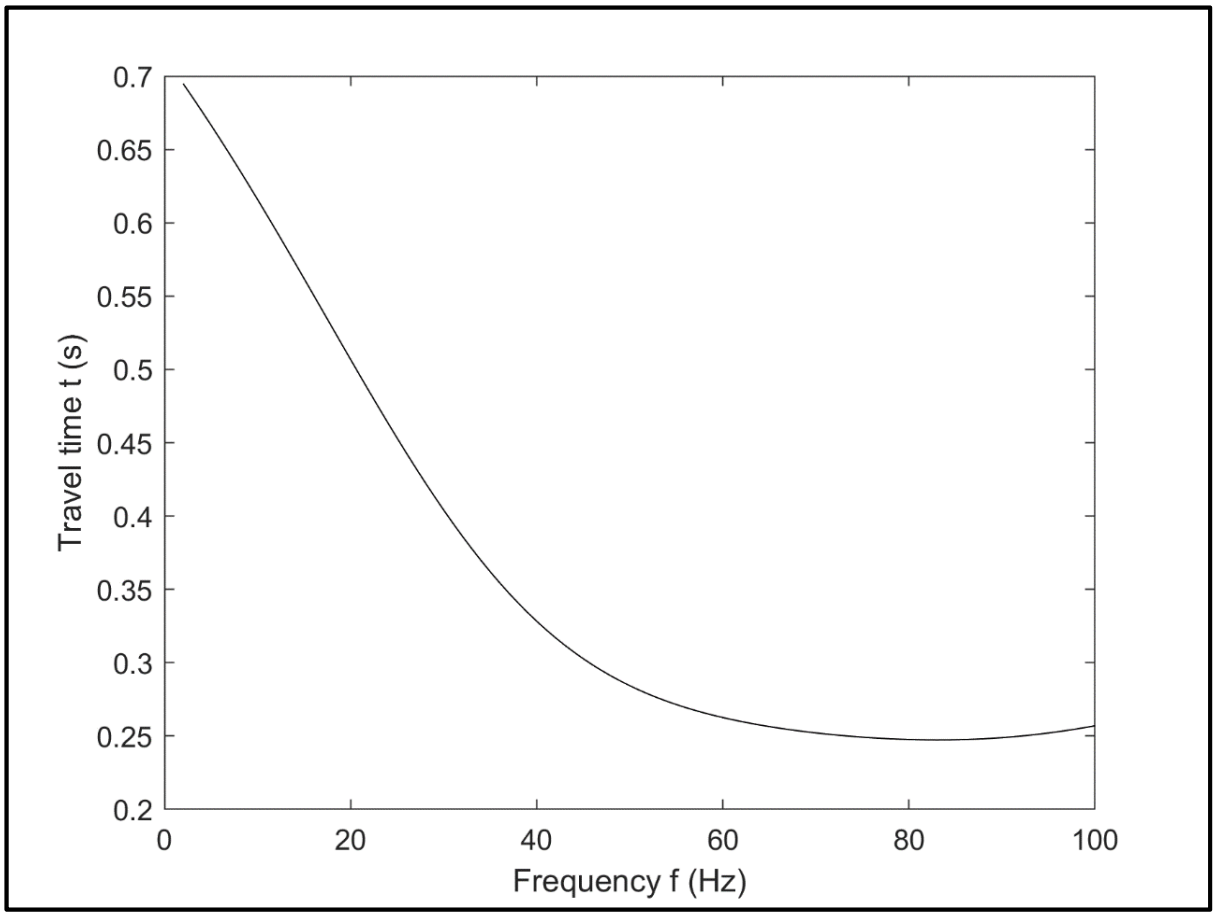

FIG 3.6b: The travel time plot of the frequencies.

3.3 Frequency-dependent phase velocity estimation

This is the velocity at which the phase of any single frequency component of the wave travels. Simply put, this is the ratio of the propagation distance of the direct P-wave arrival to the travel time of each frequency component. As mentioned before, the propagation distance can be estimated from the square root of the sum of the squares of the source offset and the depth of the accelerometer we are analysing.

Analysing the travel times of the frequencies for source offset 250m on line 2, the seismic traces evaluated are 30 traces apart (looking at it from the 3-component accelerometers perspective), which means the depth interval is 10m for accelerometers 1m apart and 20m for

accelerometers that are 2m apart. The phase velocity estimated at the different depths as it varies with frequency for this source offset is displayed in Figure 3.7.

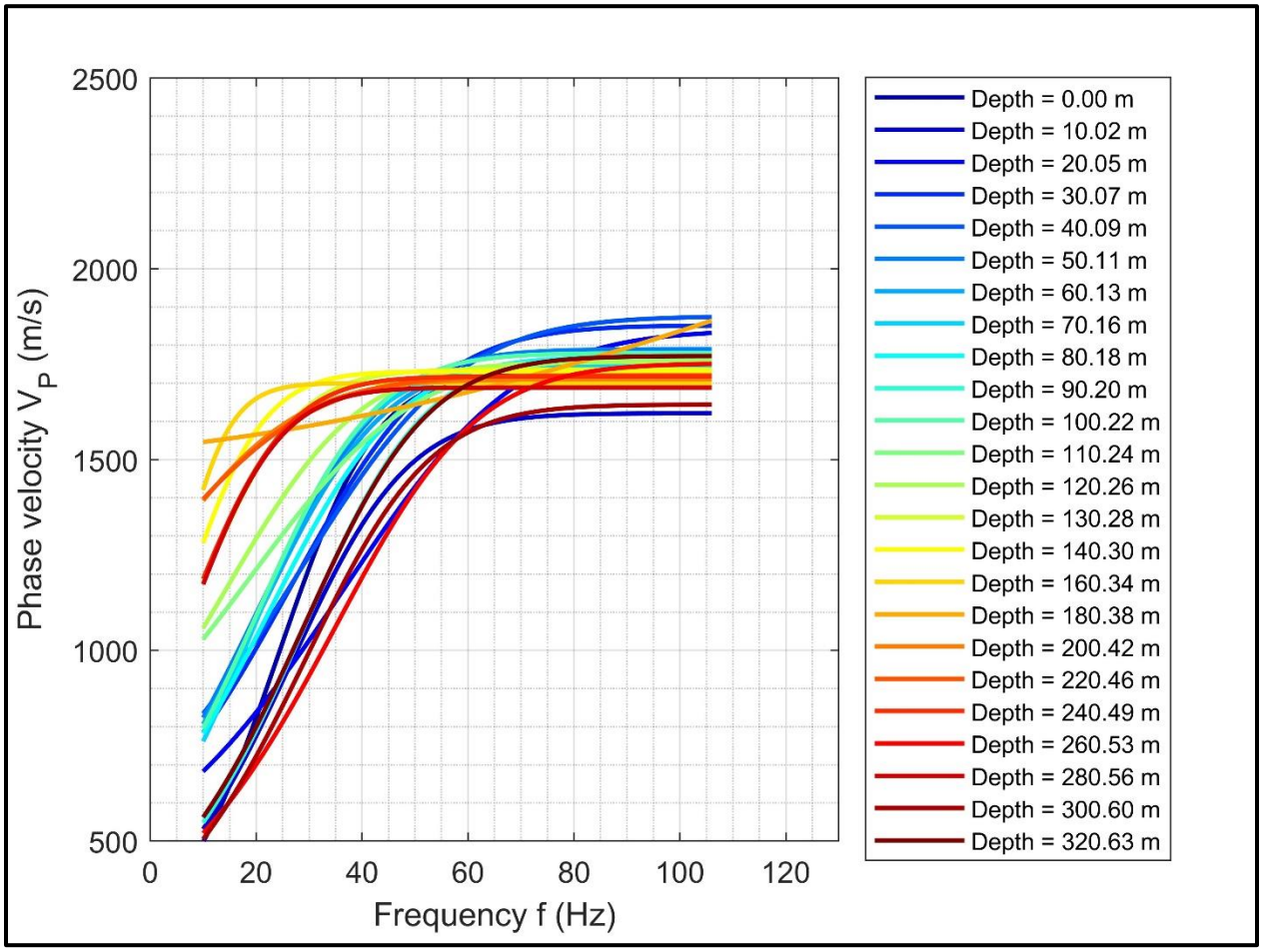

FIG 3.7: The phase velocity at different depths for source offset 250m at line 2.

3.3.1 Calibration of Phase Velocity

The phase velocity values we got from section 3.3 are called uncalibrated phase velocity. We compared the group velocity with the velocity of the direct p-wave arrival in Figure 3.8 and found that there is a discrepancy. The picking of the arrival and departure times was carried out with high accuracy, but the times were subject to a constant error. To account for this error, a constant time Tcal is applied to the phase velocities to give the calibrated phase velocity. The Tcal is estimated from the velocity of the direct p-wave arrival with equations 13.

$$U_{grp} = \frac{L}{V_{grp}} \quad (14)$$

$$T_{cal} = \Delta T - U_{grp} \quad (15)$$

Where U_{grp} is the travel time, V_{grp} is the velocity and L is the propagation distance of the P-wave. T_{cal} is the calibration time. Figure 3.9 displays the calibrated phase velocities estimated from seismic traces for source offset.

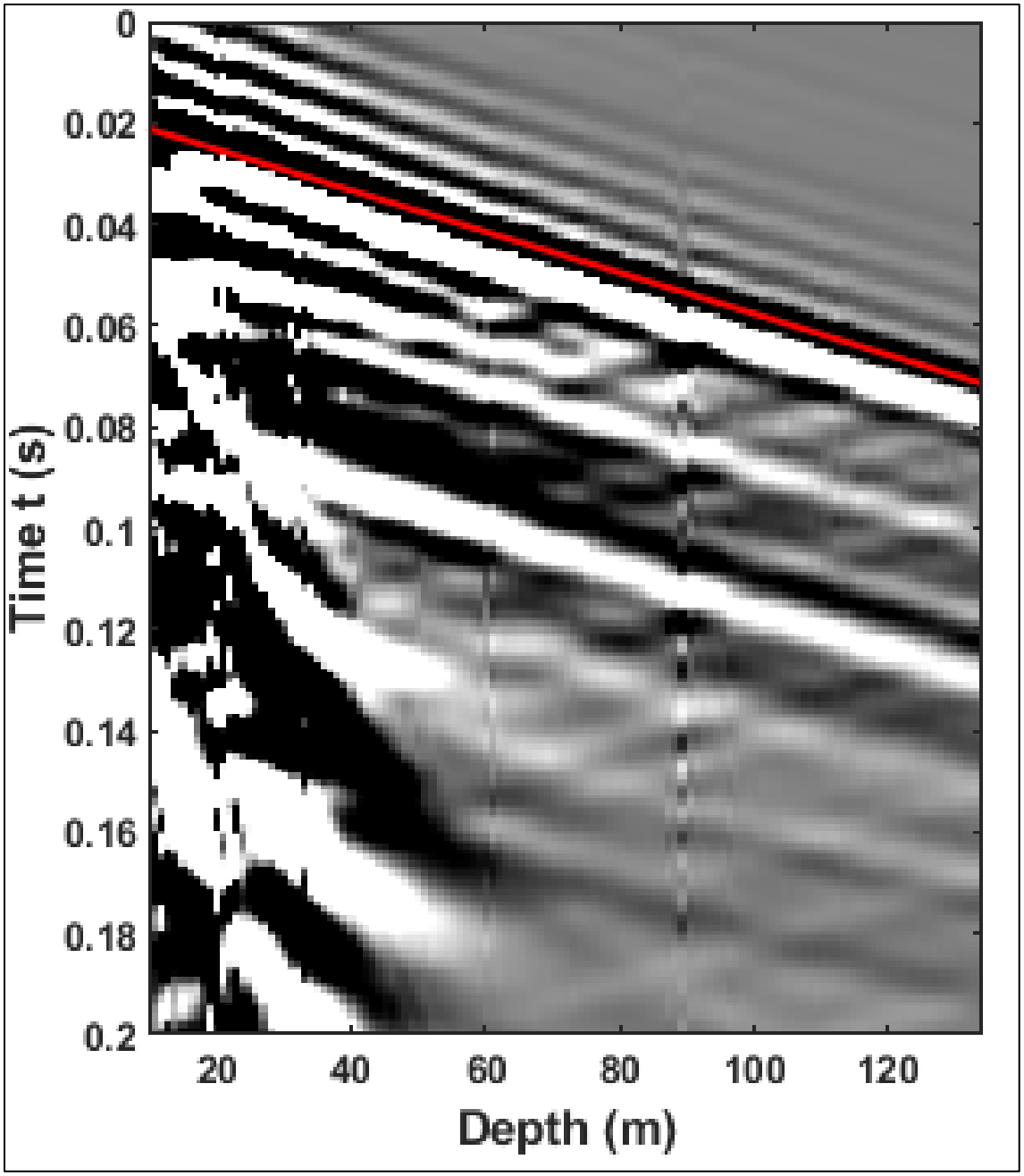

FIG 3.8: The group velocity of the direct P-wave estimated from the slope.

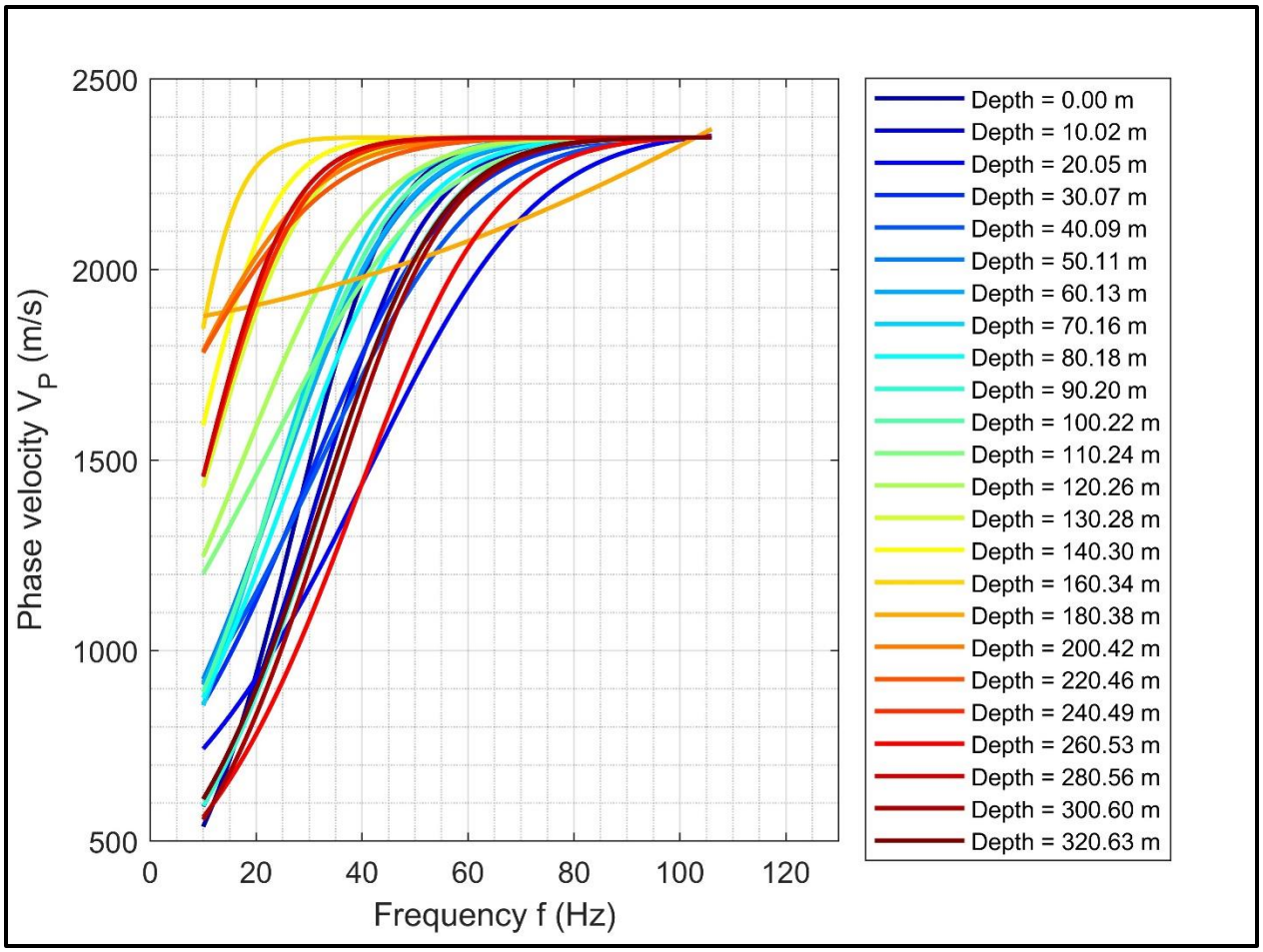

FIG 3.9: Calibrated phase velocity after applying Tcal to the uncalibrated phase velocity.

3.4 Phase velocity maps

The phase velocity was estimated for every source point on line 1, we observe the variation of phase velocity with frequency. In Figure 3.10, are the phase velocity plots at frequencies 10, 20, 40 and 80 Hz while the offsets remain unchanged in all cases. It is important to note that although there is variation in the phase velocity at these frequencies, at a depth of around 300m, there is a consistent record of low phase velocity which is attributed to the CO2 plume.

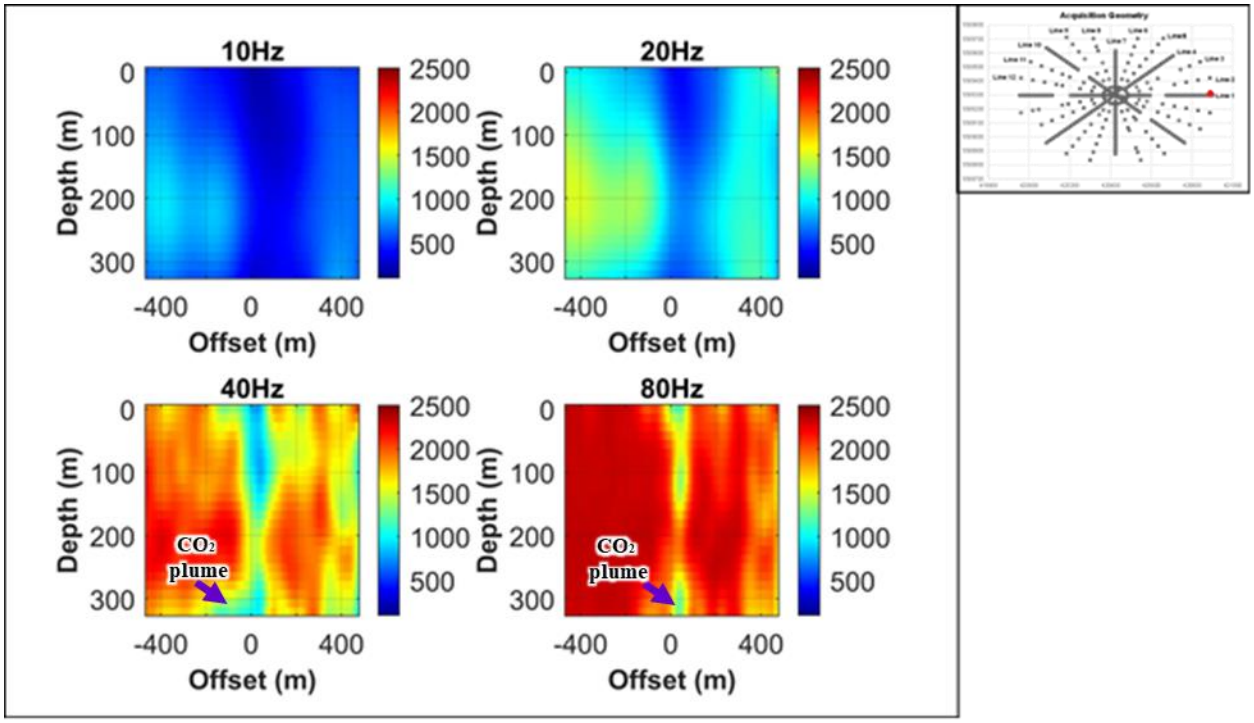

FIG 3.10: Phase velocity plots at frequencies 10, 20, 40 and 80 Hz along line 1.

This analysis was carried out for all twelve shot lines, the maps of phase velocity at frequencies 10,20,40 and 80Hz for all shot lines are displayed in Figure 3.11. We observed that phase velocity not only varies with frequency, but it also changes with the VSP azimuth, that is, it changes with the direction of wave propagation. It is also important to note a low phase velocity is recorded at a depth of around 300m in all the different source lines, for all frequencies analysed.

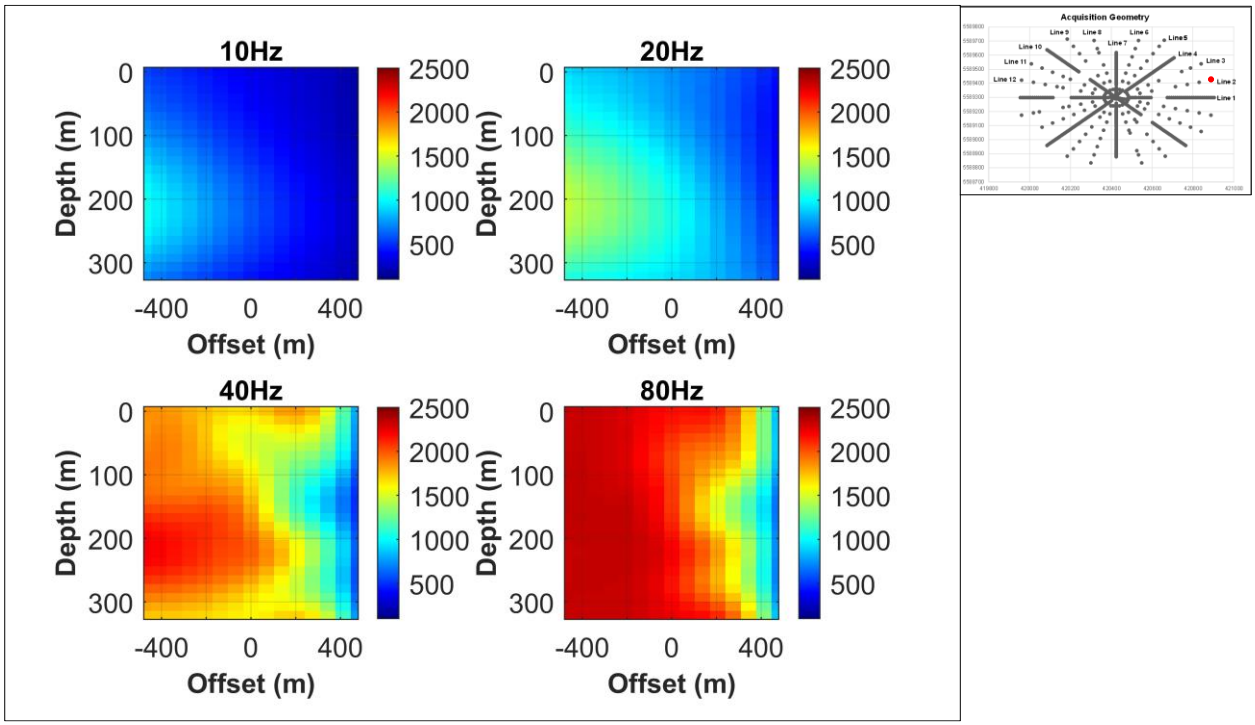

FIG 3.11a: Phase velocity plots along Line 2.

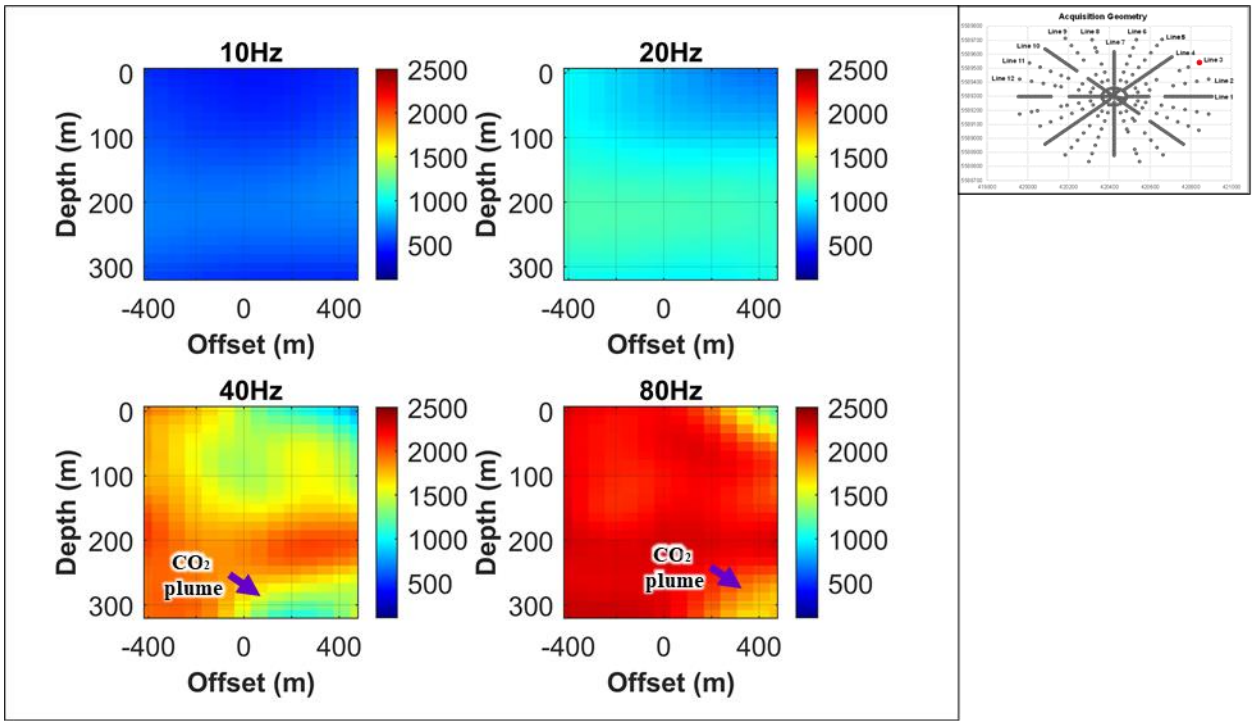

FIG 3.11b: Phase velocity plots along Line 3.

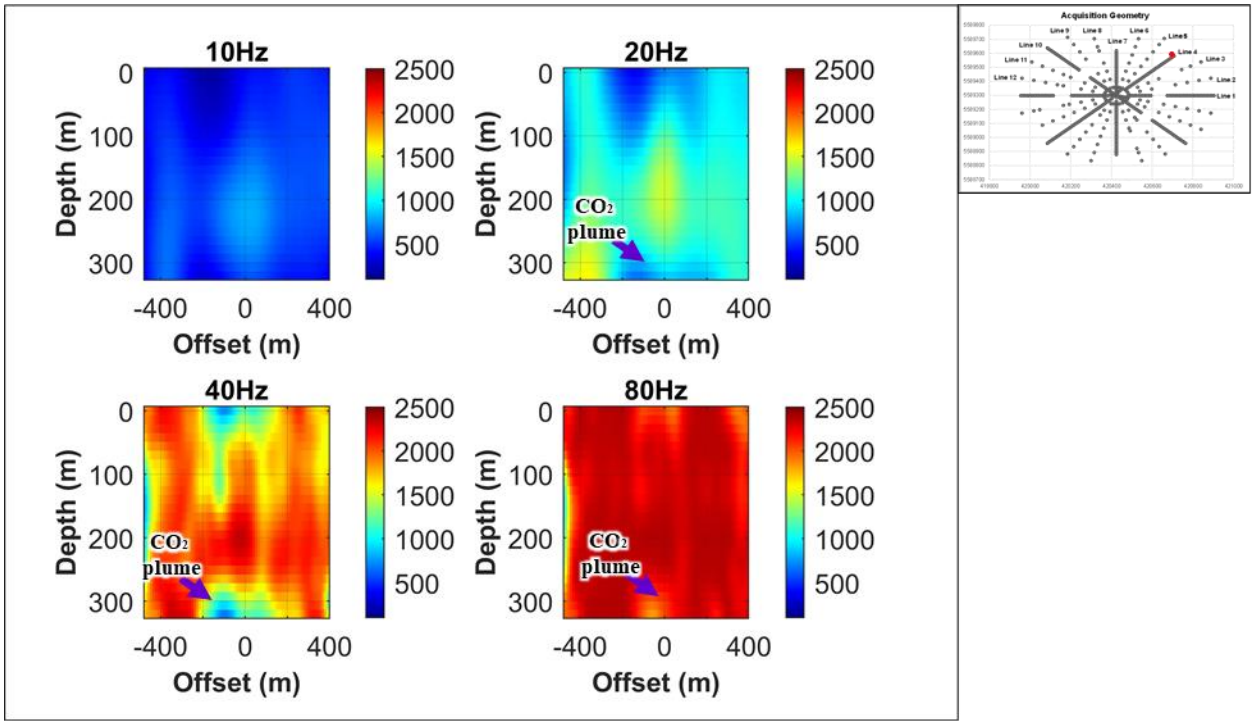

FIG 3.11c: Phase velocity plots along Line 4.

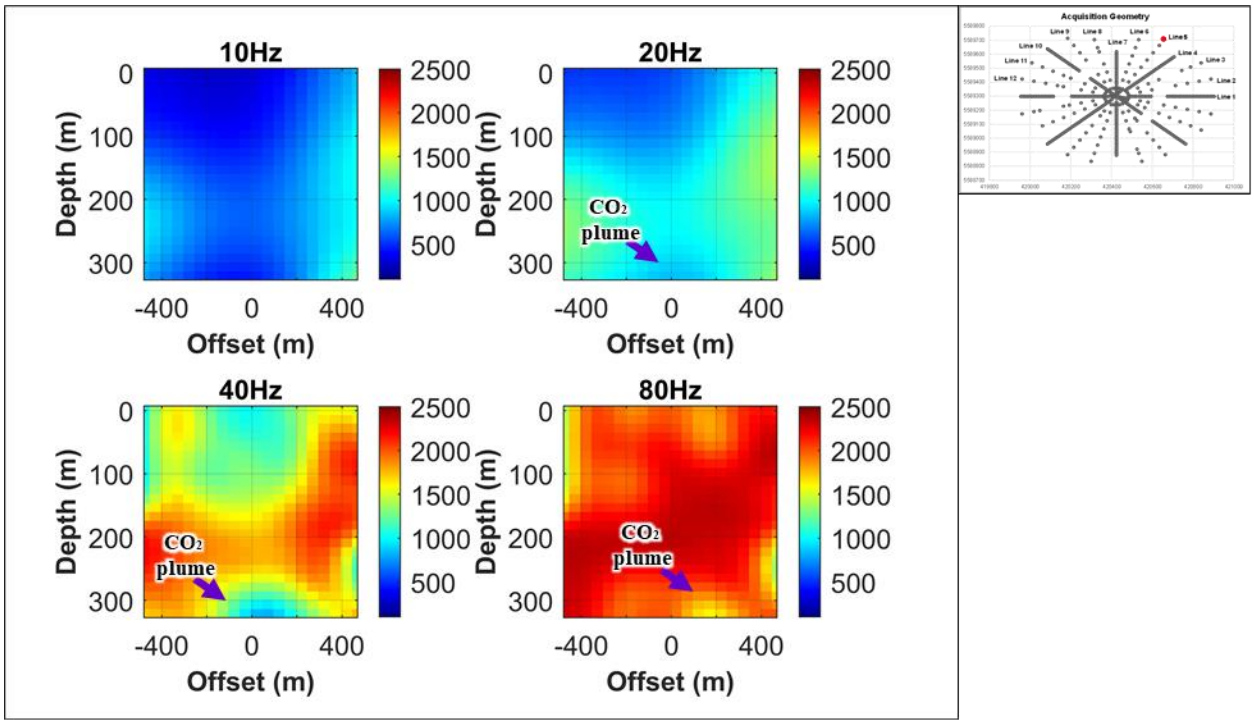

FIG 3.11d: Phase velocity plots along Line 5.

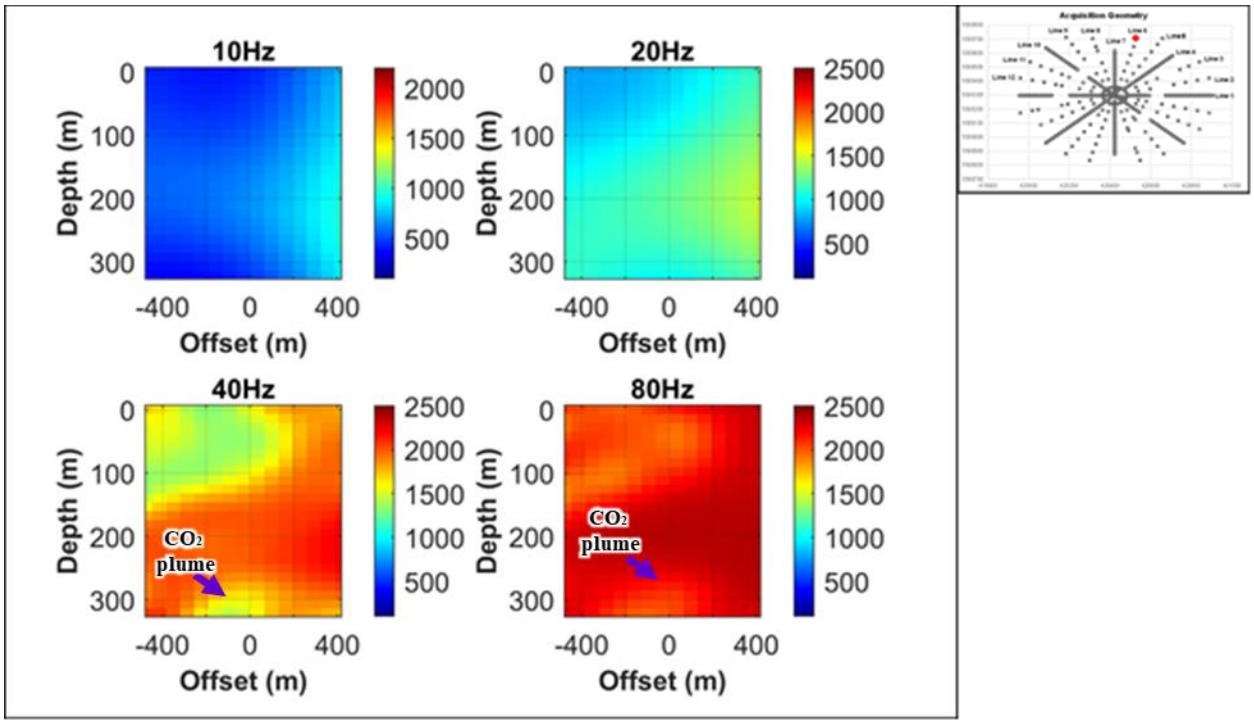

FIG 3.11e: Phase velocity plots along Line 6.

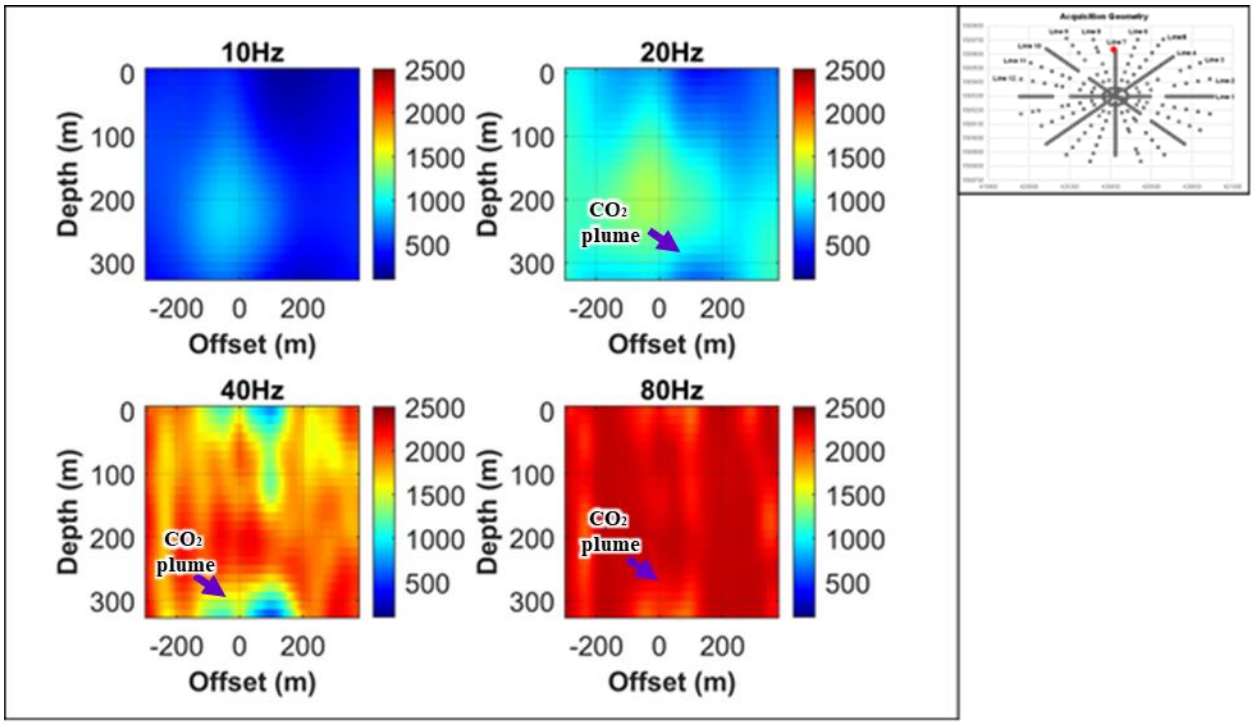

FIG 3.11f: Phase velocity plots along Line 7.

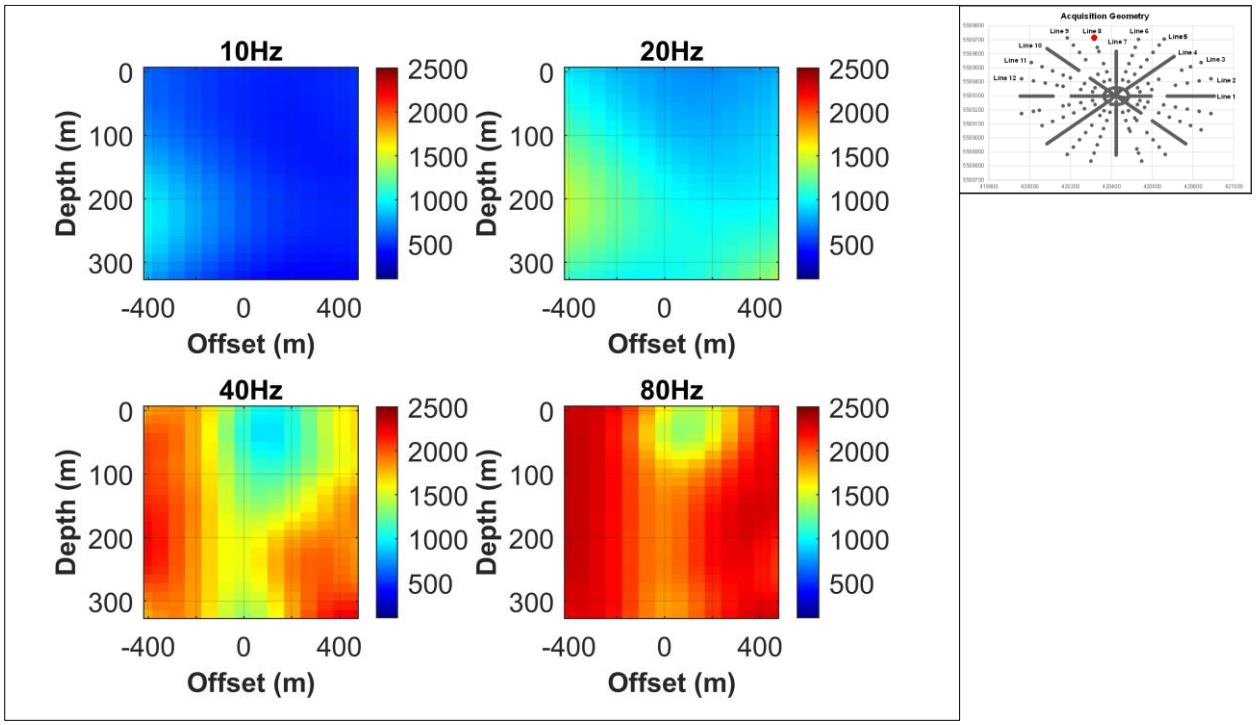

FIG 3.11g: Phase velocity plots along Line 8.

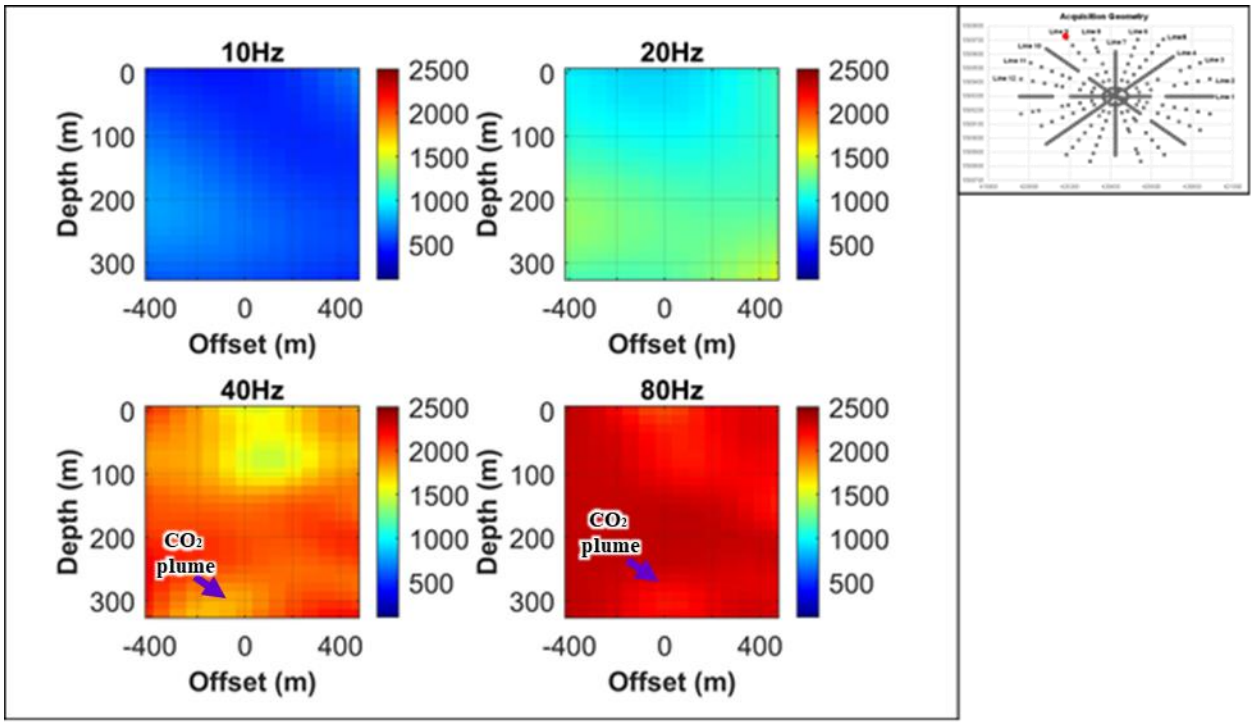

FIG 3.11h: Phase velocity plots along Line 9.

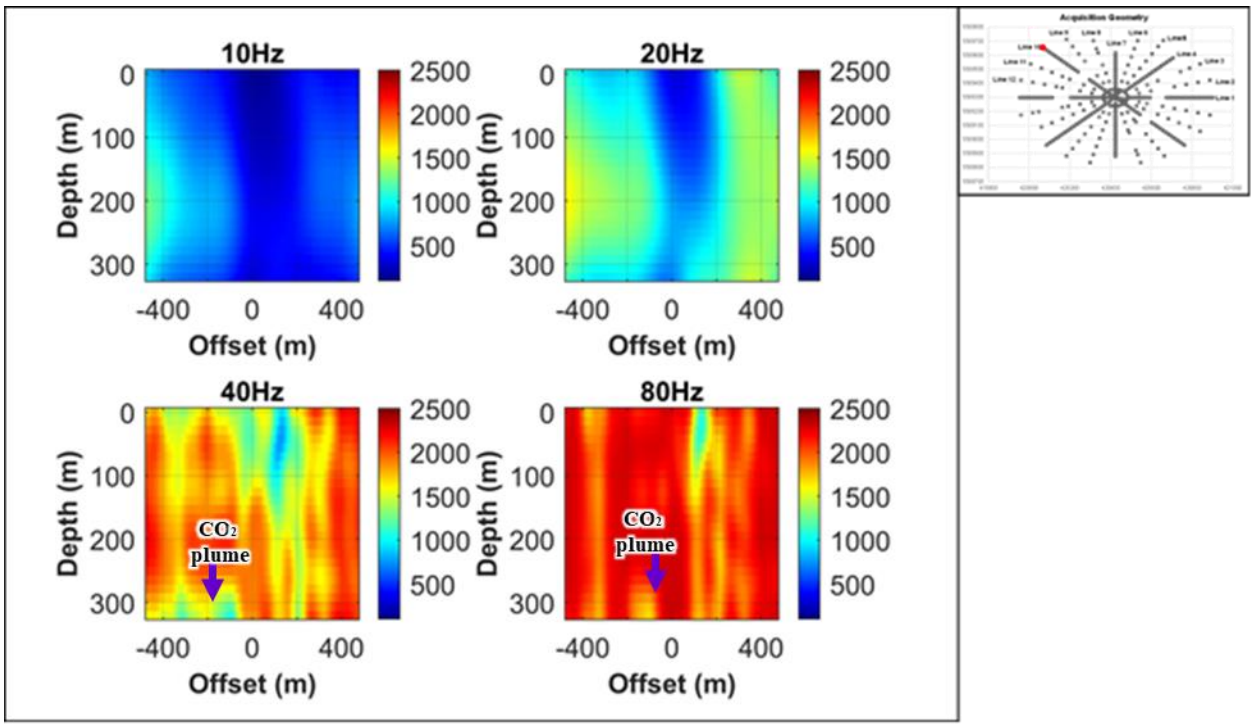

FIG 3.11i: Phase velocity plots along Line 10.

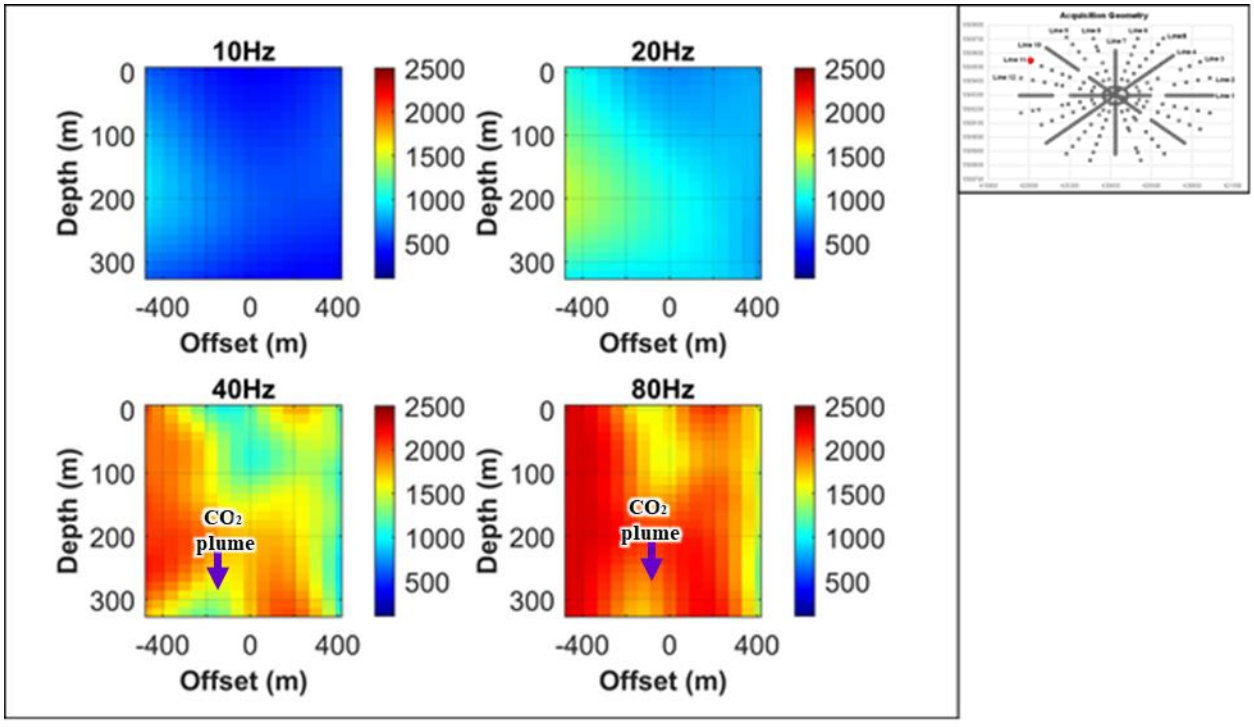

FIG 3.11j: Phase velocity plots along Line 11.

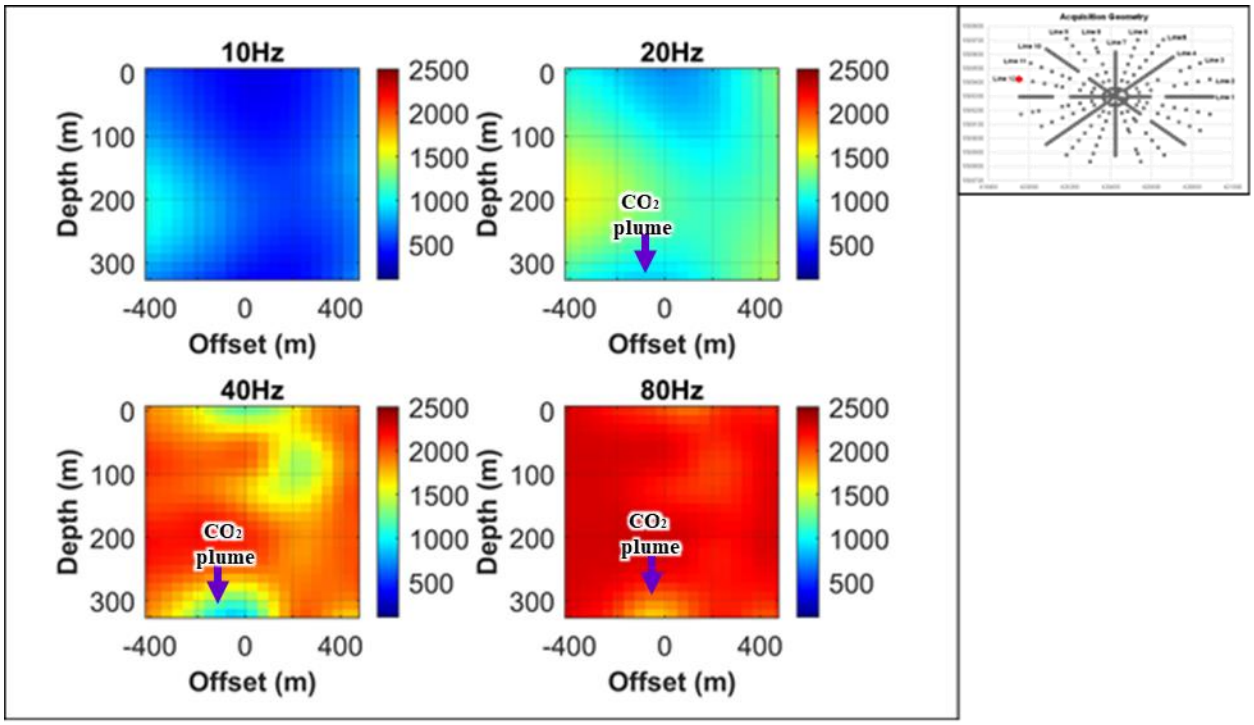

FIG 3.11k: Phase velocity plots along Line 12.

Chapter 4: Estimation of Seismic attenuation

4.1 Summary

Estimation of frequency-dependent phase velocity is a preliminary step in estimating seismic attenuation. In this chapter, we effectively used the phase velocity estimated from all the uncorrelated seismic traces. We found that the Kolsky model helps us understand the relationship between phase velocity and frequency. This helped predict phase velocities and quality factors Q.

4.2 Seismic attenuation

Seismic attenuation is a gradual decrease in seismic energy as the seismic waves propagate through the subsurface. From Aki and Richards 2002, we understand that in a dispersive medium, seismic waves of varying frequency travel with different velocities leading to frequency-dependent attenuation, which means that seismic waves of varying frequency are exposed to diverse levels of energy loss.

4.3 Quality factor

The rock quality factor Q, also referred to as the attenuation factor, is a unitless quality that is used to measure attenuation. Q is thought to be connected to the rock's physical condition. Q is inversely proportional to seismic attenuation (wiki.seg.org).

$$\propto = 1/Q \qquad 16$$

4.4 Kolsky- Futterman dispersion model

The Kolsky-Futterman model helps to understand the relationship between phase velocity and frequency. The Kolsky-Futterman model assumes that the seismic attenuation ($\propto$) is linear with

frequency over some range. It describes the non-linear relationship between phase velocity and frequency as:

$$\frac{1}{C_w} = \frac{1}{C_r}\left(1 - \frac{1}{\pi Q_r}\ln\left|\frac{w}{w_r}\right|\right) \quad 17$$

$$w_r = 2\pi f_r \quad 18$$

$$w = 2\pi f \quad 19$$

where C_w is the frequency-dependent phase velocity, C_r and Q_r are the reference phase velocity and Quality factor at the reference frequency w_r.

4.5 Reference Frequency

It is evident from Equation 17 that the value of Q_r we are estimating is highly dependent on the reference frequency chosen. Phase velocity,C_w is the observed data (estimated from the uncorrelated seismic traces), w is also known from the frequency content of the data from the chosen reference frequency, f_r we can choose the reference velocity C_r.

The linearized form of the Kolsky-Futterman dispersion model is:

$$y = M_0 + M_1 X \quad 20$$

Where y is the dependent variable, M is the model parameter and X is the input parameter. The Mean squared error cost function approach was used in formulating the objective function, $\emptyset$ and it is defined as

$$\emptyset = \frac{1}{m}\sum_{i=1}^{m}\left(p^{(i)} - y^{(i)}\right)^2 \quad 21$$

Where m is the number of data points, p is the predicted phase velocity and y is the observed phase velocity. The model parameter, M was updated using the Gradient descent optimization tool in equation 23.

$$M_{k+1} = M_K + h_k \left(\frac{\partial \emptyset}{\partial M}\right)_k \quad 23$$

k is the iteration number with 2000 being the maximum.

M is the model parameter, h is –0.01 (learning rate) and the regression line for the predicted phase velocity is:

$$p = X \cdot M \quad 24$$

Using the linearized Kolsky-Futterman dispersion model, we tested various frequencies to determine the reference frequency where the model produces predicted phase velocity that fits the observed phase velocity while yielding a realistic Q value. It was observed that a reference frequency of 80 Hz, or frequencies near this value, results in realistic Q values. In contrast, lower reference frequencies yield unrealistic Q values (see appendix).

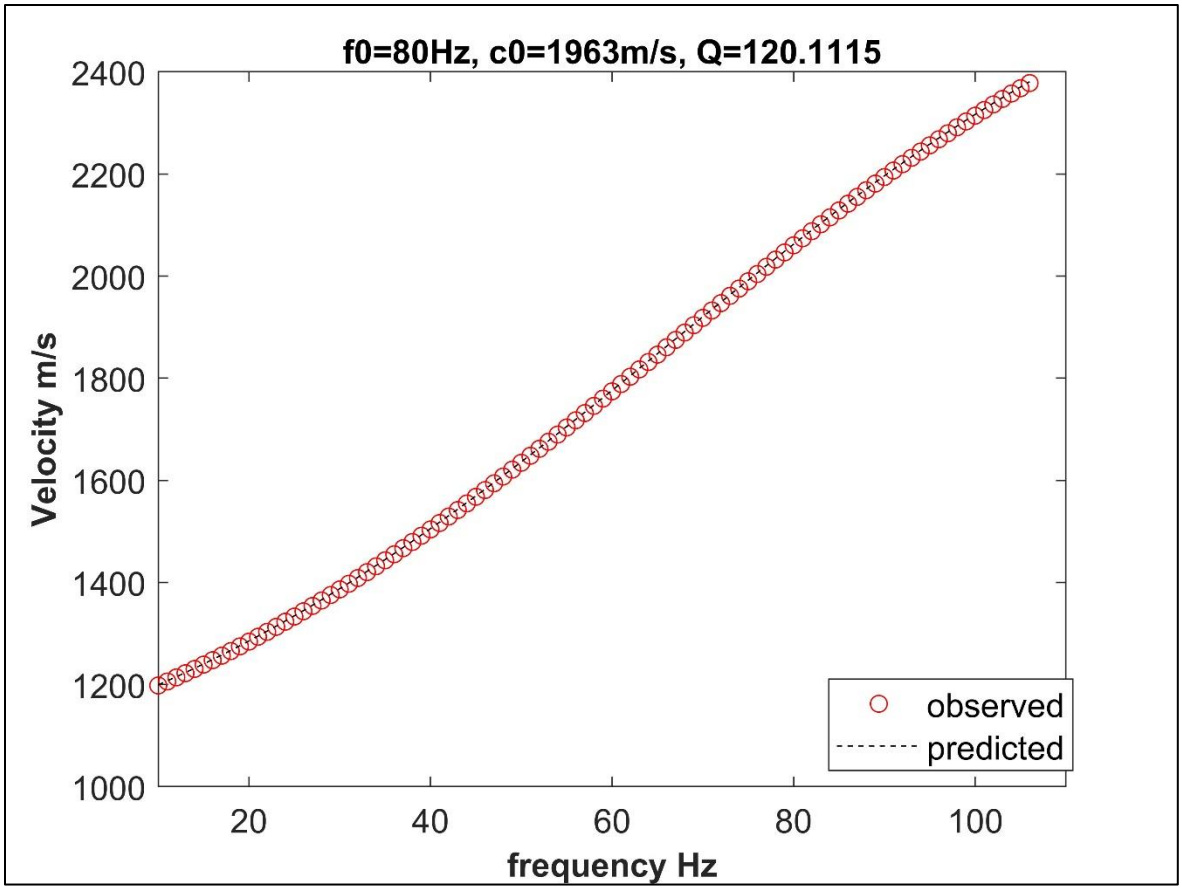

FIG 4.1: Estimating Q at a depth of 300m, Line 3 at 480m offset using a reference frequency of 80Hz and reference phase velocity of 1963m/s.

These Q values at reference frequency, 80Hz and reference phase velocities 1963m/s fall within the range of Q values from the published work of Wang and Lawton (2024), where they measured time-lapse variation in seismic attenuation from distributed acoustic sensing VSP data from the Newell County facility using the time-variant amplitude spectra approach.

The estimated Quality factor values show the measure of the energy loss as the seismic wave propagate through the subsurface. These values vary with depth as well as the VSP line azimuth.

An average of the phase velocity at reference frequency 80Hz was calculated for each line and used as the reference velocity in the Kolsky-Futterman dispersion model. This is shown in Table 4.1. Figure 4.2 shows an example of the average phase velocity at 80Hz estimated along line 3.

Table 4.1: Average phase velocity

Reference Velocity @ 80Hz	
Line 1	2134
Line 2	2130
Line 3	2155
Line 4	2150
Line 5	2126
Line 6	2207
Line 7	2244
Line 8	2075
Line 9	2270
Line 10	2098
Line 11	1987
Line 12	2199

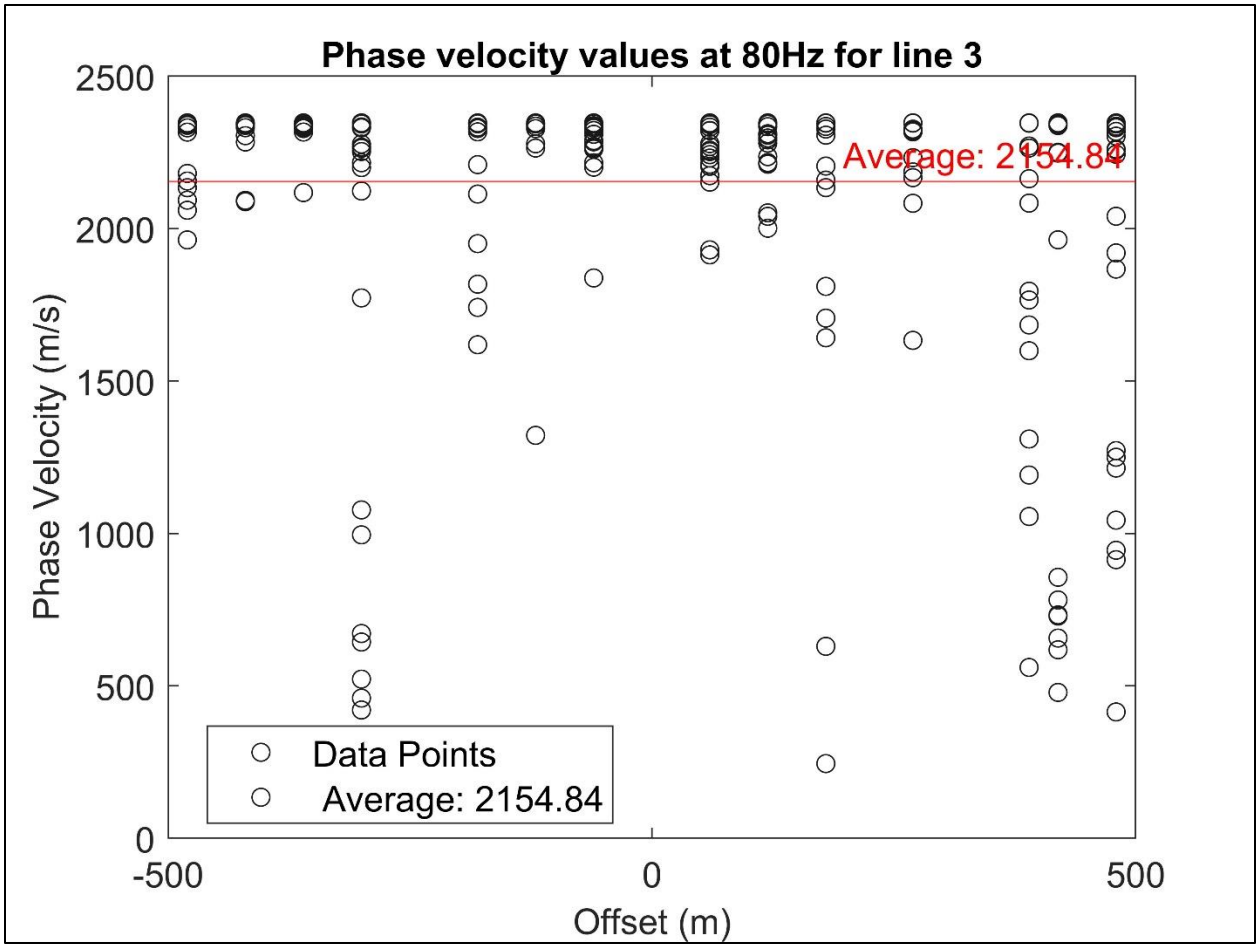

FIG 4.2: Phase velocity values at 80Hz for line 3 are shown in black circles and the average phase velocity is shown with the red line.

4.6 Seismic attenuation maps

The variation of the estimated seismic attenuation along the different source lines is shown in Figure 4.3. A consistent high attenuation is observed at depths around 300m. The seismic attenuation which is 1/Q is displayed on the colour scale with blue indicating lower seismic attenuation and red indicating higher seismic attenuation.

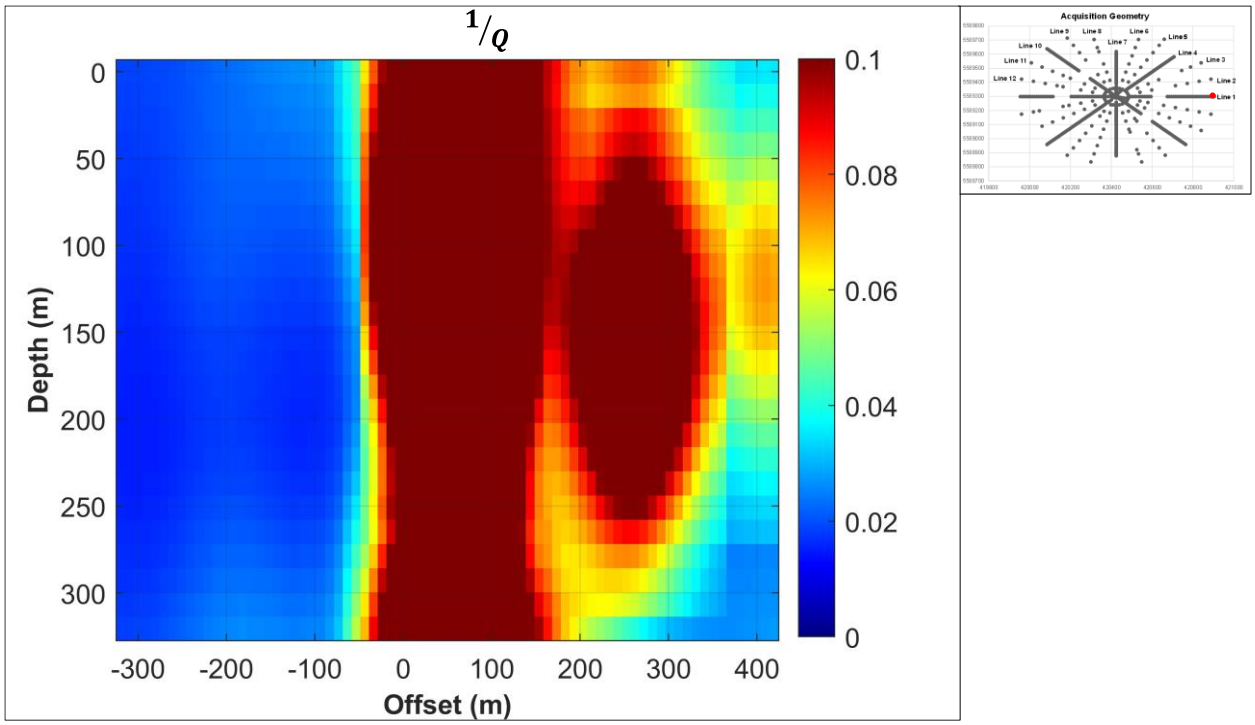

FIG 4.3a: Estimated seismic attenuation along line 1.

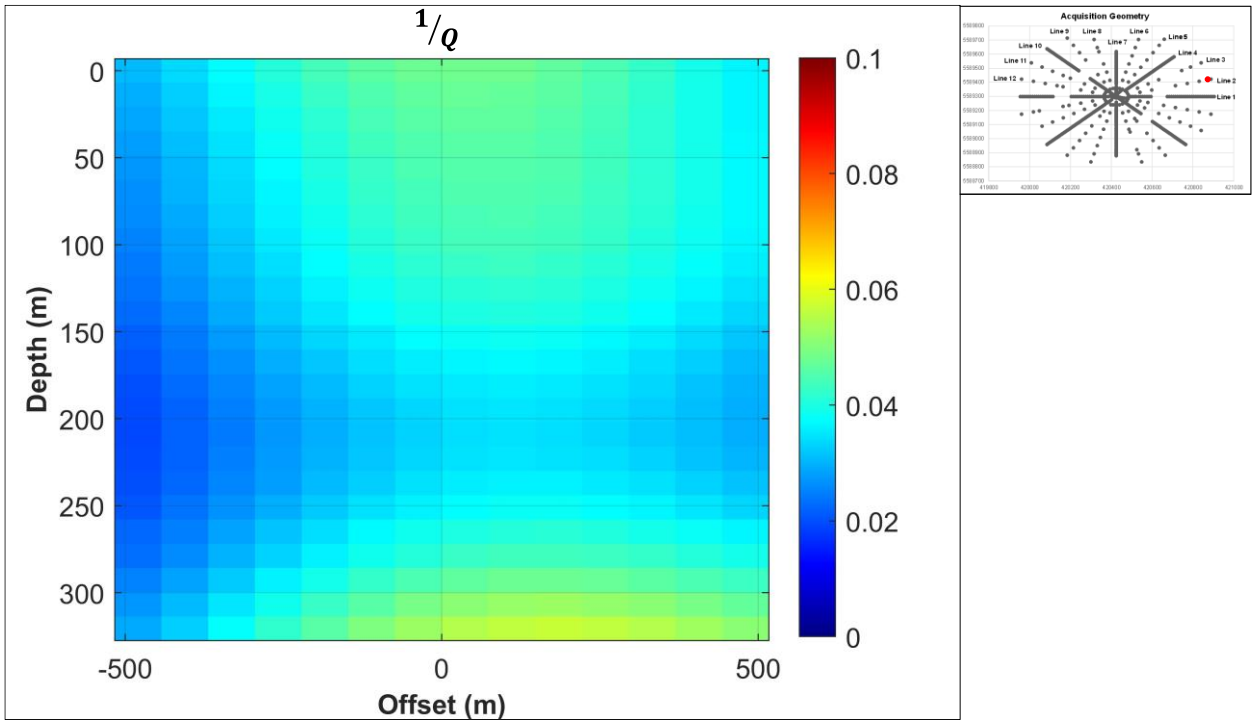

FIG 4.3b: Estimated seismic attenuation along line 2.

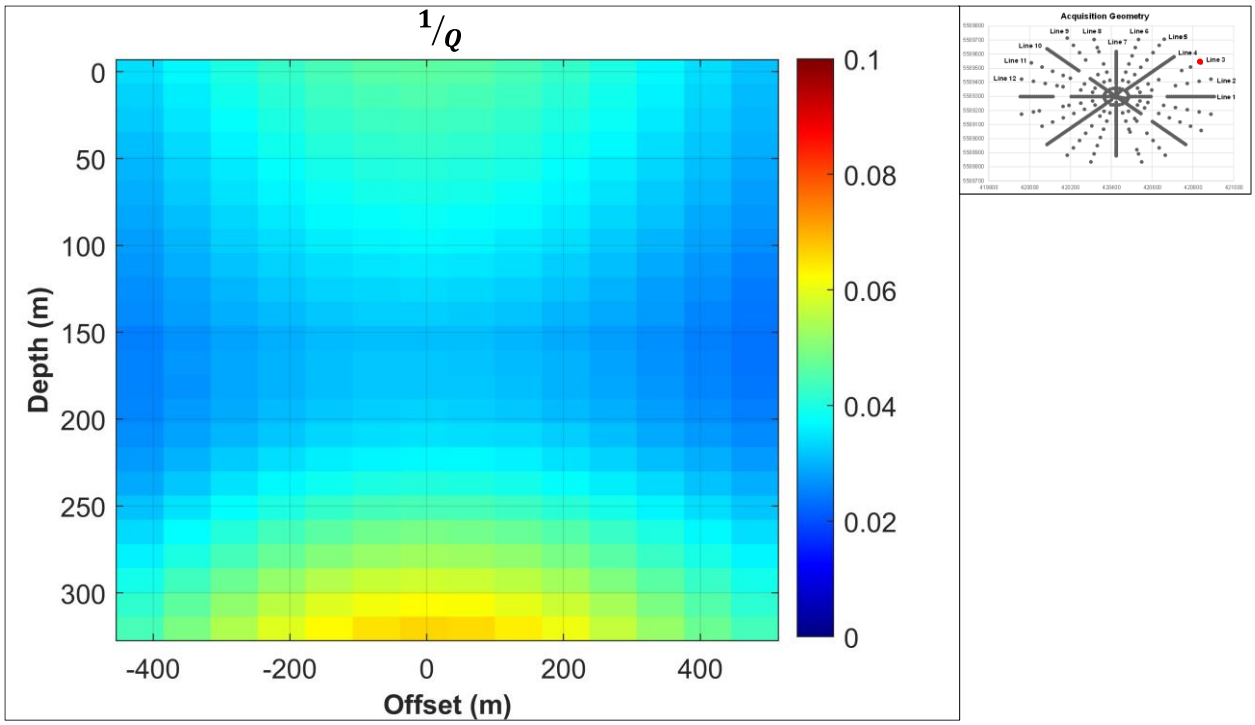

FIG 4.3c: Estimated seismic attenuation along line 3.

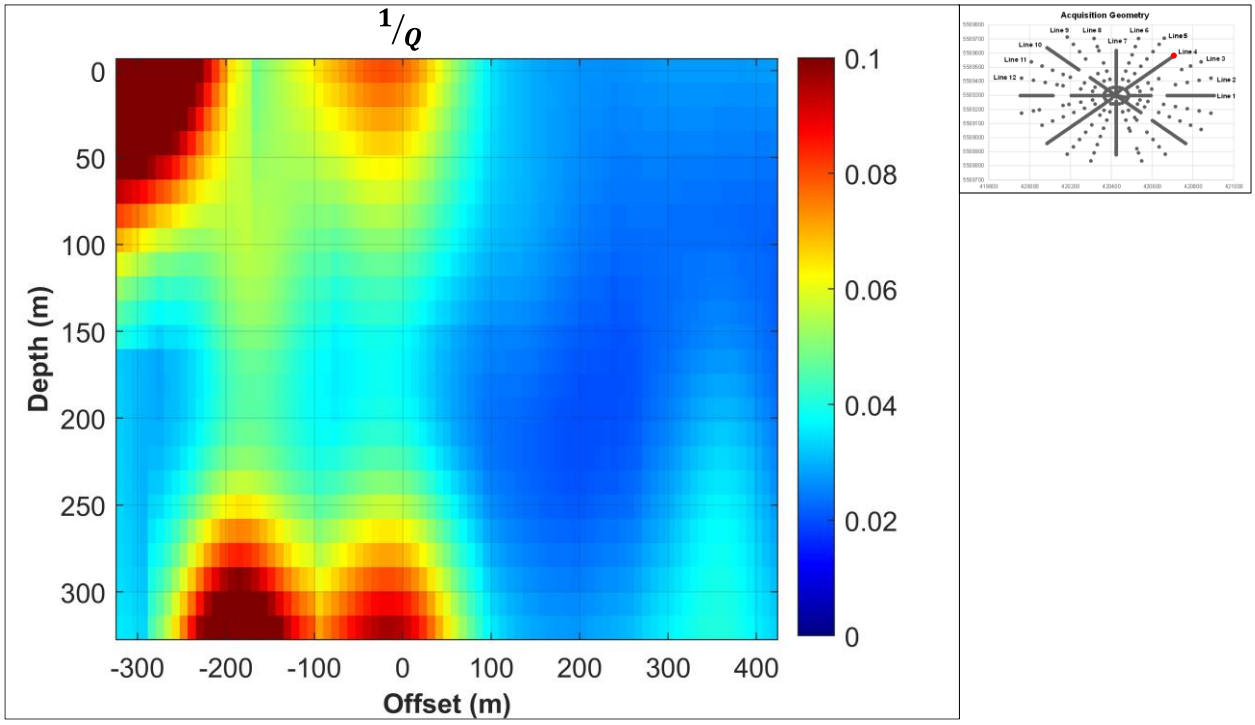

FIG 4.3d: Estimated seismic attenuation along line 4.

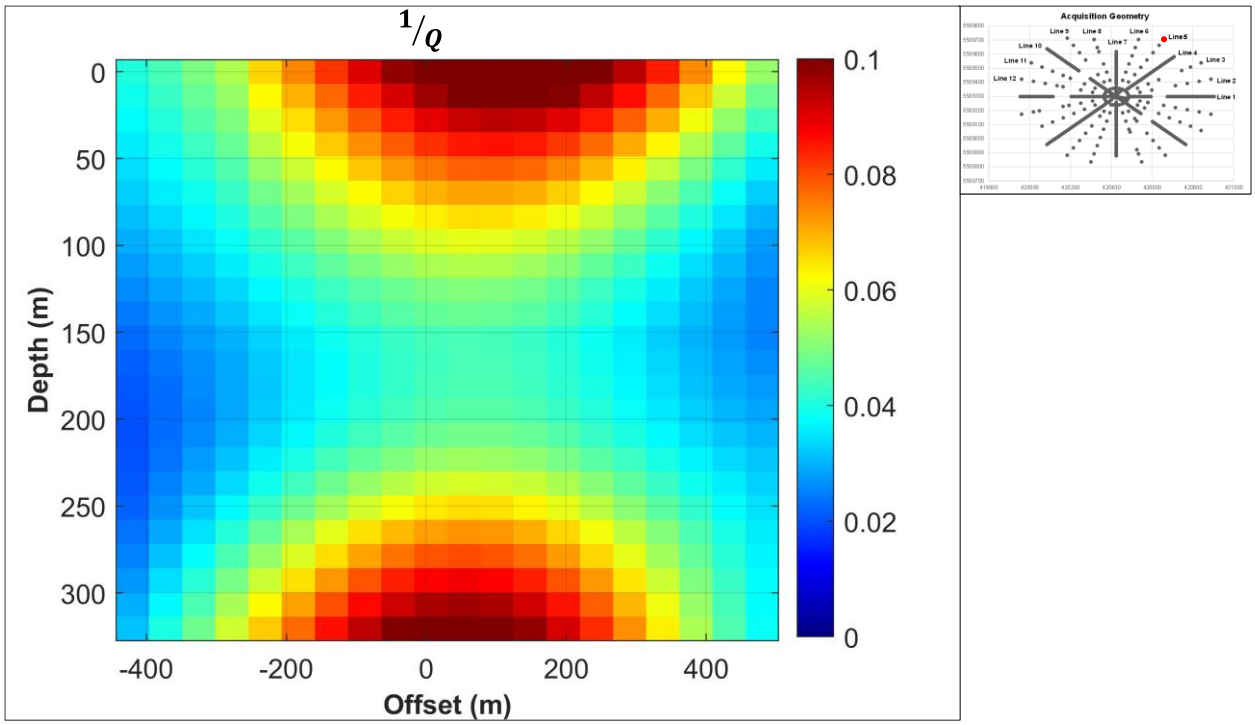

FIG 4.3e: Estimated seismic attenuation along line 5.

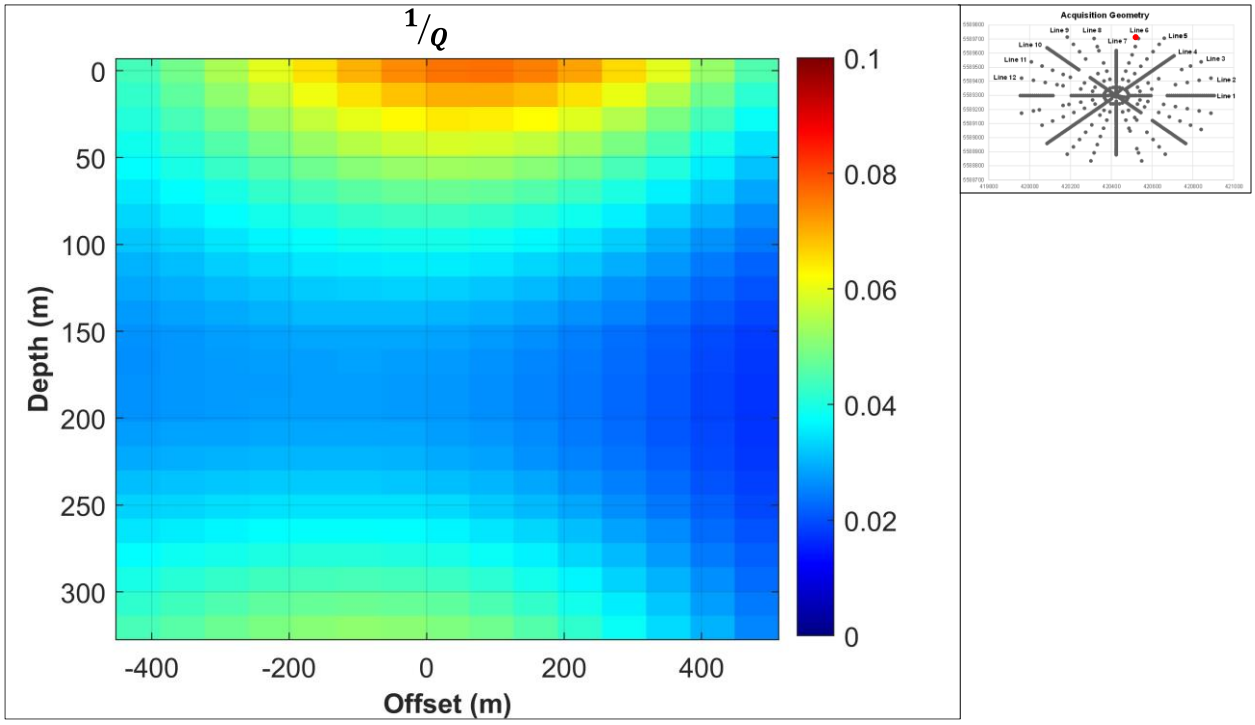

FIG 4.3f: Estimated seismic attenuation along line 6.

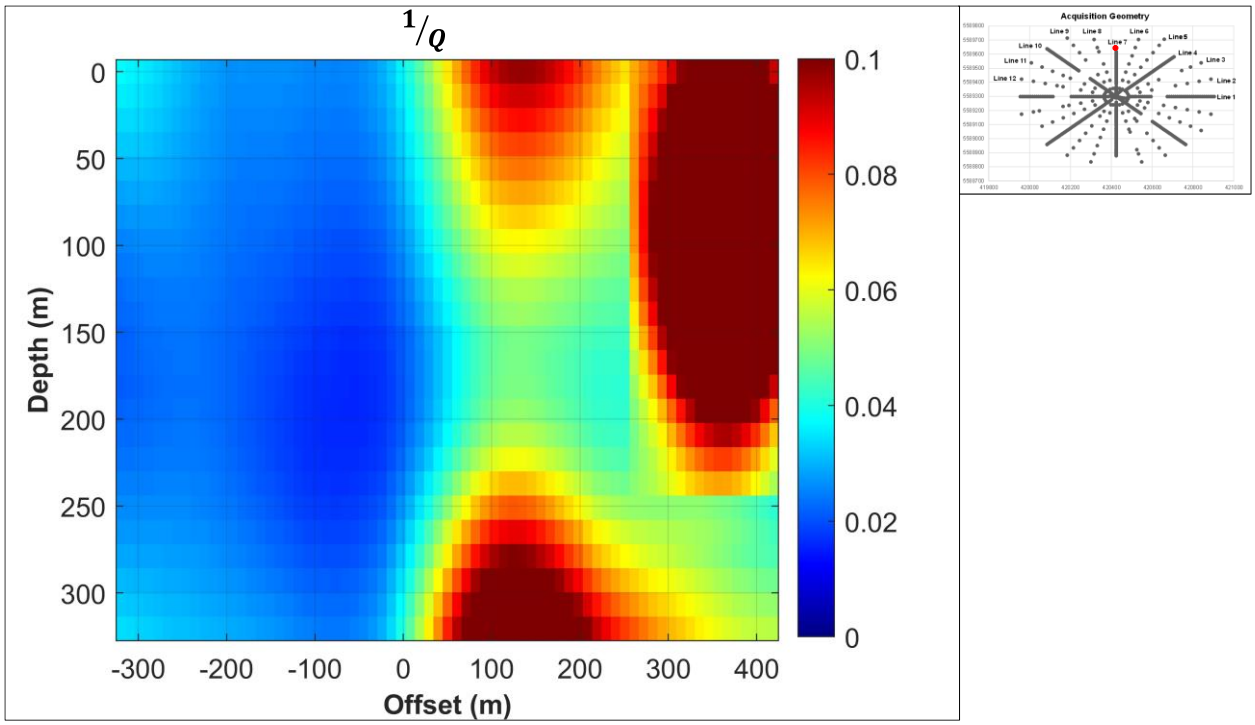

FIG 4.3g: Estimated seismic attenuation along line 7.

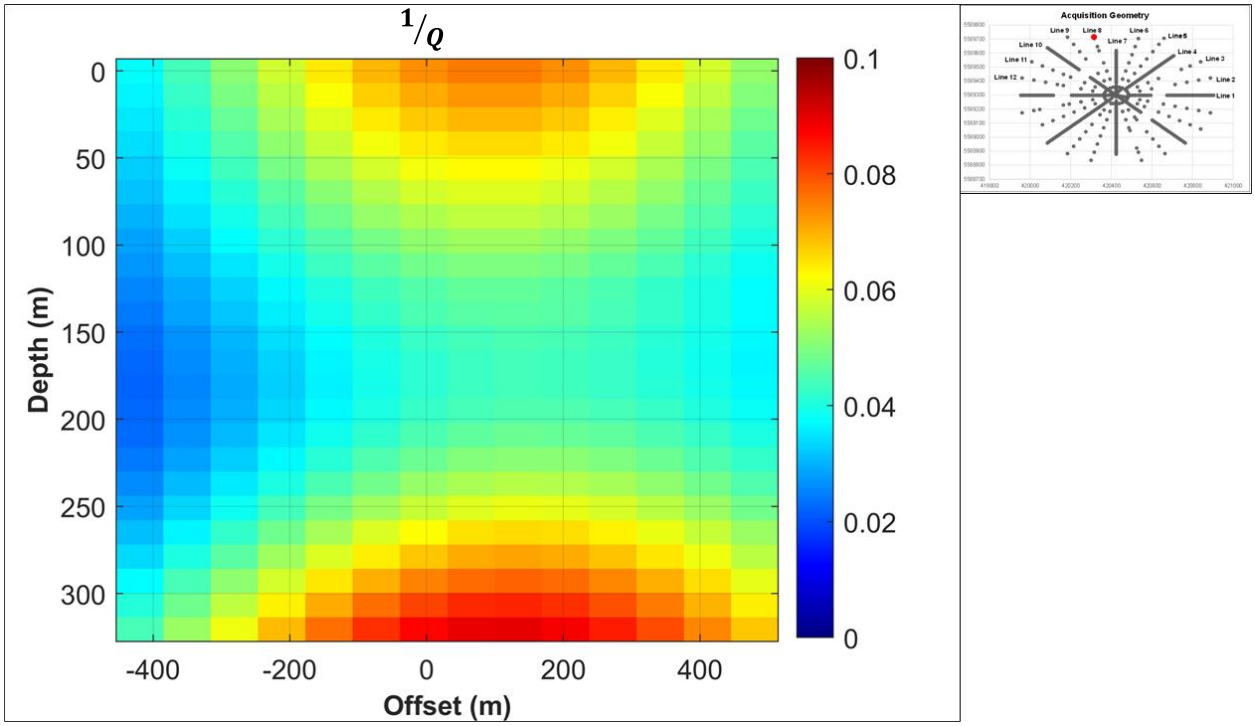

FIG 4.3h: Estimated seismic attenuation along line 8.

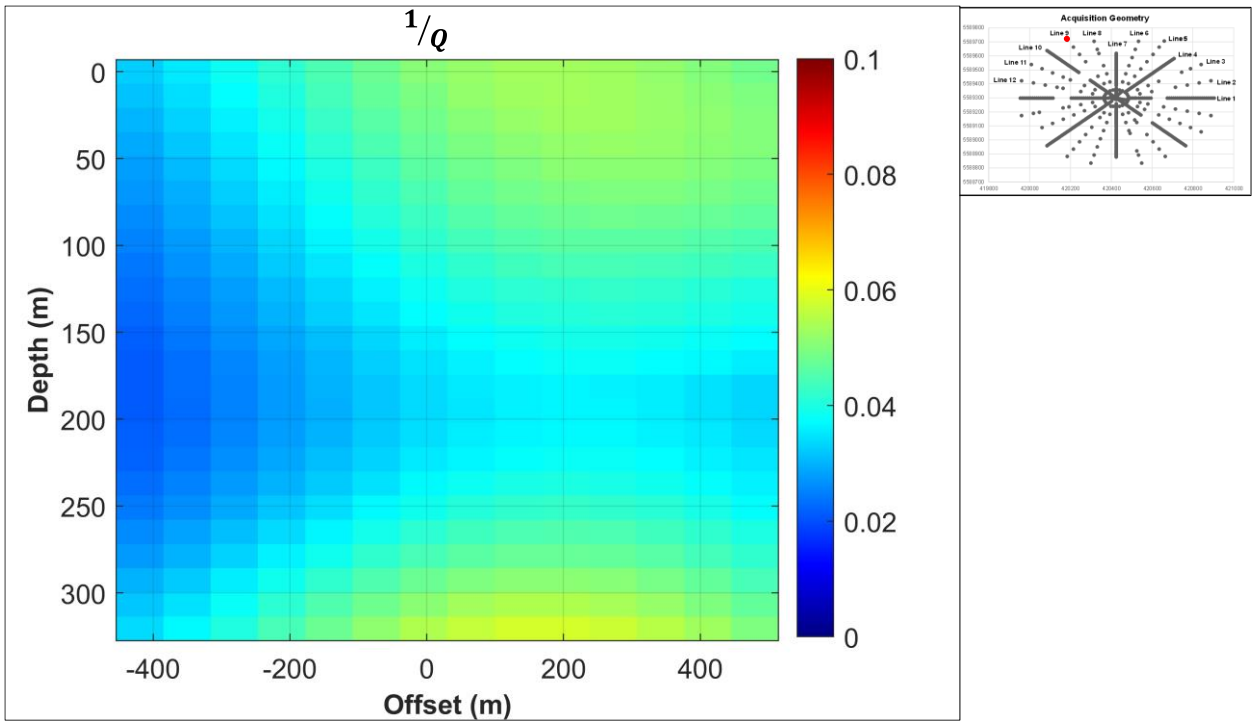

FIG 4.3i: Estimated seismic attenuation along line 9.

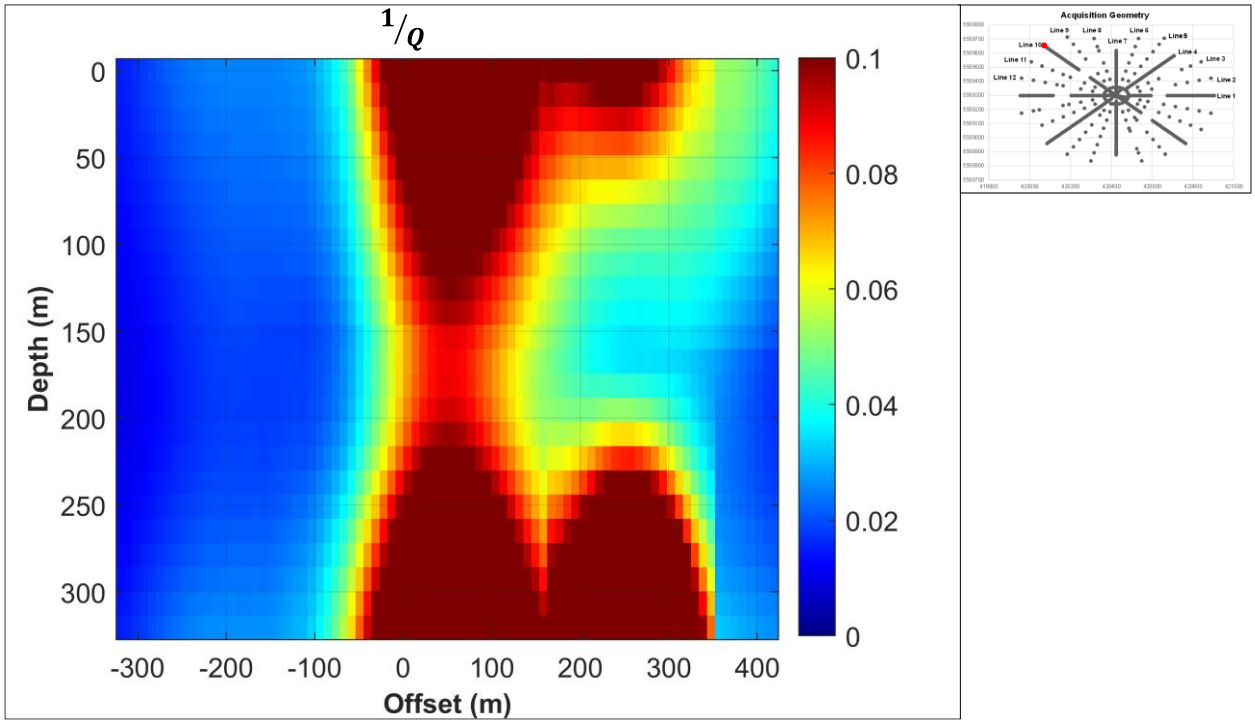

FIG 4.3j: Estimated seismic attenuation along line 10.

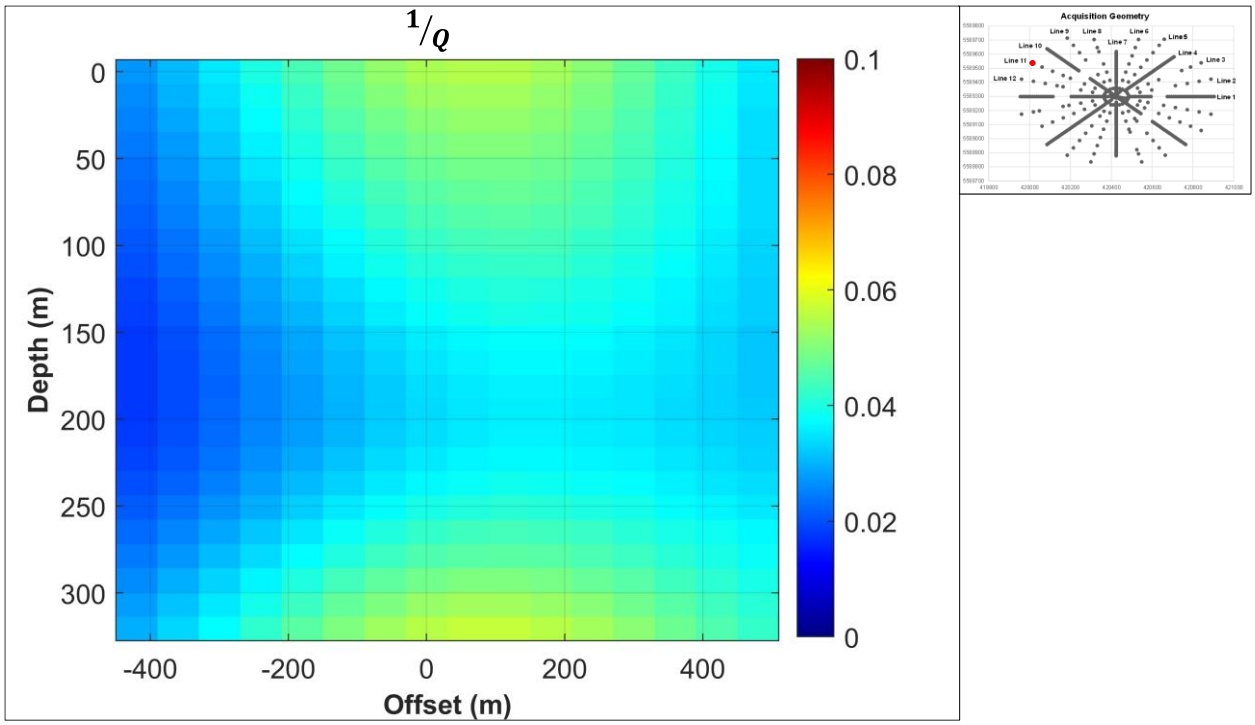

FIG 4.3k: Estimated seismic attenuation along line 11.

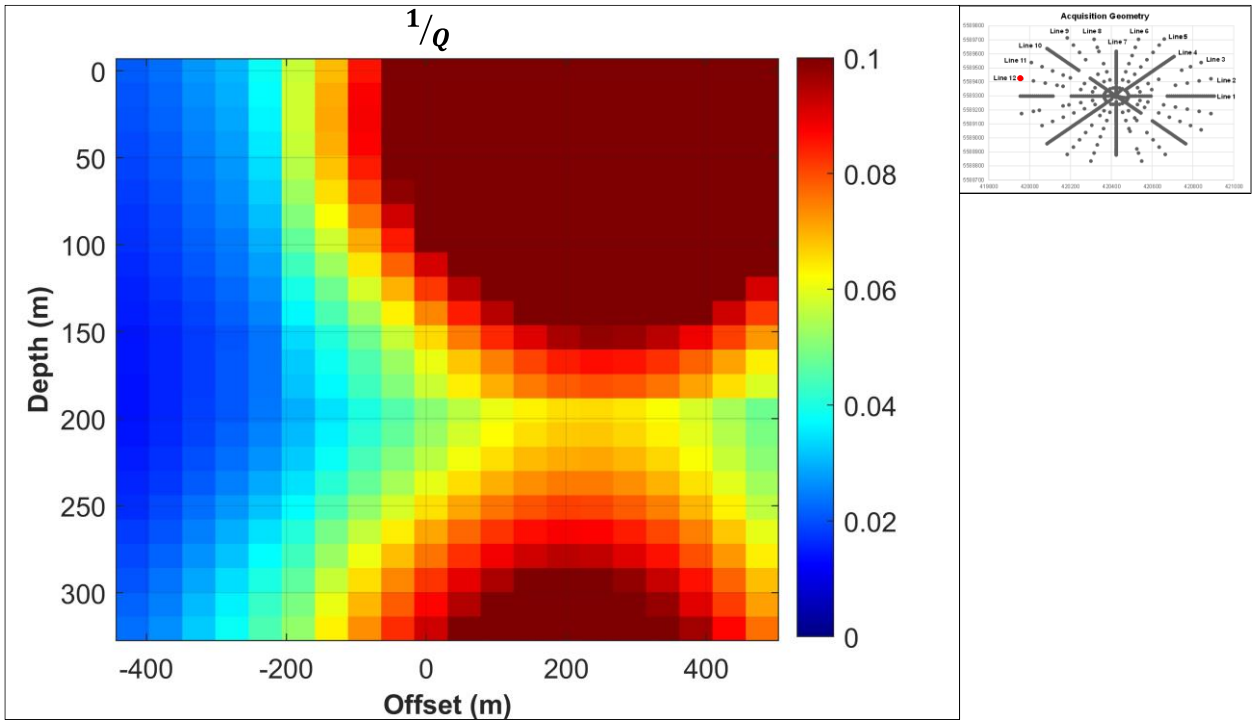

FIG 4.3l: Estimated seismic attenuation along line 12.

Looking at the seismic attenuation maps from line to line, the variation of seismic attenuation is quite evident and relatable to the variation in the observed phase velocity. These variations in seismic attenuation and phase velocity can be attributed to the heterogeneous subsurface. Zhang and Stewart (2007) related seismic attenuation with rock properties, and they observed that Q is directly proportional to the phase velocity. They observed that rocks with higher porosity will have higher seismic attenuation. We expect the rocks with low phase velocity to show high seismic attenuation and vice versa. Seismic attenuation in rocks also depends on the degree of fluid saturation and the type of fluid, with dry rocks having the least attenuation, as observed by Johnston (1981). Another important reason for the variation in both phase velocity and attenuation from line to line can be due to anisotropy which is the variation of the seismic velocities with VSP azimuth.

Chapter 5: Conclusion

Estimation of the dispersion/attenuation of the seismic waves in the near surface enhances the understanding of the CO2 plume propagation.

The geology in the near surface is complex due to the variation in rock and fluid properties. Its use as a storage for CO_2 should be accompanied by efficient monitoring to ensure the CO_2 remains contained in the subsurface.

The changes in the elastic properties of rock in the subsurface made it possible to effectively employ the sensitivity of seismic waves response to these changes in rock properties.

Newell County facility is a shallow CO_2 injection site that encourages near-surface seismic characterization. Analysing the VSP dataset from the Newell County facility provided the opportunity to understand the changes in elastic properties in the near surface. From the uncorrelated vibroseis data set, we know the importance of the interplay of the departure and arrival times of the higher and lower frequencies of the propagating seismic waves. This is an essential aspect of this method, seeing the seismic frequencies transmitted earlier into the earth by the vibroseis arriving later than the higher frequencies that were transmitted after the low frequencies. This method of estimating the frequency-dependent phase velocities in the near-surface has been able to show variation in phase velocities for the study area. We observed the changes in phase velocity with frequency while keeping the line and offsets constant. This confirms that phase velocity indeed changes with frequencies due to dispersion. The CO_2 injected around 300m depth was clearly imaged as a low phase velocity area around the 300m depth.

There is a recorded change in the phase velocity from line to line due to spatial heterogeneity in dispersion. These estimated frequency-dependent phase velocities were utilized in estimating seismic quality factor Q by using the Kolsky dispersion model. This model finds the relationship between the phase velocity estimated and the frequency of the seismic signal, although it needs a reference phase velocity which is dependent on the reference frequency selected. Several reference frequencies were tried, but we chose the 80Hz frequency because it gave resulting Q values that are similar to the Q values from the work of Wang and Lawton (2024), where they measured time-lapse variation in seismic attenuation from distributed acoustic sensing VSP data from the Newell County facility using the time-variant amplitude spectra approach. Seismic attenuation is inversely proportional to the Q, and in the seismic attenuation maps, we were able to deduce the areas with low and high seismic attenuation. The areas with high attenuation around 300m were attributed to the CO_2 plume. There are also observed changes in seismic attenuation from line to line due to spatial heterogeneity in attenuation.

Future work could include integrating seismic attenuation estimations with well-log interpretation to better understand the relationships to enhance CO_2 monitoring.

References

Aki, K., and Richards, P. G., 2002, Quantitative Seismology: University Science Books, 2nd edition.

Cheng, P., 2013, Anelastic attenuation in seismic data: modelling, measurement, and correction: Ph.D. thesis, The University of Calgary.

Daley, T., & Harbert, W. (2019). Goals of CO2 Monitoring: Why and How to Assess the Subsurface Changes Associated with Carbon Capture and Storage. In T. Davis, M. Landrø, & M. Wilson (Eds.), Geophysics and Geosequestration (pp. 54-70). Cambridge: Cambridge University Press. doi:10.1017/9781316480724.004.

Dragoset, W., 1988, Marine vibrators and the Doppler effect: SEG Expanded Abstracts, 75–78.

Futterman 1966, Dispersive body waves: SEG Expanded Abstracts, 410-411.

F. Gassmann, “Uber die Elastizitat Poroser Medien,” Veirteljahrsschrift der Naturforschenden Gesellschaft in Zzirich, Vol. 96, 1951, pp. 1-23.

Haase, A. B., 2010, q estimation from uncorrelated vibroseis VSP model data: CSEG Geonconvention Expanded Abstracts.

Johnston et al 1981 Attenuation of seismic waves: SEG Expanded Abstracts, 231-233.

Kevin W. Hall, Kevin L. Bertram, Malcolm Bertram, Kris Innanen, and Don C. Lawton 2018, CREWES 2018 multi-azimuth walk-away VSP field experiment, vol 30.

Kris Innanen, 2014, Estimating anelastic dispersion from uncorrelated vibe data, vol 16: CREWES Reports.

Macquet, M., Lawton, D. C., Saeedfar, A. A., and Osadetz K. G., 2019, A feasibility study for detection thresholds of CO2 at shallow depths at CaMI Field Research Station, Newell County, Alberta, Canada: Petroleum Geoscience, 25, No. 4, pg., 509-518.

Margrave, G. F. and Lamoureux, M. P., 2002, Gabor deconvolution: CREWES Annual Research Report, 13.

Robert R. Stewart, 2001, VSP: An in-depth seismic understanding. CSEG Recorder Vol. 26 No. 07.

Sun LF, Milkereit B, Tisato N. Analysis of velocity dispersion using multichannel sonic logging data: A case study. Geophysical Prospecting. 2016 Jun 28;64(4):1016-29.

Wang and Lawton, Time-lapse attenuation variations using distributed acoustic sensing vertical seismic profile data during CO2 injection at CaMI Field Research Station, Alberta, Canada. GEOPHYSICS, Vol. 89, No. 2 (March-April 2024)10.1190/GEO2022-0731.1.

Wong J., Picking and fitting of first-break times measured on Gabor transforms of correlated Vibroseis VSP signals. CREWES research report-Volume 35.

Zhang, Stewart, Lawton 2007 Estimating seismic attenuation (Qp & Qs) from rock properties CREWES Research Report - Volume 22 (2010).

Appendix

Testing out different frequencies as the reference frequency and predicting new sets of phase velocities using estimated phase velocities from line 3, shot offset 480m while estimating Q. The tested depths are 50, 260 and 300m.

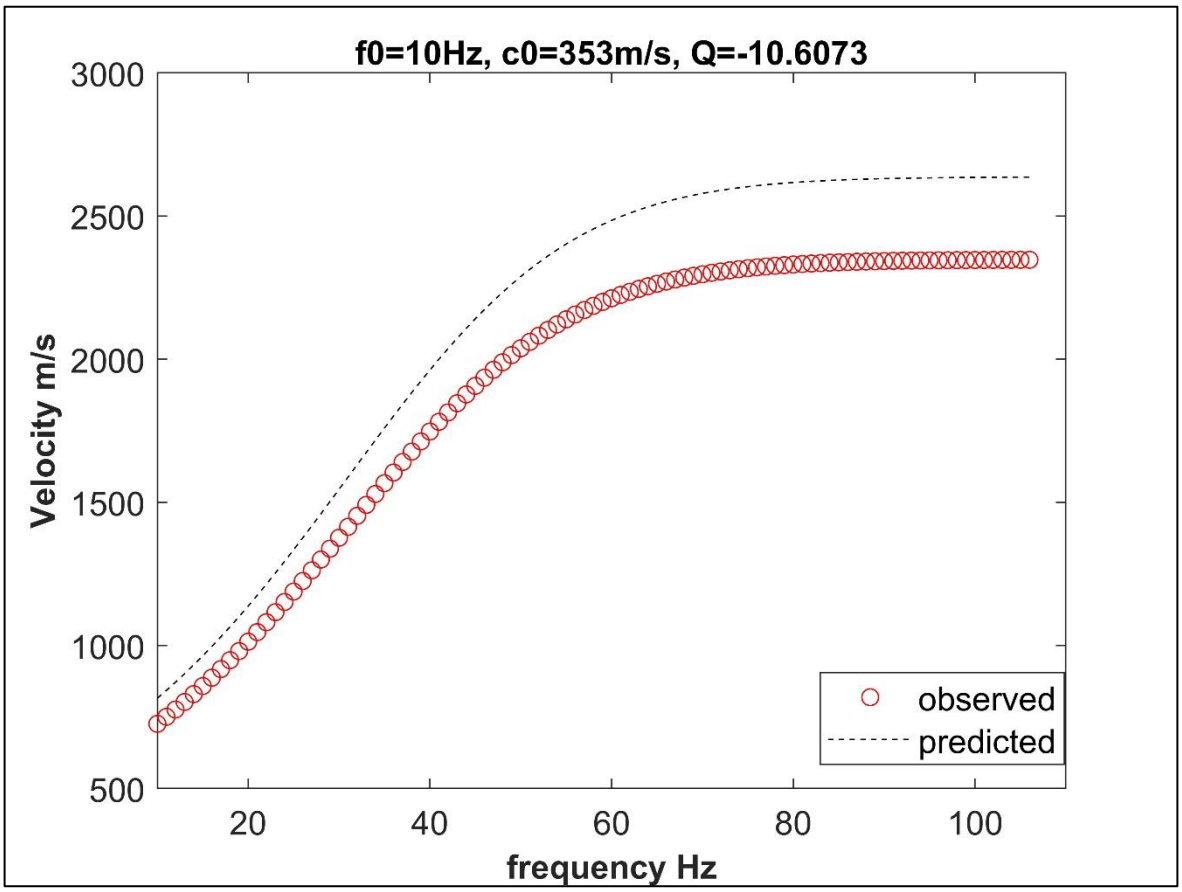

FIG 4.1a: Estimation of Q at a depth of 50m, Line 3 at 480m offset using a reference frequency of 10Hz and reference velocity of 353m/s.

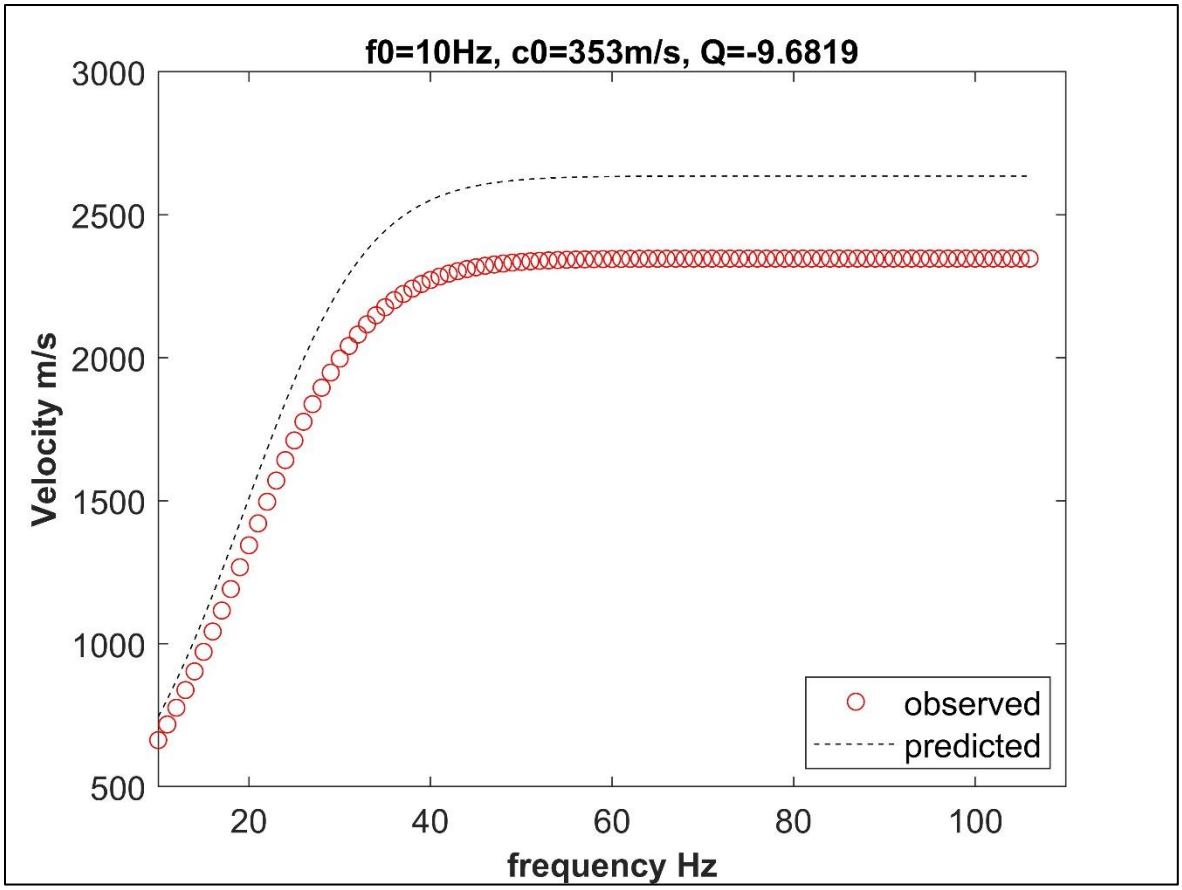

FIG 4.1b: Estimation of Q at a depth of 260m, Line 3 at 480m offset using a reference frequency of 10Hz and reference velocity of 353m/s.

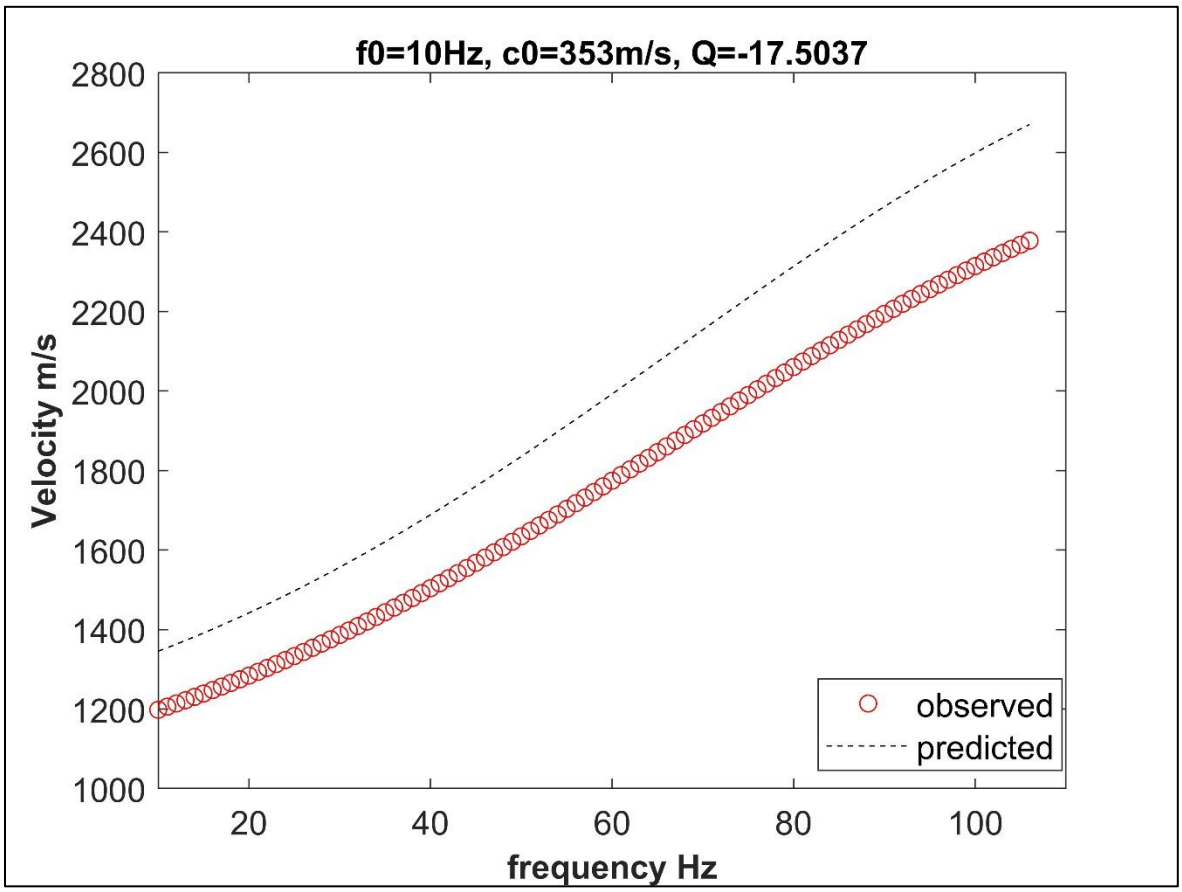

FIG 4.1c: Estimation of Q at a depth of 300m, Line 3 at 480m offset using a reference frequency of 10Hz and reference velocity of 353m/s.

Repeating the same process, we used a reference phase velocity of 1200 which is equivalent to the highest phase velocity at 10Hz for Line 3, offset 480m. There remains a difference between the predicted and observed phase velocity, and the Q ranges from -5.1 to 2.8, as shown in Figure 4.2

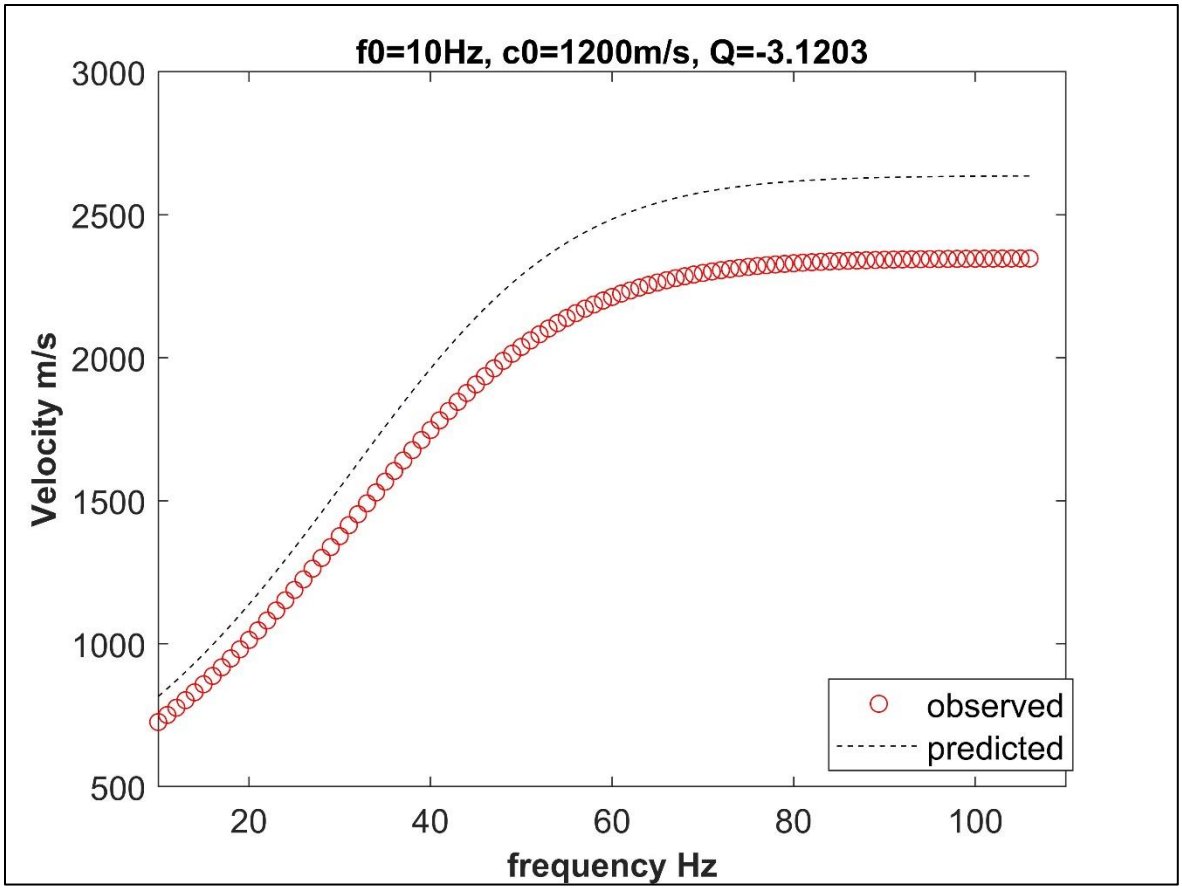

FIG 4.2a: Estimation of Q at a depth of 50m, Line 3 at 480m offset using a reference frequency of 10Hz and reference velocity of 1200m/s.

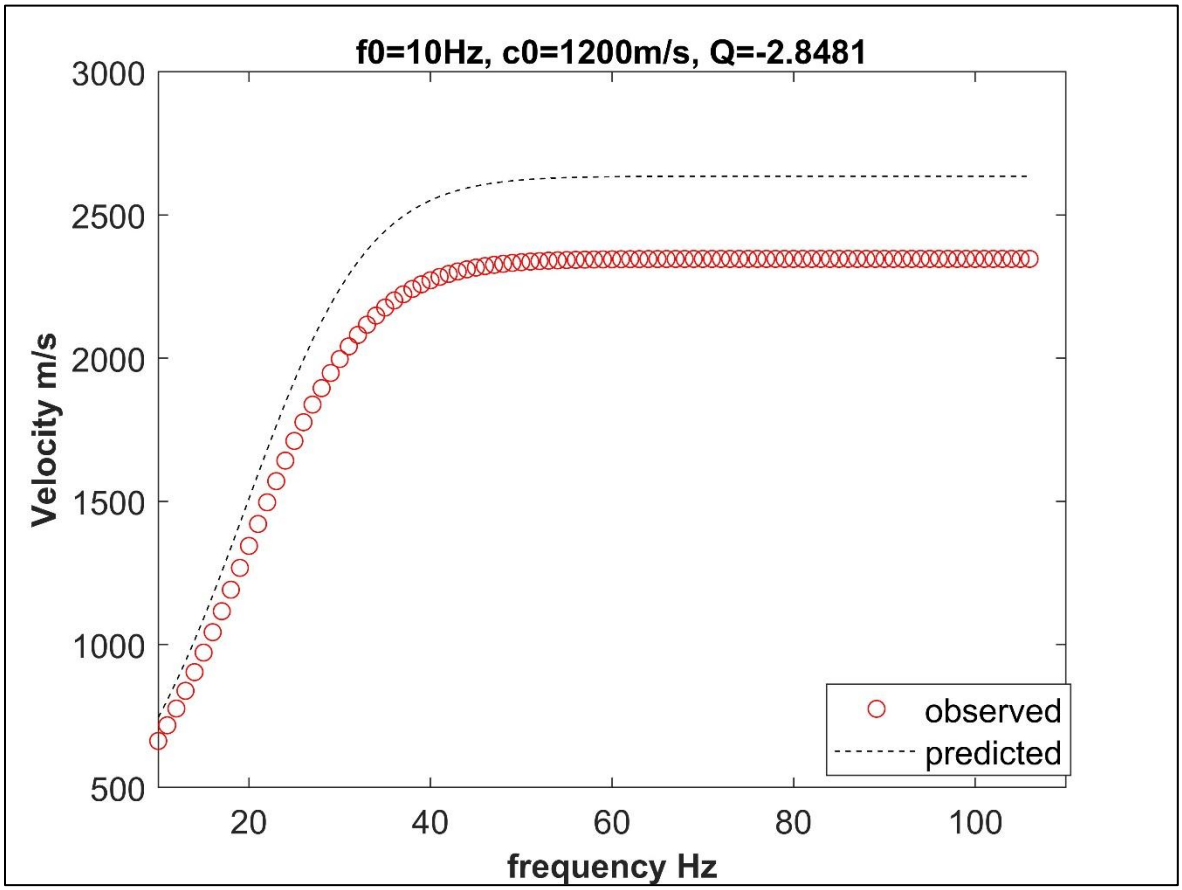

FIG 4.2b: Estimation of Q at a depth of 260m, Line 3 at 480m offset using a reference frequency of 10Hz and reference velocity of 1200m/s.

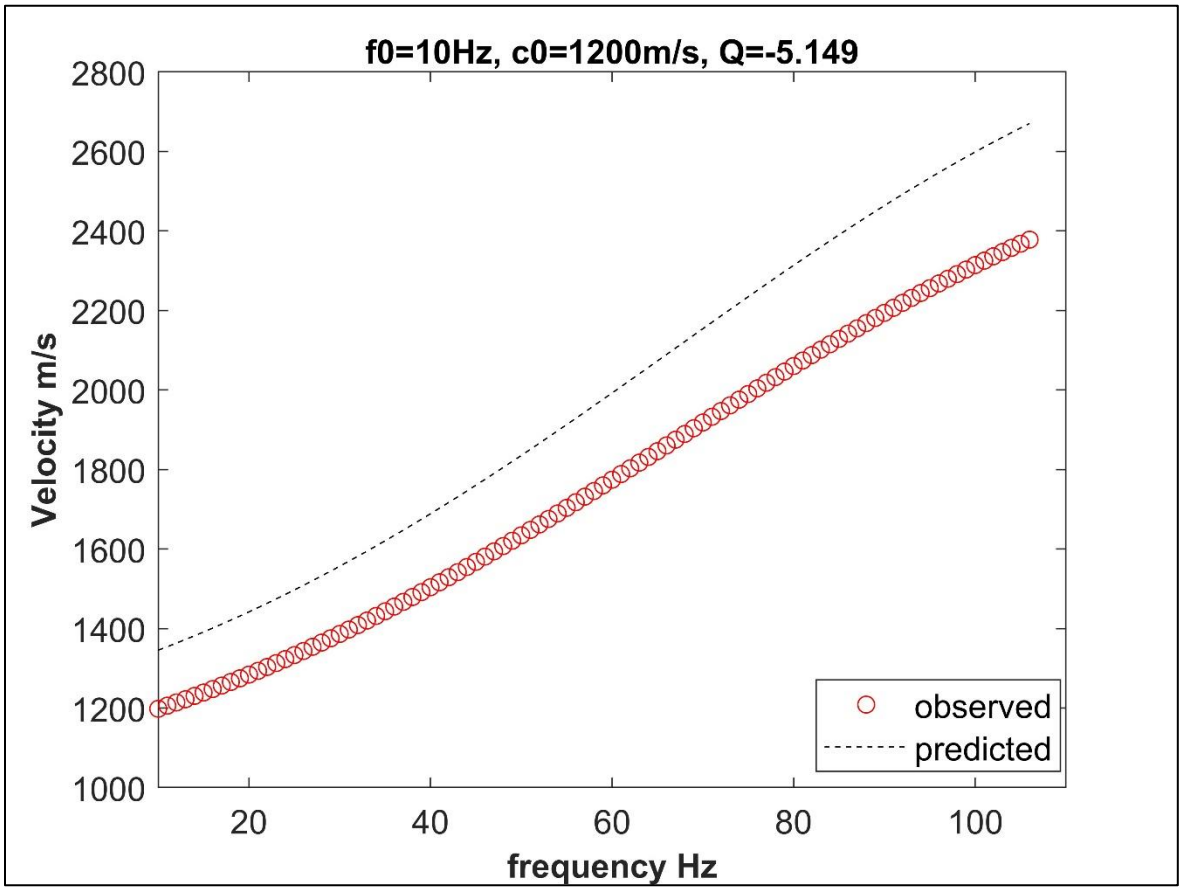

FIG 4.2c: Estimating Q at a depth of 300m, Line 3 at 480m offset using a reference frequency of 10Hz and reference velocity of 1200m/s.

Choosing the lowest phase velocity of 1328m/s at a 30Hz reference frequency, we observed that the Q that minimizes the difference between the predicted and observed phase velocities ranges between –152.1343 and –84.15, as shown in Figure 4.3.

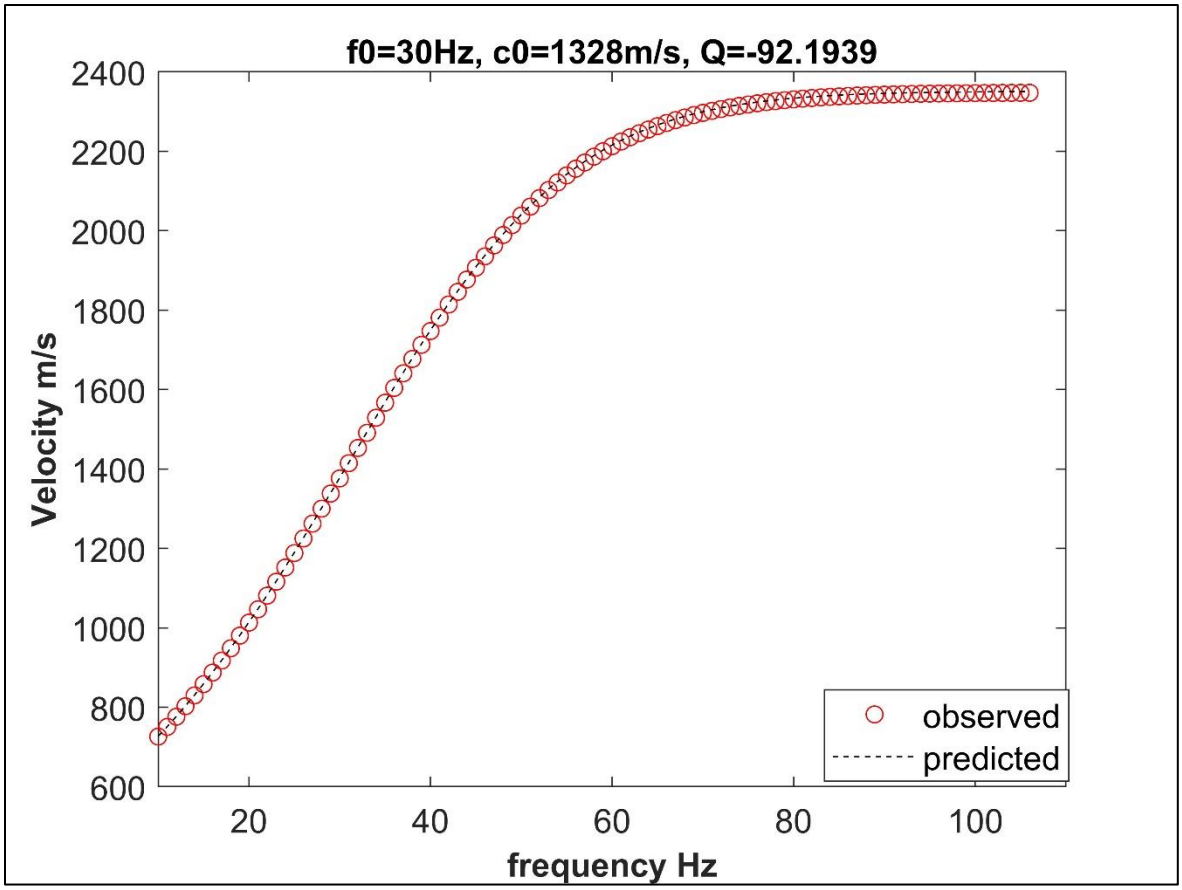

FIG 4.3a: Estimating Q at a depth of 50m, Line 3 at 480m offset using a reference frequency of 30Hz and reference velocity of 1328m/s.

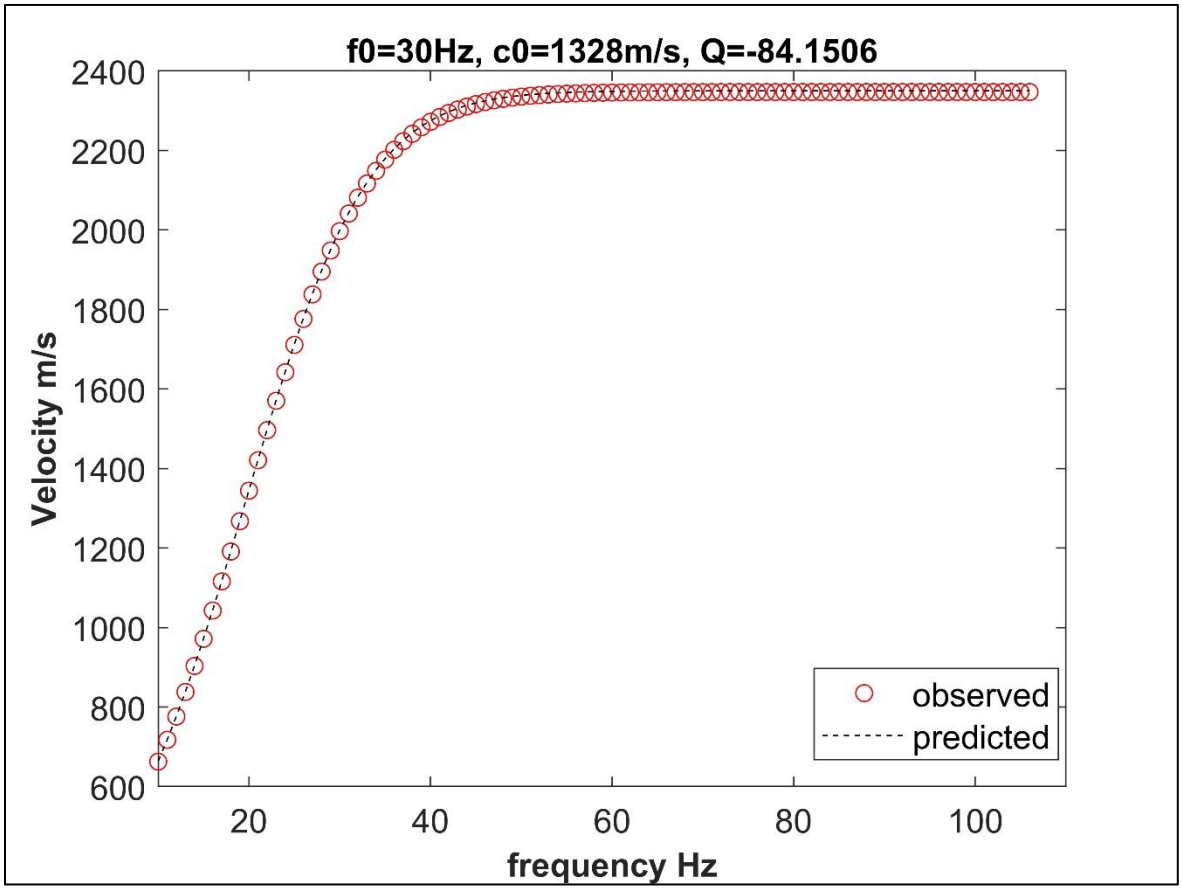

FIG 4.3b: Estimating Q at a depth of 260m, Line 3 at 480m offset using a reference frequency of 30Hz and reference velocity of 1328m/s.

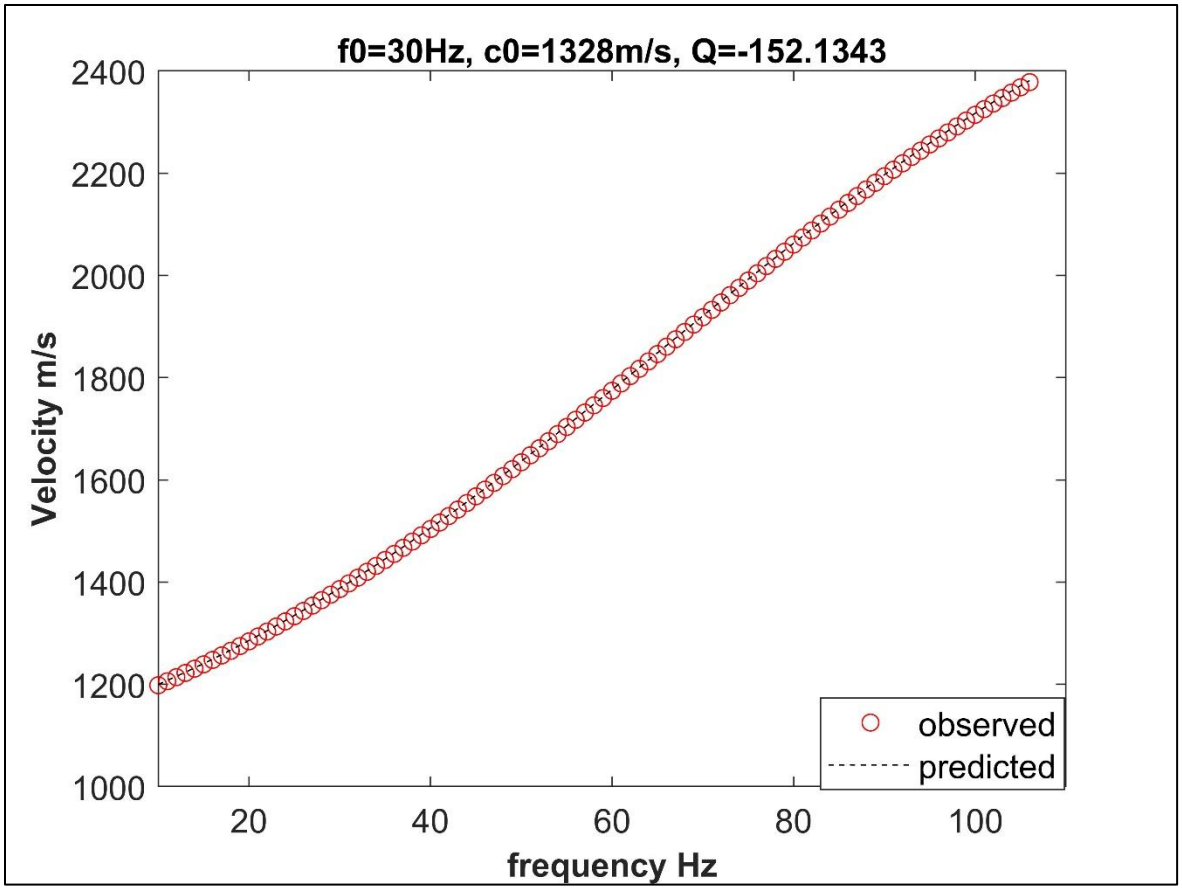

FIG 4.3c: Estimating Q at a depth of 300m, Line 3 at 480m offset using a reference frequency of 30Hz and reference velocity of 1328m/s.

At the same reference frequency of 30 Hz and inputting the highest phase velocity as the reference phase velocity, it was observed that the Q that minimized the difference between the predicted and observed phase velocity range between -52.67 and -95.2 as displayed in Figure 4.4.

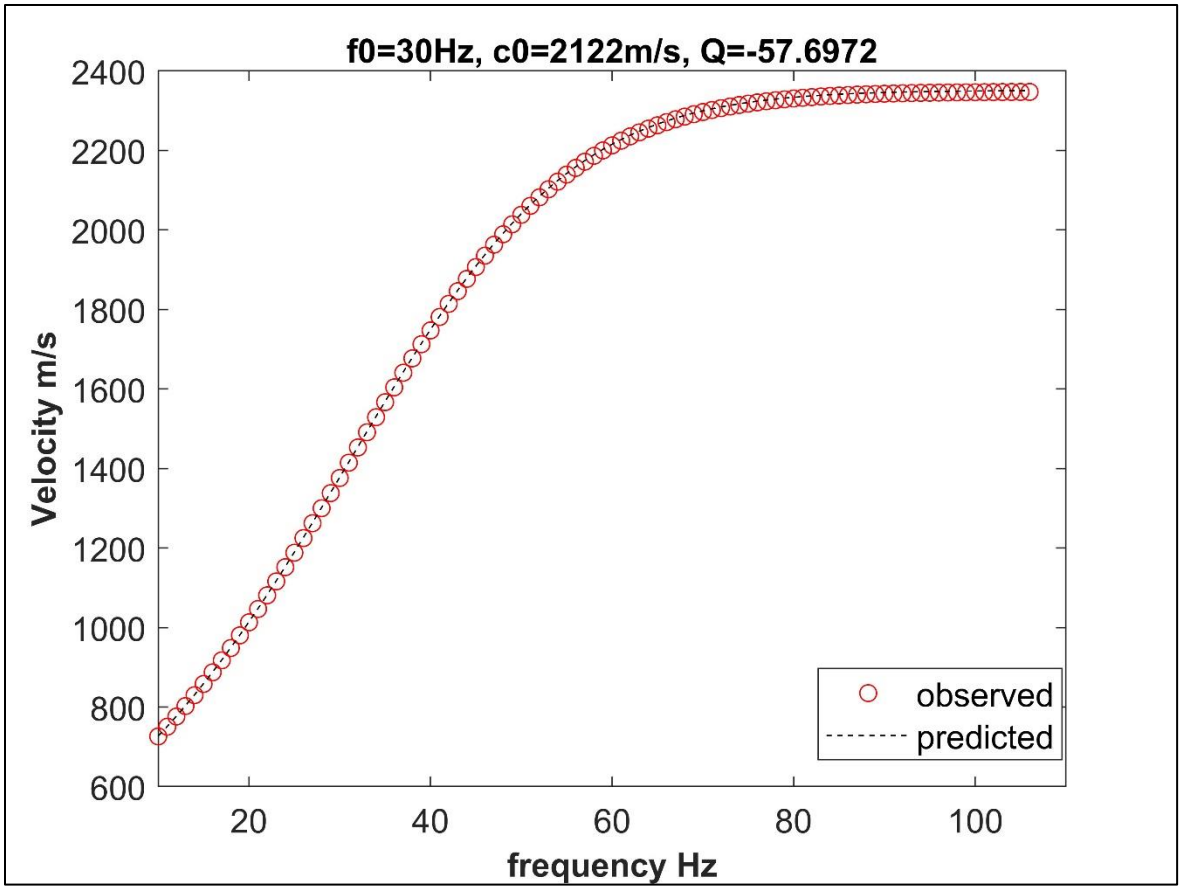

FIG 4.4a: Estimating Q at a depth of 50m, Line 3 at 480m offset using a reference frequency of 30Hz and reference velocity of 2122m/s.

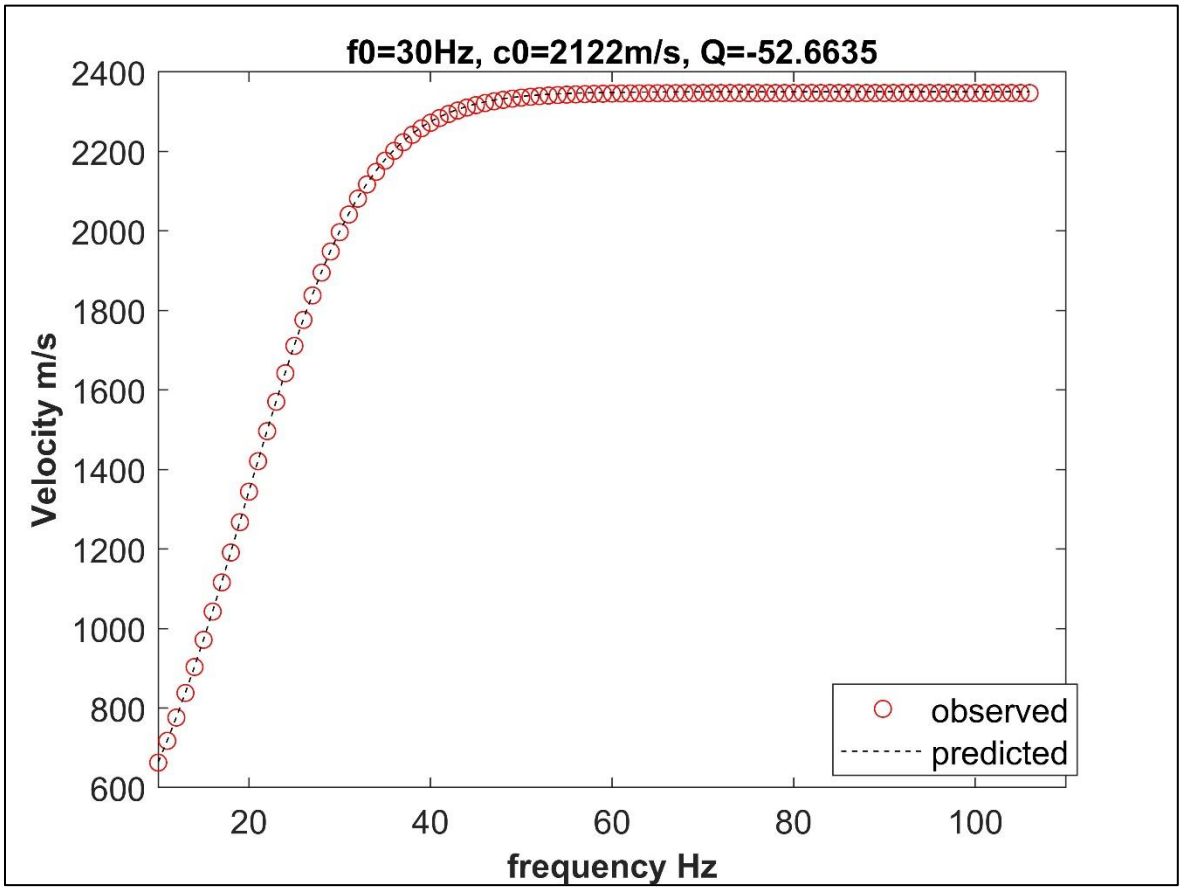

FIG 4.4b: Estimating Q at a depth of 260m, Line 3 at 480m offset using a reference frequency of 30Hz and reference velocity of 2122m/s.

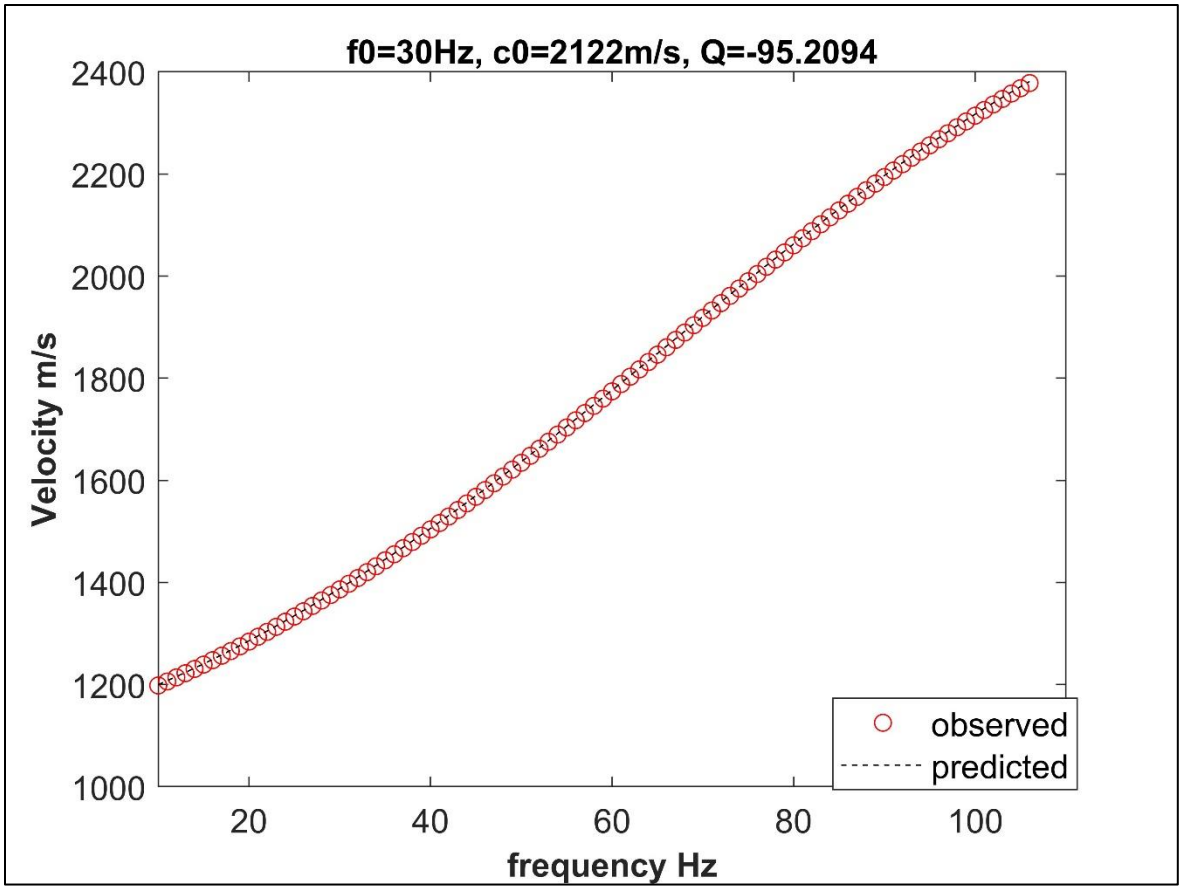

FIG 4.4c: Estimating Q at a depth of 300m, Line 3 at 480m offset using a reference frequency of 30Hz and reference velocity of 2122m/s.

Using a reference frequency of 80Hz and reference phase velocity of 1963m/s, which is the lowest phase velocity at 80Hz for line 3, at 480m offset, we got Q values ranging between 66.44 and 120.1115 as shown in Figure 4.5.

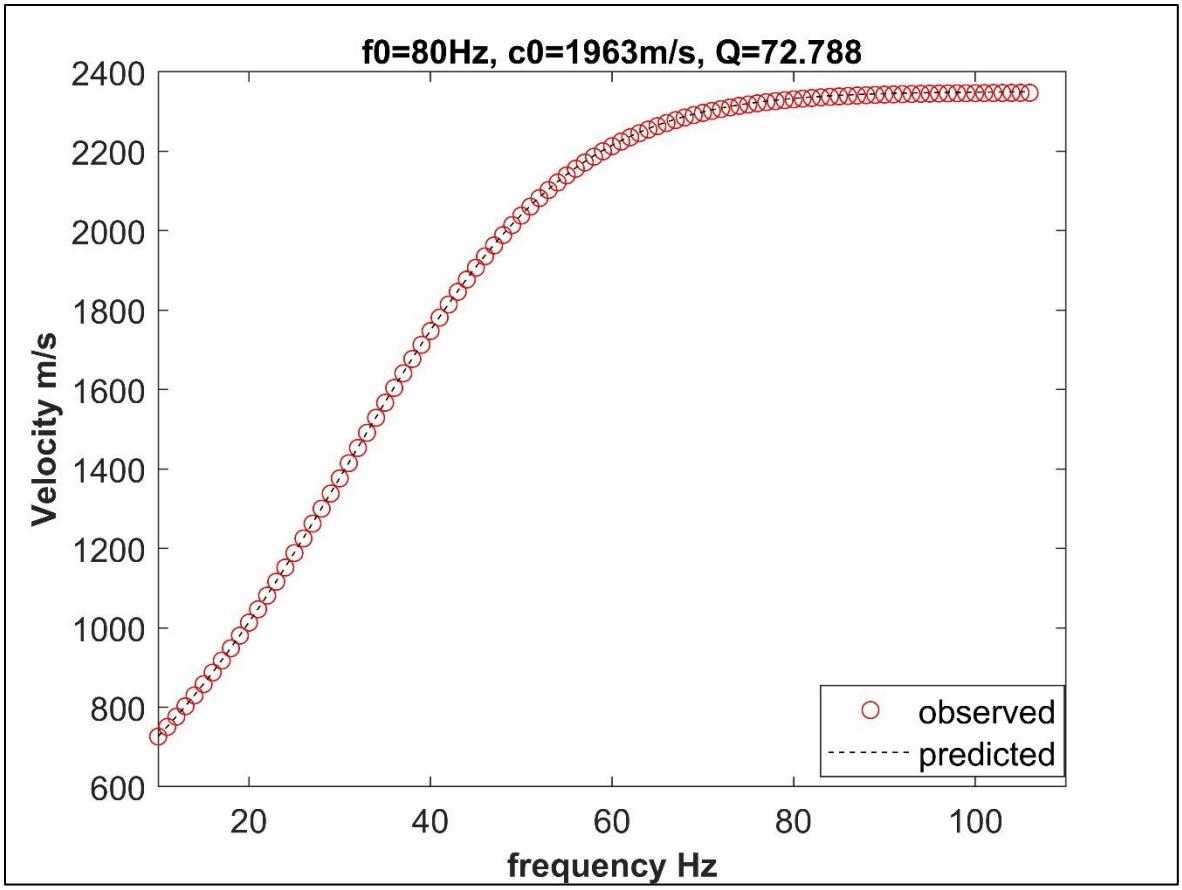

FIG 4.5a: Estimating Q at a depth of 50m, Line 3 at 480m offset using a reference frequency of 80Hz and reference phase velocity of 1963m/s.

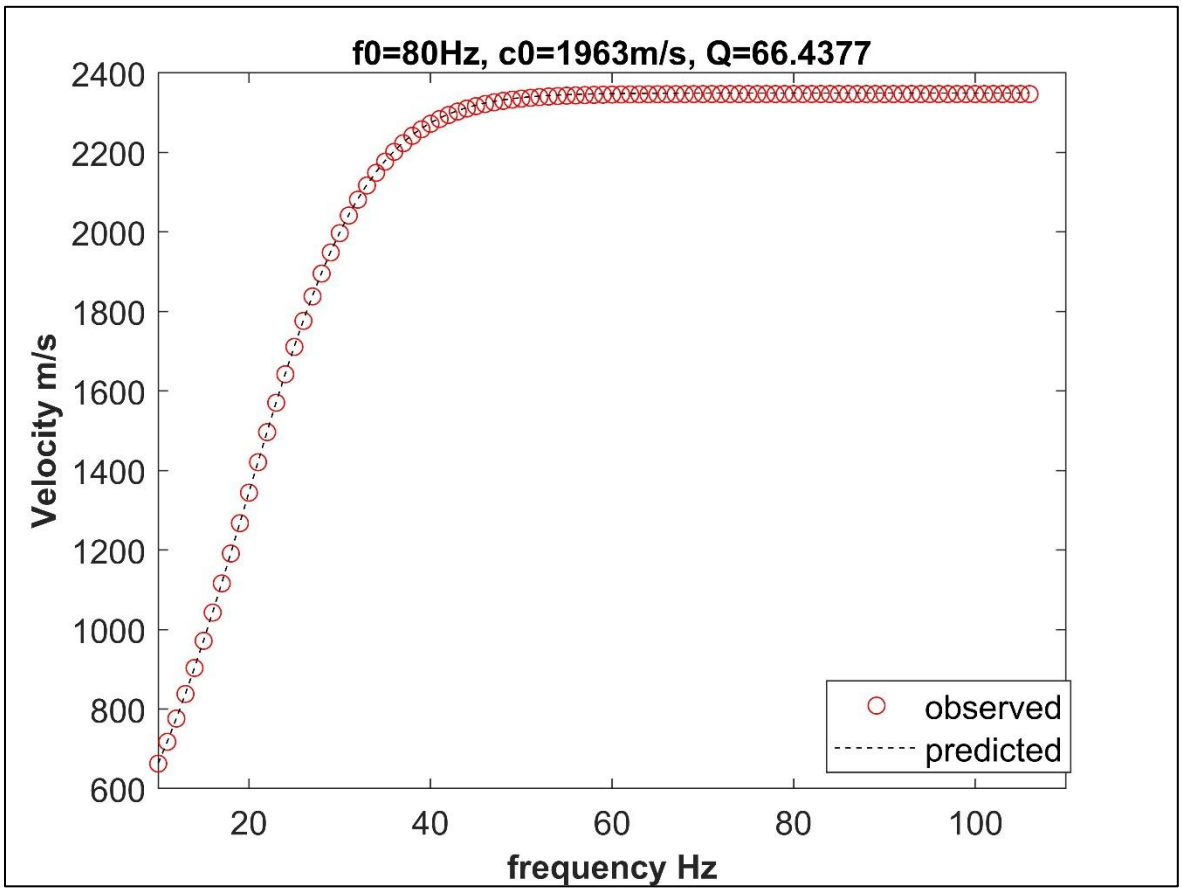

FIG 4.5b: Estimating Q at a depth of 260m, Line 3 at 480m offset using a reference frequency of 80Hz and reference phase velocity of 1963m/s.

We also used 2347m/s, the highest phase velocity at 80Hz for line 3 at offset 480m, and we got

Q values between 55.57 and 100.46, as shown in Figure 4.6.

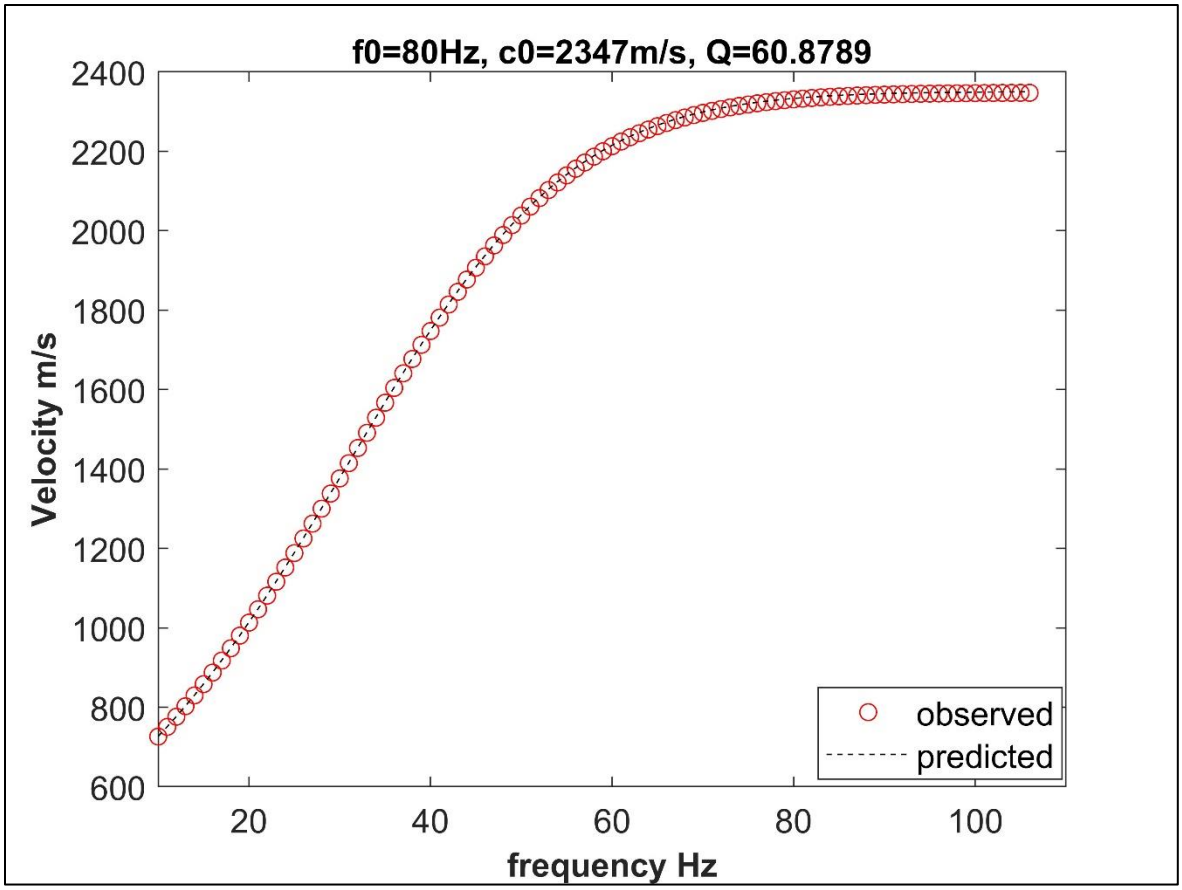

FIG 4.6a: Estimating Q at a depth of 50m, Line 3 at 480m offset using a reference frequency of 80Hz and reference phase velocity of 2347m/s.

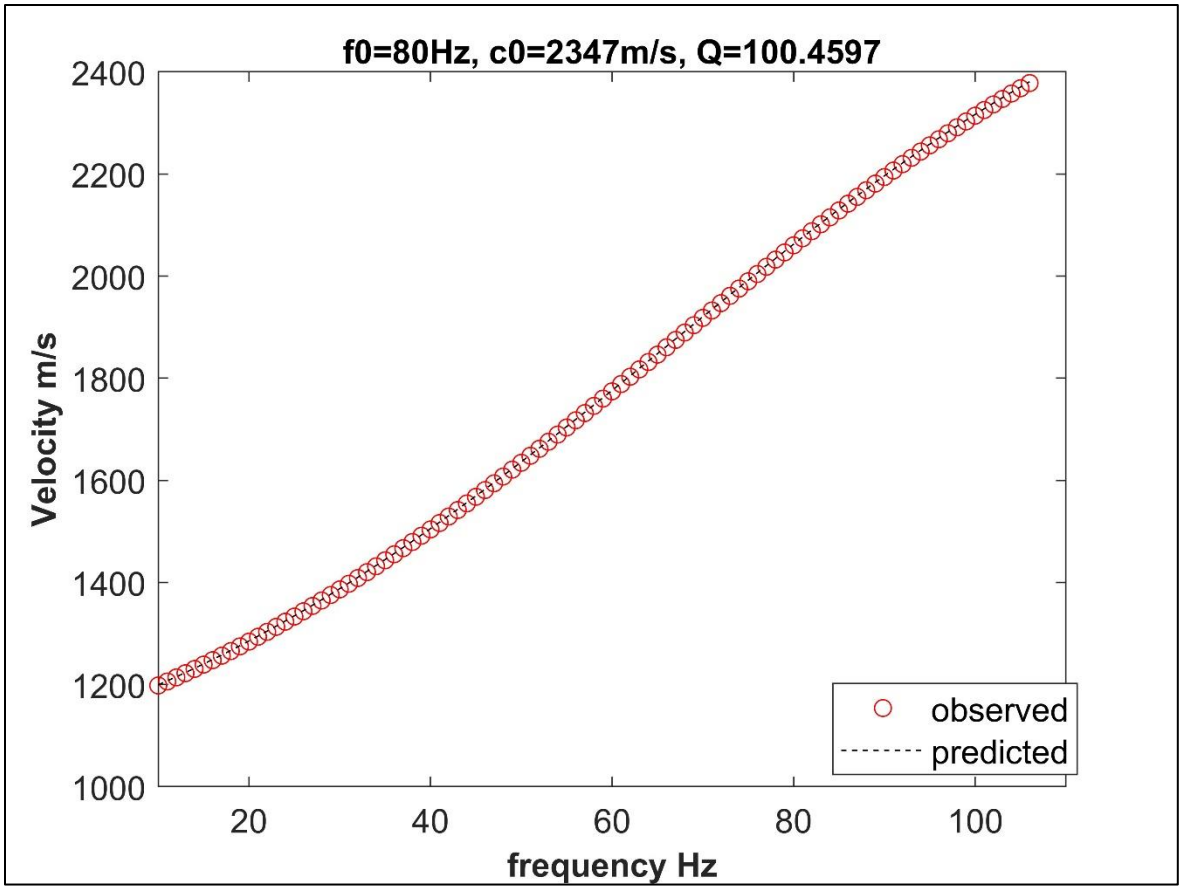

FIG 4.6c: Estimating Q at a depth of 300m, Line 3 at 480m offset using a reference frequency of 80Hz and reference phase velocity of 2347m/s.

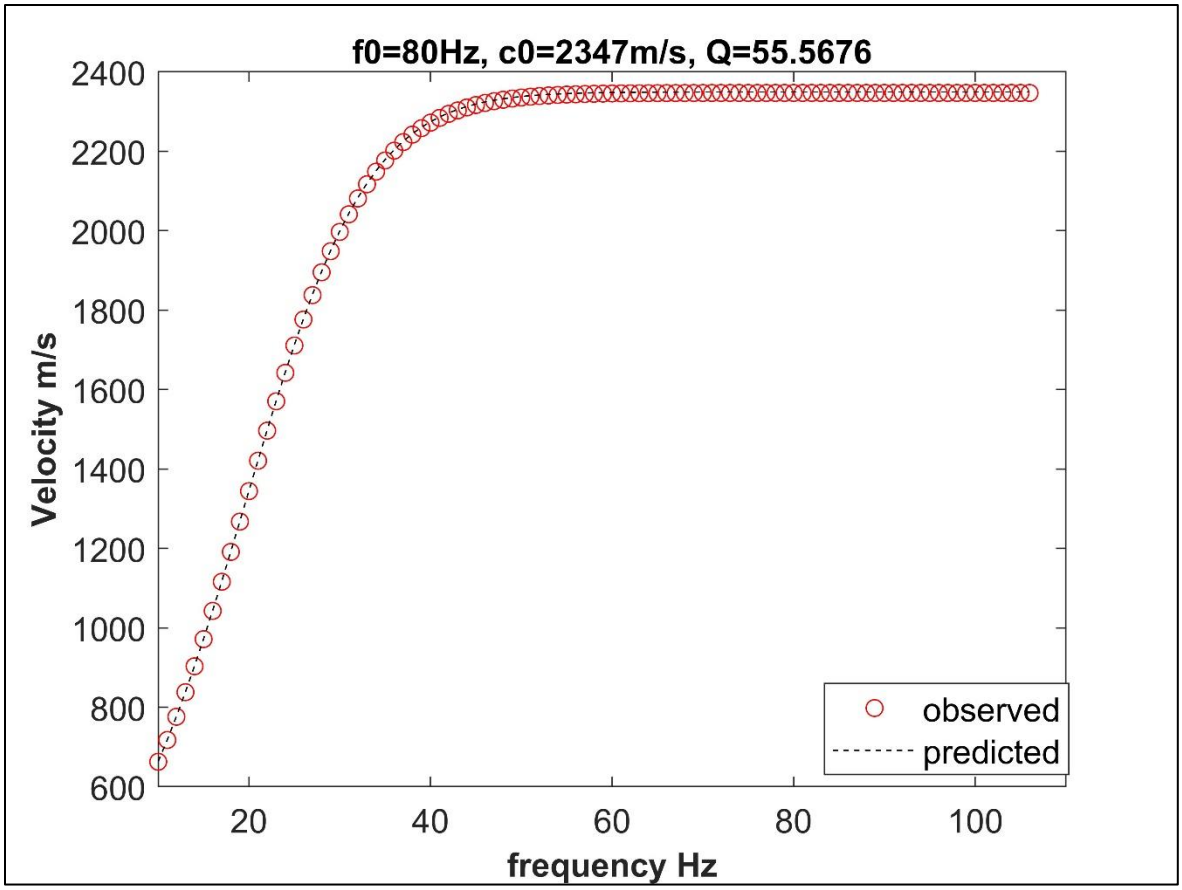

FIG 4.8b: Estimating Q at a depth of 260m, Line 3 at 480m offset using a reference frequency of 80Hz and reference phase velocity of 2347m/s.